LATERAL VARIATIONS OF DENSITY IN THE EARTH'S MANTLE

by

JAFARGHOLI ARKANI HAMED

Engineering Degree

University of Tehran (1962)

WITHDRAWN
MASS. INST. TECH.
FROM
MIT LIBRARIES
LINDGREN

SUBMITTED IN PARTIAL FULFILLMENT
OF THE REQUIREMENTS FOR THE
DEGREE OF DOCTOR OF
PHILOSOPHY
at the
MASSACHUSETTS INSTITUTE OF
TECHNOLOGY
February, 1969

Signature of Author.....
Department of Geology and Geophysics, January 13, 1969

Certified by .....
Thesis Supervisor

Accepted by .....
Chairman, Departmental Committee
on Graduate Students

Lindgren
WITHDRAWN
MASS. INST. TECH.
MAR 12 1969
FROM
MIT LIBRARIES

تقدیم بمادرم

To My Mother

ABSTRACT

LATERAL VARIATIONS OF DENSITY IN THE EARTH'S MANTLE

by

Jafargholi Arkani Hamed

Submitted to the Department of Geology and Geophysics on 13 January 1969 in partial fulfillment of the requirement for the degree of Doctor of Philosophy.

Lateral variations of the earth's gravitational field, deduced from orbital data of artificial satellites, indicate the existence of lateral density variations within the earth. A density model is computed for the the mantle with the following constraints: 1) the model presents the perturbations for Gutenberg's earth model specified by spherical harmonics with n = 2, . . ., 6; 2) the density anomalies are confined to the mantle and the crust; 3) the anomalies of the crust are determined for n = 2, . . ., 6 from crustal thickness, crustal P wave velocity, and P_n velocity, and those of the upper mantle for n = 2 and 3 are related to the lateral variations of seismic travel time residuals; 4) the unknown density anomalies of the mantle are determined such that the total shear strain energy of the earth is a minimum, 5) the gravitational potential of the deformed earth (subject to the density anomalies) on its surface equals the first six degrees of the spherical harmonic representation of the measured geopotential; and, 6) an isotropic, elastic, and cold mantle and a liquid core are assumed in the stress analysis.

The density anomalies thus obtained exhibit a decreasing feature with depth. In the crust they are on the order of 0.03 g/cc, in the upper mantle 0.1 g/cc, and in the lower mantle 0.04 g/cc, which are within the values deducted from seismic measurements.

Maximum shear stresses associated with the density anomalies are about 400 bars throughout the mantle. It is concluded that the real mantle subject to these density anomalies is in the creep state.

Thesis Supervisor: M. Nafi Toksöz
Title: Associate Professor of Geophysics

ACKNOWLEDGEMENTS

I would like to express my sincere gratitude and appreciation to my thesis supervisor, Professor M. Nafi Toksöz, for introducing me to the present thesis problem and for his invaluable time, encouragement and patience during the course of this work. I am very grateful to my advisor, Professor Theodore Madden, for the tremendous help I have received in the mathematical formulation as well as deep understanding of the problem. I would also like to thank Dr. Ralph Wiggins for the benefit of discussion which I received in the early stages of my thesis and for his help in the computer programmings and computations. Thanks also are due to Professor Keiiti Aki and Dr. John Minear for their careful reading of my thesis and many of their invaluable suggestions and criticism. Others with whom discussions have been helpful are Professor Gene Simmons and Dr. John Fairborn. I am also thankful to my previous advisor, Professor David Strangway, and Professor Patrick Hurley for their moral support during my moments of depression. Mr. Muawia Barazangi kindly permitted me to include his unpublished figure in my thesis. I am also grateful to Miss Mariann Pilch for her careful typing of the manuscript.

It is beyond any doubt that without the financial assistance of the Iranian Government I would not have been able to perform the

present work and it would have been very difficult for me to pursue my graduate studies. It would simply take more than a mere note of thanks.

BIOGRAPHICAL NOTE

The author was born on February 2, 1940, in Tabriz, Iran. He attended elementary and high schools in Tabriz before receiving Engineering Degree from the Engineering Faculty of the University of Tehran in 1962. He spent 1963 working for Minak Mining Company as a responsible engineer for two coal mines in Iran. Having received a scholarship from the Iranian Government, the author started his graduate work at the Massachusetts Institute of Technology in 1964.

TABLE OF CONTENTS

Table of Continents - continued

CHAPTER 1

Introduction

The observed perturbations of close satellite orbits have yielded accurate determinations of the low order harmonics of the lateral variations of the earth's gravitational field. These results indicate that the lateral variations of density exist within the earth. Seismic and heat flow measurements have also shown lateral variations. Thus, detailed studies of the lateral variations of the properties of the earth's interior are in order.

In this study we will be concerned with the larteral variations of density in the mantle. Kaula (1963) made a start on this problem, but we wish to extend his work by making use of seismic data on crustal thickness and crustal seismic velocities to fix the crustal density variations. This extension is made possible by the close relationship between density and seismic velocity in igneous rocks (Birch, 1961). Similar determinations of upper mantle density variations are made by using seismic travel time residuals. We determine the density variations in the mantle by using these seismically inferred loads as inputs, and by minimizing the total shear strain energy in the earth while satisfying the satellite gravity data.

(1 - 1) - Historical Review

The departure of the earth from a spherically symmetric body has been known for about three centuries. Richer (1671) observed that a pendulum oscillates with different frequencies at different latitudes and concluded that the earth is not a perfect sphere. Assuming an equilibrium state for a self-gravitating, rotating, uniform liquid earth, Newton pointed out that the earth is spheroidal. His conclusion was later confirmed by the measurements of the length of the meridian arc of 1^{o} in Peru and Lapland which were conducted by Bouguer (1735) and DeMaupertuis (1736) respectively (see Spencer Jones, 1954, for the cited references). The lateral heterogeneity of the earth is also manifested in the theory of isostasy (Airy, 1855; Pratt, 1855; (see Jeffreys, 1959)) which explains the lack of gravity effects of surface topography by compensation through variation of the crustal thickness and/or density. These crustal variations have been observed by seismic investigations.

Unlike the radial density variations in the earth, which have been studied in great detail, the lateral density variations have not been studied satisfactorily. This is partly due to the fact that the gross data of the earth, the total mass and the moment of inertia, are unable to yield any information about the lateral distribution of the density inside the earth (except for the second degree zonal spherical harmonic which contributes to the earth's moment of

inertia about the polar and an equatorial axis). Jeffreys (1941) pointed out that the spherical harmonic representation of geopotential has harmonics of degree 3, 4 and 6 and concluded that their sources must be below the thin crustal layer. Vening Meinesz (1962) also related the third and the fifth degrees of these harmonics, to the convection currents possibly existing in the earth's mantle.

In the last few years the artificial satellite data have indicated the lateral undulations of geopotential. These have been related to density anomalies in the earth (Wang, 1965; and Kaula, 1963 and 1967). Kaula (1963) presented two models for the lateral density variations of the crust and mantle. These models assume the topography of the surface of the earth as a surface load and also yield gravitational fields similar to the observed geopotential expressed by spherical harmonics through the fourth degree. However, in his determination of the models he had only used surface loads, so his models may not be realistic. An example is shown by the following table where the degree correlation coefficients of the crustal thickness with his crustal anomalies are listed.

n	Crust. Thick. and Model 1	Crust. Thick and Model 2
2	.39	.97
3	-.86	.057
4	-.83	.31

This table shows that the second degree harmonics of model 1 and all of the harmonics of model 2 have positive correlations with those of

crustal thickness. That is, the thicker crust has higher densi ty and vice versa. Considering the oceanic and the continental crust and their associated densities these results are not geophysically realistic. Therefore, we consider Kaula's work as a mathematical problem and adopt his procedure and use more data in order to determine a more realistic model of lateral density variations of the mantle.

(1-2) - Thesis Outline

Including the present chapter, this thesis is made up of five chapters.

Chapter 2 presents the data collected on crustal thickness and P_n velocity. The crustal thickness and the P wave travel time residuals are analyzed in terms of spherical harmonics through the sixth and the third degrees respectively. Using the coefficients of the harmonics we then calculate the linear correlation coefficients between any two sets of data: geopotential, surface equivalent rock topography, crustal thickness, and P wave travel time residuals. These coefficients are used to demonstrate the existance of, or lack of, linear relationships between the various types of geopotential data.

From crustal thickness, crustal P wave velocity, and P_n velocity we determine the average density of a surface layer (with 50 km. thickness) beneath 297 stations by using a linear density-velocity relationship (Birch, 1961). Because of the strong correlation

between the density and the actual crustal thickness we employ an emphirical relationship in order to compute the shperical harmonic coefficients of the density of the layer from those of crustal thickness. In the case of the upper mantle we relate the lateral variations of density to those of P wave velocity through Birch's (1964) formula and, thus, calculate the density anomalies from P wave travel time residuals.

In Chapter 3 we compute the density variations inside the mantle through the stress analysis in an isotropic, elastic and cold mantle overlying a laterally homogeneous liquid core. The density anomalies obtained in Chapter 2 together with the geopotential and equivalent rock topography are utilized in the analysis. From all possible density anomalies we select the one which exhibits a smoothly varying radial dependence and, moreover, produces a minimum total shear-strain energy in the earth.

Chapter 4 is devoted to the geophysical interpretation of the results of Chapter 3. These results are compared with the lateral variations of seismic structure of the mantle and with tectonically active regions. Furthermore, we determine the relaxation time of the stresses produced by the density anomalies in the mantle.

As a suggestion for further development of the present work we formulate in Chapter 5 the equations of a visco-thermo-elastic mantle model.

So as not to burden the text, mathematical formulas are developed in appendices.

CHAPTER 2

Lateral Variations of Geophysical Data

In recent years an increasing number of geophysical measurements have become available on a global basis. The joint studies of these data provide excellent means for understanding the properties of the earth's interior. This chapter focuses attention on the geophysical data that yield detailed information about the crust and the upper mantle. The physical quantities considered are: gravitational field of the earth (geopotential), surface equivalent rock topography, crustal thickness, seismic velocities in the crustal layers, seismic velocity at the top of the upper mantle (P_n velocity), and P wave travel time residuals.

The lateral variations of geopotential have been studied from the measurements of the undulations of close satellite orbits. From such measurements the coefficients of the spherical harmonic representation of geopotential have been determined (Guier, 1963; Izsak, 1964; Guier and Newton, 1965; Kaula, 1963, 1966, 1967; and, Gaposchkin, 1967). The correlation of Kaula's (1967) and Gaposchkin's (1967) values yields the degree correlation coefficients greater than 0.9 through the 6th degree, 0.7 for the 7th, and 0.3 for the 8th degree harmonics. Thus, Kaula's (1967) coefficients are reliable for the first 6 degrees of the harmonics which will be used throughout the

present studies. Spherical harmonic coefficients of the equivalent rock topography are also available (Lee and Kaula, 1967).

Deviations of seismic travel times from Jeffreys-Bullen tables are well known for certain distance ranges (Herrin and Taggart, 1966; Carder, et al., 1966; Cleary and Hales, 1966; Doyle and Hales, 1967; Chinnery and Toksöz, 1967). In addition to these variations, individual seismic stations exhibit well-defined residuals which are independent of the epicentral distances. These residuals are discussed and analyzed through the 3rd degree of spherical harmonics by Toksöz and Arkani-Hamed (1967). Recently Herrin, et al. (1968) have compiled all of the available P wave travel time residuals. We re-analyze these data through the 3rd degree.

In this chapter we present and analyze the most recent collection of crustal data, through which we deduce the crustal effects on the lateral variations of geopotential and P wave travel time residuals. Moreover the linear correlation coefficients of any two sets of the data are calculated in order to acquire some detailed information about the lateral density variations of the upper mantle.

2.1 - Spherical harmonic analysis of crustal thickness and P wave travel time residuals

Study of the lateral variations of crustal thickness involved the collection of all the data available through 1967. These are listed in Table (2-1). Included in the data are the results of seismic refraction, reflection, and surface wave dispersion measurements. P wave travel time residuals, however, are taken from the station corrections of Herrin, et al. (1968) for 320 stations. They have expressed the correction Δt, at a station by:

$$\Delta t = A + B\sin(c + d) \qquad (2\text{-}1)$$

where c is the station-source azimuth and A, B, and d are the constants of the station which have been determined from at least 10 observations at that station. Our main interest is in the first term, A, which presents the overall travel time residual of the station. In addition to these data, we also use the data obtained from three ocean bottom seismic observatories located on the Pacific ocean floor which provide the only information from the oceanic areas. Figures (2-1) and (2-2) display the global distribution of crustal thickness and travel time residuals, averaged over grids of $5^{o} \times 5^{o}$ latitude and longitude. This averaging is required in order to minimize the baising effect of the varying density of the stations on the spherical harmonic analysis of the data.

The averaged data are, then, expressed in terms of the following spherical harmonics:

$$Z(\theta,\varphi) = \sum_{n=1}^{N} \sum_{m=0}^{n} \{ A_{nm} \cos m\varphi + B_{nm} \sin m\varphi \} P_{nm}(\cos\theta) \qquad (2\text{-}2)$$

where A_{nm} and B_{nm} are the coefficients to be determined. Since we are primarily interested in the lateral variations of the data we first remove their mean values which correspond to the zero degree coefficient. The remaining coefficients are determined through two different techniques. For crustal thickness that has fairly uniform spatial distribution the simple least squares method is used. For the travel time residuals which are mainly available on the continents and islands and have a non-uniform distribution, a weighted least squares procedure is employed. Both of these methods are described in Appendix I. Spherical harmonic coefficients through N = 3 for travel time residuals and N = 6 for crustal thickness are computed and are tabulated in Table (2-2). These coefficients were used to construct the contours of the lateral variations of crustal thickness and travel time residuals, which are shown in Figures (2-3) and (2-4). The contours of crustal thickness outline oceans and continents fairly well and those of travel time residuals delineate the ocean basins, the shield areas, and the tectonic regions in the northern hemisphere. The shield areas in North America, Europe and Asia are characterized by the early arrivals indicating higher average velocities, while Pacific Ocean seems to be late.

The harmonic coefficients obtained are subject to the aliasing effect. That is, the low harmonics are probably biased by the higher order variations that may exist in the data. This biasing was examined for the case of travel time residuals by generating artificial data at the same points where we have real data, and re-expanding the data thus obtained in terms of spherical harmonics through N = 3. The resulting coefficients were, then, compared with those used to generate the data. For values of $N \leqslant 6$ the corresponding coefficients did not, in general, differ by more than 30 %. Including the N-values of 7, 8 and 9 changed the coefficients significantly. This indicates that the location of the stations is such that the harmonics of the degree higher than 6 contributes to the lower degree harmonics. In the case of crustal thickness, because of the uniform distribution of data, the aliasing effect is less pronounced.

2.2 - Crustal effects on geopotential and P wave travel time residuals

The lateral variations of crust affect all the measurements made on the earth's surface and, thus, obscure the effects of the lateral variation of the mantle on the measurements. To separate the crustal effects we consider a surface layer with 50 km. thickness. This imaginary boundary lies below the Mohorovicic discontinuity almost everywhere. We then determine the average density of this layer at 297 points by the following equation:

$$\bar{\rho}_j = \frac{\sum_{i=1}^{N_j} \rho_{ij} H_{ij}}{\sum_{i=1}^{N_j} H_{ij}} \qquad (2\text{-}3)$$

where H_{ij} and ρ_{ij} are the thickness and the density of the i^{th} layer and N_j is the number of the layers under the j^{th} station. Density of each layer is determined from its P wave velocity (Tabulated by Arkani-Hamed and Toksöz, 1968) and the Birch's (solution 8; 1961) experimental relationship:

$$\rho = 0.41 + 0.3597\, V_p \qquad (2\text{-}4)$$

Table (2-1) also includes the densities, thus obtained. Woolard (1959) demonstrated the validity of utilizing seismic velocities in order to calcuate the crustal densities.

Figure (2-5) displays $\bar{\rho}$ versus crustal thickness. The strong negative correlation between these quantities (their linear correlation coefficient is -.83) indicates that the thicker crust is associated with the lower average density and vice versa. This is because the oceanic crust is primarily made up of basic rocks with densities higher than those of the continental areas. Furthermore, continents have deep roots in the mantle while the oceanic crust is so thin that a large part of the "equivalent crust" must be filled up by heavy materials of the upper mantle. Because of the strong correlation, the empirical relationship:

$$\bar{\rho} = 3.311 - 0.0239\,(\mathrm{CRTH}) + 0.000247\,(\mathrm{CRTH})^2 \qquad (2\text{-}5)$$

is used to relate the density of the surface layer to actual crustal thickness. Here crustal thickness (CRTH) is in km and $\bar{\rho}$ is in g/cc. This relationship enables us to determine the spherical harmonic coefficients of $\bar{\rho}$ from those of crustal thickness. Table (2-2) contains the coefficients of $\bar{\rho}$ and Figure (2-6) displays the spherical harmonic synthesis of $\bar{\rho}$.

The spherical harmonic coefficients of the gravitational field of this layer and the equivalent rock topography over lying the layer are related to those of $\bar{\rho}$ and σ by:

$$\Phi_n(a) = \frac{4\pi G}{2n+1}\left[\frac{1}{a^{n+1}}\left(\frac{a^{n+3} - R^{n+3}}{n+3}\right)\bar{\rho}_n + a\sigma_n\right] \qquad (2\text{-}6)$$

where a is the mean radius of the earth, R is the radial distance to the bottom of the layer ($R = a - 50$ km.) and σ is the surface mass density corresponding to surface equivalent rock topography (the topography is reduced to a surface mass by using 2.7 g/cc for the average density of its materials, Lee and Kaula, 1967).

Table (2-3) is the list of the spherical harmonic coefficients of the gravitational potentials of the equivalent rock topography, the surface layer, and their total contribution to geopotential. The coefficients of geopotential are also listed in the same table for easy

comparison. The gravitational potentials of the topography or the surface layer are an order of magnitude greater than the observed geopotential variations, indicating the existence of some compensating density anomalies in the deep mantle.

Because of the lateral variations of the crust, travel times of P waves propagating vertically through the surface layer under different stations are different. Table (2-4) gives the locations of $5^{o} \times 5^{o}$ squares where the crustal data together with the travel time residuals are available. The square with the asterisk is chosen as the reference point, and other residuals are reduced to this point and are listed in the same table (STTR*). Using the average crustal velocity and P_n velocity, the travel times of P waves propagating from the surface to the bottom of the surface layer are determined and their residuals with respect to the reference point (the crustal residuals, CSTTR) are computed and also included in table (2-4). The crustal effect on the travel time residuals is very pronounced. Figure (2-7) illustrates the observed travel time residuals (STTR) versus the crustal residuals. Their linear correlation coefficient is -.47. The negative sign of the coefficient indicates that areas with positive crustal residuals (low P wave velocity of the layer), are associated with negative observed residuals and vice versa. This result is geophysically important and denotes that wherever the surface layer velocities are low (the continents) the upper mantle velocities are high and, thus, the layer compensates for the large lateral variations

of the velocities of the upper mantle.

Table (2-4) also includes the travel time residuals associated with the upper mantle (the mantle residual, MSTTR) which are computed through the following formula:

$$MSTTR = STTR - CSTTR \tag{2-7}$$

Comparison of these residuals with crustal residuals shows that not only do they have, in general, opposite signs but that also the MSTTR is about three times larger than the CSTTR.

2.3 - Correlation of Geophysical Data and Upper Mantle Density-Anomalies

To demonstrate the existence of or the lack of the linear relationships between the sets of geophysical data, we compute the correlation coefficients between any two sets. Wherever the data have common locations, which is the case for crustal thickness versus average density of the surface layer, or observed travel time residuals versus crustal residuals, the correlation coefficients are determined by (Lee, 1960):

$$r_{xy} = \frac{\overline{(x - \bar{x}) \cdot (y - \bar{y})}}{\sigma_x \cdot \sigma_y} \tag{2-8}$$

where $\bar{x}$ is the mean value of x and σ_x is the standard deviation of x. In the cases where the data do not have a common spatial distribution,

their spherical harmonic coefficients are used to display their correlation. If A_{nm}, B_{nm}, and A'_{nm}, B'_{nm} are the spherical harmonic coefficients of the two phenomena their correlation coefficients will be expressed by (Appendix II):

$$r = \frac{\sum_{n=1}^{N}\sum_{m=0}^{n}\{A_{nm}\cdot A'_{nm} + B_{nm}\cdot B'_{nm}\}}{\left[\sum_{n=1}^{N}\sum_{m=0}^{n}\{A_{nm}^2 + B_{nm}^2\}\right]^{1/2}\cdot\left[\sum_{n=1}^{N}\sum_{m=0}^{n}\{A'^2_{nm} + B'^2_{nm}\}\right]^{1/2}} \qquad (2\text{-}9)$$

Equation (2-9) and the coefficients listed in Table (2-2) were used to calculate the correlation coefficients between the foregoing sets of geophysical data used in this study. These are given in a matrix form in Table (2-5). In all these computations the value of n is determined by the lower value of the two sets. Moreover, the C_{20} coefficient of geopotential is omitted since its large value is primarily due to the improper correction for the flattening of the earth.

The correlation coefficients listed in Table (2-5) are in general low except for a few cases. The highest correlation is between surface topography and crustal thickness. This is in excellent agreement with value r = .76 of Lee and Taylor (1967) obtained by linear regression analysis. Such a high correlation means that higher regions are associated with thicker crust; this is an obvious conclusion when we consider the oceans and the continents and the associated crustal thicknesses. There is comparatively good correlation between geopotential and P wave travel time residuals. Its negative sign indicates that the zones with higher densities are

associated with higher seismic velocities. The negative correlation between travel time residuals and equivalent rock topography or crustal thickness means that the oceanic areas are associated with relatively lower average velocities than the continental ones, which implies that the upper mantle velocities under the oceans are slower than those under the continents to offset the crustal delays.

The lack of correlation between geopotential and equivalent rock topography or crustal thickness is very significant. These results, which have also been observed by Munk and MacDonald (1960), Birch (1964), and Kaula (1967), indicate that the lower harmonics of geopotential variations are controlled by the mass distributions in the mantle.

Table (2-5) displays overall correlations between the data. For a detailed study of the correlation coefficients, however, we have correlated the harmonics of similar degrees for two sets of data (the degree correlation) by using equation (2-9) for a given value of n. The results are listed in Table (2-6), which also includes the degree power and degree cross-power spectra of the data and shows the dominant degree of harmonics in the data. Harmonics with n greater than one are considered because of the lack of first degree harmonics in geopotential and, hence, in the lateral density variations of the earth with which we are concerned in the present studies. The almost equal degree correlation coefficients of crustal thickness and equivalent rock topography indicates a very close relationship between them and,

hence, confirms Airy's theory of isostasy. The large and negative degree correlation coefficients of travel time residuals and crustal thickness are very interesting. They mean that the thicker crust is associated with the shorter travel times. This indicates that materials under lying a thick crust are characterized by high P wave velocities. The small magnitudes and alternative sign of degree correlations of geopotential and crustal thickness are very significant. This indicates that geopotential is not due to the uncompensated part of the crustal anomalies but, rather, mantle density anomalies are responsible for the lateral variations of geopotential. The negative and high degree correlation coefficient of the second degree harmonics of travel time residuals and those of geopotential once more delineates the existence of large lateral variations in the properties of the upper mantle.

The foregoing discussion leads us to conclude that some large lateral density variations exist in the upper mantle and moreover, the lateral variations of P wave velocity of the upper mantle are somewhat linearly related to those of density. Therefore, the upper mantle density variations were determined from the mantle residuals by the assumption that Birch's (solution II, 1964) formula:

$$\Delta \rho = 0.3788\, \Delta V_p \qquad (2\text{-}10)$$

holds between these variations. In the absence of any realistic

equation of state this assumption is in order. To evaluate the mantle residuals, the travel time residuals corresponding to the surface layer are first calculated from its average density by using the following relationship:

$$\Delta t = -2.78 \times \frac{50}{V^2} \Delta \rho \qquad (2\text{-}11)$$

which is derived from equation (2-4). Then the mantle residuals are readily determined through equation (2-7). Using these residuals and equation (2-10) the upper mantle density anomalies are computed by the following equation:

$$\Delta \rho = \frac{-0.3788 \times MSTTR}{\sum_i (H_i / V_i^2)}$$

Here H_i and V_i are the thickness and the velocity of the $_i$th layer in the upper mantle. In the numerical calculations, Gutenberg's earth model is used and it is assumed that $\Delta \rho$ does not change with depth. If we use Jeffreys' model instead, there will not be any significant difference in the results. Both of these models are listed by Alterman, et al. (1961).

LIST OF TABLES FOR CHAPTER 2

Table

Table (2-1)

NO	LAT. D	M	LONG. D	M	ELEV KM	TH. KM	PN KM/S	RR	RL	SW	RHO G/CC	REF.
1	114	34	57	27	-4.9	4.6	8.06	1	0	0	3.24	47
2	116	56	58	10	-5.5	5.5	8.12	1	0	0	3.25	47
3	121	29	61	52	-4.3	5.5	8.16	1	0	0	3.26	27
4	122	55	62	26	-4.8	6.1	8.39	1	0	0	3.33	27
5	129	45	63	58	-5.0	4.4	8.13	1	0	0	3.27	27
6	125	46	73	40	-4.0	4.0	7.99	1	0	0	3.21	27
7	126	51	76	23	-3.2	3.9	8.23	1	0	0	3.28	27
8	127	15	78	31	-1.9	8.5	7.61	1	0	0	3.03	27
9	127	56	87	39	-3.8	8.2	7.80	1	0	0	3.11	27
10	123	48	96	1	-4.3	7.1	8.06	1	0	0	3.20	27
11	122	45	102	45	-4.8	7.7	8.18	1	0	0	3.21	27
12	124	11	105	55	-5.6	6.9	8.24	1	0	0	3.26	27
13	122	50	108	41	-5.3	4.7	7.87	1	0	0	3.14	27
14	119	42	111	31	-5.3	5.9	8.28	1	0	0	3.27	27
15	115	3	104	12	-5.1	5.0	8.11	1	0	0	3.24	27
16	110	43	97	12	-5.8	6.2	8.14	1	0	0	3.24	27
17	106	25	89	19	-5.7	4.2	7.94	1	0	0	3.20	27
18	103	9	93	13	-5.2	7.5	8.07	1	0	0	3.21	27
19	104	57	108	9	-5.6	6.1	8.28	1	0	0	3.28	27
20	103	47	115	33	-5.7	9.0	8.23	1	0	0	3.21	27
21	103	31	118	26	-5.7	8.4	8.09	1	0	0	3.17	27
22	41	54	273	56		63.9	8.39	1				73
23	42	55	269	16		37.6	8.52	1				73
24	42	14	274	10		72.0	8.52	1				73
25	43	05	268	05		34.0	8.39	1				73
26	43	15	267	25		33.6	8.28	1				73
27	41	40	265	00		50.6	8.28	1				73
28	52	0	240	50	1.9	42.9	7.80	1	1	0	2.78	39
29	52	35	242	30	3.4	34.9	7.80	1	1	0	2.87	39
30	53	20	243	45	1.3	33.8	7.80	1	1	0	2.85	39
31	53	54	245	12	0.3	31.6	7.80	1	1	0	2.86	39
32	52	0	238	0	0.0	21.0	7.90	1	0	1	2.97	77
33	51	30	240	0	1.4	27.4	7.90	1	0	1	2.82	77
34	50	45	241	0	1.0	36.0	7.90	1	0	1	2.78	77
35	39	47	248	50	0.7	48.0	8.25	0	1	0	2.59	40
36	39	33	246	50	1.4	48.0	8.25	0	1	0	2.65	40
37	40	3	249	40	0.8	48.0	8.01	0	1	0	2.61	40
38	39	0	247	0	4.0	44.0	8.20	1	0	0	2.63	81
39	39	0	242	0	8.0	32.0	7.80	1	0	0	2.78	81
40	39	0	240	0	2.0	32.0	7.80	1	0	0	2.84	81
41	40	0	234	0	4.0	54.0	8.10	1	0	0	2.99	81
42	46	0	295	0	0.0	36.3	8.11	1	0	0	2.79	5
43	45	30	296	0	0.0	32.8	8.11	1	0	0	2.81	5
44	46	0	298	30	0.0	32.6	8.11	1	0	0	2.84	5
45	12	30	261	0	0.0	38.0	8.20	1	0	0	2.88	65
46	13	30	266	0	0.0	37.8	8.20	1	0	0	2.73	65
47	46	00	290	00		37.0	8.20	1				75
48	47	00	286	00		36.0	8.10	1				75
49	49	00	283	00		33.0	8.20	1				75
50	52	00	277	00		39.0	8.10	1				75

****** CONTINUE ******

NO	LAT. D	M	LONG. D	M	ELEV KM	TH. KM	PN KM/S	RR	RL	SW	RHO G/CC	REF.
51	43	30	271	30		37.0	8.10	1				75
52	44	30	270	00		37.0	8.00	1				75
53	42	30	265	30		37.0	8.10	1				75
54	53	00	268	30		41.0	8.20	1				75
55	60	00	263	00		33.0	8.20	1				75
56	43	30	253	00		53.0	8.10	1				75
57	43	30	246	30		41.0	7.90	1				75
58	49	00	253	00		48.0	8.00	1				75
59	55	00	253	00		51.0	8.20	1				75
60	48	00	250	00		41.0	8.00	1				75
61	55	30	251	30		31.0	7.90	1				75
62	47	00	243	30		47.0	7.90	1				75
63	50	00	240	00		50.0	7.90	1				75
64	50	00	243	00		22.0	7.80	1				75
65	51	00	240	00		45.0	7.90	1				75
66	51	30	239	00		16.0	7.90	1				75
67	52	30	243	00		28.0	7.80	1				75
68	53	30	244	30		30.0	7.80	1				75
69	52	30	238	00		23.0	8.00	1				75
70	55	30	240	30		23.0	8.20	1				75
71	35	0	258	0	0.3	31.0	7.90	1	0	0	2.94	34
72	37	0	258	30	0.3	34.0	7.90	1	0	0	2.89	34
73	39	0	303	0	0.0	31.1	7.98	1	0	0	2.87	11
74	41	30	301	0	0.0	34.7	7.98	1	0	0	2.82	11
75	42	30	295	30	0.0	48.7	8.50	1	0	0	2.75	11
76	43	15	299	0	0.0	42.5	8.50	1	0	0	2.82	11
77	44	30	299	30	0.0	32.5	8.10	1	0	0	2.84	11
78	46	00	295	00		36.3	8.10	1				11
79	46	0	300	30	0.0	34.8	8.00	1	0	0	2.59	11
80	48	0	301	0	-4.0	11.6	7.96	1	0	0	2.95	11
81	56	10	137	0	-2.2	14.4	8.03	1	0	0	2.89	52
82	56	30	136	30	-2.1	13.9	8.03	1	0	0	2.89	52
83	152	0	220	0	-3.4	6.5	7.79	0	0	1	3.13	1
84	150	0	225	0	-3.4	6.5	7.79	0	0	1	3.13	1
85	135	0	240	0	-3.7	6.5	7.79	0	0	1	3.13	1
86	140	0	230	0	-3.7	6.5	7.79	0	0	1	3.13	1
87	140	0	250	0	-3.7	6.5	7.79	0	0	1	3.13	1
88	145	0	217	0	-3.7	10.0	7.79	0	0	1	3.08	18
89	155	0	180	0	-3.7	30.0	7.79	0	0	1	2.85	18
90	143	0	290	0	-3.8	10.0	7.79	0	0	1	3.08	18
91	125	0	305	0	-3.8	10.0	7.79	0	0	1	3.08	18
92	155	0	270	0	0.0	25.0	7.79	0	0	1	2.89	18
93	142	0	5	0	-4.4	5.0	7.79	0	0	1	3.15	18
94	175	0	70	0	3.9	35.0	7.79	0	0	1	2.76	18
95	137	0	97	0	-3.7	10.0	7.79	0	0	1	3.08	18
96	137	0	107	0	-3.8	10.0	7.79	0	0	1	3.08	18
97	155	0	135	0	1.0	35.0	7.79	0	0	1	2.76	18
98	140	0	115	0	-3.8	10.0	7.79	0	0	1	3.08	18
98	150	0	140	0	0.0	35.0	7.79	0	0	1	2.76	18
100	134	0	97	0	-3.9	10.0	7.79	0	0	1	3.08	18

****** CONTINUE ******

NO	LAT. D	M	LONG. D	M	ELEV KM	TH. KM	PN KM/S	RR	RL	SW	RHO G/CC	REF.
101	150	0	135	0	0.0	35.0	7.79	0	0	1	2.76	18
102	125	0	287	0	0.7	30.0	7.79	0	0	1	2.83	18
103	143	0	275	0	-4.4	5.0	7.79	0	0	1	3.15	18
104	155	0	220	0	0.0	25.0	7.79	0	0	1	2.89	18
105	127	0	290	0	0.7	30.0	7.79	0	0	1	2.83	18
106	144	0	282	0	-4.2	5.0	7.79	0	0	1	3.15	18
107	160	0	240	0	0.0	25.0	7.79	0	0	1	2.89	18
108	120	0	302	0	0.1	30.0	7.79	0	0	1	2.83	18
109	140	0	310	0	-3.8	10.0	7.79	0	0	1	3.08	18
110	160	0	50	0	2.9	35.0	7.79	0	0	1	2.76	18
111	135	0	40	0	-4.5	5.0	7.79	0	0	1	3.15	18
112	158	0	90	0	0.0	35.0	7.79	0	0	1	2.76	18
113	140	0	46	0	-4.2	5.0	7.79	0	0	1	3.15	18
114	126	00	178	00	-2.4	15.5	7.79			1		76
115	132	00	173	00	0.0	35.0	7.79			1		76
116	43	45	8	10		36.0	8.15	1				28
117	44	00	8	05		37.0	8.15	1				28
118	44	00	7	10		37.0	8.15	1				28
119	44	30	8	00		49.0	8.15	1				28
120	44	30	7	05		44.0	8.15	1				28
121	44	40	7	00		43.0	8.15	1				28
122	44	35	7	00		42.0	8.15	1				28
123	44	32	7	05		45.0	8.15	1				28
124	44	40	7	20		40.0	8.15	1				28
125	44	45	7	30		42.0	8.15	1				28
126	44	50	7	00		39.0	8.15	1				28
127	44	51	7	10		47.0	8.15	1				28
128	44	55	6	55		47.0	8.15	1				28
129	44	55	6	45		46.0	8.15	1				28
130	44	55	6	50		42.0	8.15	1				28
131	44	58	6	40		44.0	8.15	1				28
132	45	00	6	35		36.0	8.15	1				28
133	45	00	7	16		39.0	8.15	1				28
134	44	55	7	16		38.0	8.15	1				28
135	44	54	7	26		43.0	8.15	1				28
136	44	57	7	40		53.0	8.15	1				28
137	45	02	6	30		36.0	8.15	1				28
138	45	02	6	50		42.0	8.15	1				28
139	45	05	6	10		28.0	8.15	1				28
140	45	05	6	20		33.0	8.15	1				28
141	45	05	7	00		46.0	8.15	1				28
142	45	10	6	20		29.0	8.15	1				28
143	45	10	7	08		46.0	8.15	1				28
144	45	12	6	28		30.0	8.15	1				28
145	45	12	7	00		45.0	8.15	1				28
146	45	12	7	30		44.0	8.15	1				28
147	45	18	6	35		31.0	8.15	1				28
148	45	18	6	52		34.0	8.15	1				28
149	45	18	7	30		47.0	8.15	1				28
150	45	20	7	00		35.0	8.15	1				28

****** CONTINUE ******

NO	LAT. D	M	LONG. D	M	ELEV KM	TH. KM	PN KM/S	RR	RL	SW	RHO G/CC	REF.
151	45	20	7	07		47.0	8.15	1				28
152	45	21	6	55		35.0	8.15	1				28
153	45	25	6	35		28.0	8.15	1				28
154	45	25	6	55		34.0	8.15	1				28
155	45	25	7	25		43.0	8.15	1				28
156	45	30	6	57		34.0	8.15	1				28
157	45	30	7	04		36.0	8.15	1				28
158	45	30	7	20		41.0	8.15	1				28
159	54	20	60	35		47.5	8.40		1			7
160	54	22	60	30		48.0	8.40		1			7
161	54	24	60	25		51.0	8.40		1			7
162	54	30	60	12		51.0	8.40		1			7
163	47	30	112	0	1.8	30.8	7.80	1	0	0	2.88	82
164	48	30	110	30	2.4	36.8	7.80	1	0	0	2.85	82
165	50	25	254	0	6.5	56.0	8.00	1	1	0	3.01	38
166	22	10	20	26	0.4	33.9	8.05	0	1	0	2.89	6
167	35	20	3	20	-0.2	29.7	8.30	1	0	0	2.71	15
168	40	00	8	40		30.0	8.20	1	1			31
169	38	00	10	00		27.0	8.20	1	1			31
170	40	35	8	40		28.5	8.20	1	1			31
171	40	30	11	40		29.8	8.20	1	1			31
172	48	48	16	31	0.0	39.0	8.25	1	0	0	2.88	24
173	91	45	42	7	-2.1	16.6	8.10	1	0	0	2.86	26
174	92	40	43	28	-3.6	9.9	8.08	1	0	0	3.01	26
175	92	31	44	56	-4.2	8.3	8.14	1				26
176	92	55	47	2	-4.8	11.1	8.10	1	0	0	3.07	26
177	93	28	49	36	-5.0	4.2	7.88	1				26
178	93	36	51	29	-5.1	3.4	8.18	1	0	0	3.28	26
179	92	12	57	18	-4.4	6.8	8.14	1	0	0	3.21	26
180	94	46	55	4	-0.1	31.9	8.10	1	0	0	2.94	26
181	68	20	202	0	-0.1	5.4	7.60	0	0	0	3.01	29
182	68	40	201	55	-0.2	4.7	7.65	1	0	0	3.06	29
183	68	50	202	10	-0.6	20.6	8.80	1	0	0	3.07	29
184	46	20	9	0	-2.5	10.5	8.00	1	0	0	3.03	23
185	46	45	8	30		11.5	8.00	1				23
186	47	15	7	30	-2.5	8.5	8.00	1	0	0	3.06	23
187	48	15	6	30	-2.5	8.0	7.70	1	0	0	2.98	23
188	48	45	5	0	-2.5	9.7	7.70	1	0	0	2.95	23
189	48	15	34	55		26.5	8.20	1	1			53
190	44	30	236	40	0.0	15.9	8.00	1	0	0	3.03	10
191	45	20	236	20	0.0	15.8	8.00	1	0	0	3.03	10
192	60	0	76	0	0.4	37.9	8.10	0	0	1	2.81	30
193	43	40	7	0	1.5	49.5	8.10	0	0	1	2.71	44
194	44	0	6	20	1.5	42.5	8.10	0	0	1	2.77	44
195	43	0	8	0	1.0	40.0	8.10	0	0	1	2.80	44
196	42	50	8	40	0.6	37.5	8.10	0	0	1	2.80	44
197	42	20	9	30	0.3	42.5	8.10	0	0	1	2.74	44
198	42	10	7	40	0.0	30.0	8.10	0	0	1	2.87	44
199	170	0	45	0	0.0	42.0	7.85	0	0	1	2.68	32
200	67	0	320	0	-5.8	11.5	8.10	0	0	1	3.11	9

****** CONTINUE ******

NO	LAT. D	M	LONG. D	M	ELEV KM	TH. KM	PN KM/S	RR	RL	SW	RHO G/CC	REF.
201	66	0	330	0	-5.3	5.3	8.10	0	0	1	3.28	9
202	62	30	330	0	-5.3	5.3	8.10	0	0	1	3.28	9
203	50	0	337	0	-4.8	4.8	8.10	0	0	1	3.28	9
204	54	0	335	0	-5.3	5.3	8.10	0	0	1	3.28	9
205	33	30	61	00		45.0	8.30	1				43
206	33	20	60	00		45.0	8.30	1				43
207	33	30	62	00		42.5	8.30	1				43
208	33	15	63	30		42.5	8.30	1				43
209	32	45	65	30		41.5	8.20	1				43
210	33	20	57	40		42.5	8.20	1				43
211	49	50	4	40	0.3	20.0	7.65	0	0	1	2.91	56
212	51	0	8	0	0.3	20.0	7.65	0	0	1	2.91	56
213	53	0	9	30	0.3	25.0	7.65	0	0	1	2.85	56
214	51	0	4	0	0.5	25.0	7.65	0	0	1	2.85	56
215	52	0	18	0	0.5	23.0	8.10	0	0	1	2.68	56
216	56	0	32	0	0.5	23.0	8.10	0	0	1	2.68	56
217	56	0	30	0	0.3	23.0	8.10	0	0	1	2.68	56
218	51	20	15	30	0.3	20.0	7.30	0	0	1	2.77	56
219	86	00	17	00		35.0	8.10			1		58
220	40	20	37	00		41.0	8.00	1				74
221	40	45	36	40		38.5	8.20	1				74
222	41	20	36	00		50.0	8.40			1		74
223	42	30	35	30		46.0	8.20			1		74
224	43	10	34	50		44.0	8.00			1		74
225	43	50	34	30		40.0	8.40			1		74
226	44	20	34	20		40.0	8.40			1		74
227	45	30	34	20	-2.5	27.5	8.20			1		74
228	47	00	34	20		25.0	8.20			1		74
229	47	45	42	00		42.0	8.20	1				41
230	47	50	43	30		47.0	8.20	1				41
231	48	00	44	40		50.0	8.20	1				41
232	48	40	45	15		46.0	8.20	1				41
233	47	40	40	00		28.0	8.20	1				41
234	47	30	36	00		28.0	8.20	1				41
235	35	00	79	00		40.0	8.20	1				46
236	37	00	81	00		43.0	8.20	1				46
237	38	00	160	00	-3.5	31.5	8.15	1				79
238	39	00	158	00	-1.0	29.0	8.15	1				79
239	38	45	160	00	-5.0	20.0	8.15	1				79
240	39	15	156	00	-0.6	29.4	8.15	1				79
241	39	00	157	00	-0.5	24.5	8.15	1				79
242	42	00	156	00	-5.0	25.0	8.15	1				79
243	42	30	156	00	-7.0	13.0	8.15	1				79
244	41	15	158	00	-5.5	9.5	8.15	1				79
245	45	00	155	40	-5.0	5.0	8.15	1				79
246	44	20	152	00	-2.0	18.0	8.15	1				79
247	43	45	152	00	-2.0	13.0	8.15	1				79
248	44	50	150	10	-1.0	24.0	8.15	1				79
249	41	10	152	00	-2.0	18.0	8.15	1				79
250	42	00	151	00	-3.0	12.0	8.15	1				79

****** CONTINUE ******

NO	LAT. D	M	LONG. D	M	ELEV KM	TH. KM	PN KM/S	RR	RL	SW	RHO G/CC	REF.
251	41	00	154	00	-2.0	23.0	8.15	1				79
252	52	30	60	40		46.5	8.20					80
253	51	00	63	30		45.0	8.30					80
254	50	20	64	20		46.5	8.30					80
255	49	20	65	40		40.0	8.10					80
256	49	40	69	40		42.0	8.20					80
257	49	20	73	30		55.0	8.30					80
258	50	18	141	10		25.0	7.52			1		2
259	50	17	140	06		26.0	7.52			1		2
260	53	51	139	23		39.0	7.52			1		2
261	53	20	138	12		46.0	7.52			1		2
262	54	44	136	15		27.0	7.52			1		2
263	55	38	132	26		29.0	7.52			1		2
264	54	59	135	44		23.0	7.52			1		2
265	62	36	238	25	-4.2	7.4	8.41	1	0	0	3.31	47
266	70	38	231	30	-4.8	5.9	8.05	1	0	0	3.23	47
267	79	17	214	07	-5.2	5.4	8.24	1				47
268	75	19	208	6	-5.8	5.3	8.15	1	0	0	3.25	47
269	69	34	205	6	-5.2	7.2	7.92	1	0	0	3.12	47
270	70	58	182	41	-4.8	8.2	8.28	1	0	0	3.24	47
271	77	33	168	22	-4.9	6.3	8.42	1	0	0	3.28	47
272	78	48	165	10	-4.5	8.7	8.28	1	0	0	3.18	47
273	78	40	161	35	-3.9	12.5	8.09	1				47
274	89	13	169	11	-4.4	13.0	8.16	1	0	0	3.13	47
275	80	59	174	56	-5.2	6.5	8.14	1	0	0	3.23	47
276	103	36	174	56	-2.5	5.6	8.14	1	0	0	3.22	47
277	108	59	177	34	-2.6	12.5	8.51	1	0	0	3.20	47
278	111	55	178	33	-4.1	10.6	8.42	1	0	0	3.20	47
279	109	57	187	27	-6.1	6.1	8.25	1	0	0	3.25	47
280	110	30	186	40	-9.2	11.2	8.29	1	0	0	3.23	47
281	110	02	186	53	-8.9	11.1	8.29	1				47
282	106	16	191	29	-5.1	11.2	8.77	1	0	0	3.35	47
283	107	28	199	1	-4.8	6.1	8.17	1	0	0	3.25	47
284	107	32	201	20	-5.2	5.8	8.21	1	0	0	3.27	47
285	102	47	216	27	-4.6	7.1	8.43	1	0	0	3.31	47
286	101	20	217	35	-4.6	7.4	8.34	1	0	0	3.29	47
287	100	45	226	25	-4.2	6.4	8.14	1	0	0	3.24	47
288	101	46	231	3	-4.1	5.6	8.00	1	0	0	3.21	47
289	104	16	240	50	-3.6	5.2	8.12	1	0	0	3.23	47
290	97	20	241	20	-4.3	4.8	8.30	1	0	0	3.31	47
291	89	49	236	34	-4.5	5.5	8.21	1	0	0	3.26	47
292	84	13	236	1	-4.3	5.4	8.16	1	0	0	3.24	47
293	75	2	235	48	-4.4	6.4	8.46	1	0	0	3.35	47
294	36	43	198	12	-6.9	7.8	7.78	1	0	0	3.06	47
295	34	48	191	8	-2.1	18.8	8.41	1	0	0	2.96	47
296	34	35	192	10	-0.2	28.8	8.08	1	0	0	2.76	47
297	33	15	207	11	-0.1	23.3	8.07	1	0	0	2.83	47
298	34	15	207	37	-5.4	9.6	8.19	1				47
299	39	17	211	38	-4.6	6.3	8.17	1				47
300	38	37	214	49	-4.2	6.6	8.15	1	0	0	3.24	47

****** CONTINUE ******

NO	LAT. D	M	LONG. D	M	ELEV KM	TH. KM	PN KM/S	RR	RL	SW	RHO G/CC	REF.
301	37	24	218	50	-3.7	6.9	8.36	1	0	0	3.26	47
302	36	53	221	15	-3.5	7.3	8.30	1				47
303	36	3	224	6	-2.9	6.5	8.13	1	0	0	3.17	47
304	35	37	227	28	-0.4	25.8	8.50	1	0	0	2.97	47
305	37	16	183	37	-3.6	9.9	7.60	1	0	0	2.89	47
306	39	41	182	21	-7.3	6.1	7.57	1				47
307	63	18	190	56	-4.4	6.9	8.00	1	0	0	3.16	47
308	63	57	191	10	-3.2	9.9	8.28	1	0	0	3.19	47
309	64	33	191	33	-1.1	13.1	8.42	1	0	0	3.14	47
310	69	15	253	33	-4.1	8.2	8.29	1	0	0	3.18	47
311	70	56	254	32	-4.9	4.2	7.64	1	0	0	3.05	47
312	73	50	260	15	-5.1	6.6	8.24	1	0	0	3.25	47
313	76	36	268	45	-0.1	10.3	8.18	1	0	0	3.13	47
314	77	0	268	20	-6.1	8.7	8.04	1	0	0	3.13	47
315	78	4	268	17	-3.6	4.5	7.76	1	0	0	3.11	47
316	78	30	271	56	-5.1	10.8	8.60	1	0	0	3.26	47
317	61	32	287	48	-4.3	9.0	8.40	1	0	0	3.29	47
318	66	43	289	10	-3.1	19.5	8.20	1	0	0	2.99	47
319	66	43	288	38	-8.0	10.5	8.02	1	0	0	3.16	47
320	66	30	287	1	-3.7	8.7	8.20	1	0	0	3.21	47
321	76	25	280	51	-4.5	6.4	8.10	1	0	0	3.22	47
322	77	22	281	24	-6.0	10.7	8.36	1	0	0	3.23	47
323	67	10	206	39	-5.0	5.4	8.68	1	0	0	3.43	47
324	67	23	205	56	-4.6	5.5	8.50	1	0	0	3.37	47
325	68	0	203	26	-4.9	7.3	8.10	1	0	0	3.18	47
326	66	40	203	40	-4.3	5.9	8.08	1	0	0	3.23	47
327	68	55	203	45	-0.9	12.3	8.05	1	0	0	3.03	47
328	67	47	204	47	-4.5	5.2	7.99	1	0	0	3.20	47
329	67	12	204	6	-4.3	6.3	7.97	1	0	0	3.20	47
330	66	51	203	22	-4.3	6.7	8.71	1	0	0	3.42	47
331	42	00	225	00	-4.0	4.6	8.10	1				47
332	60	56	246	40	-1.1	10.9	7.60	1				47
333	62	48	248	40	-1.7	7.7	7.80	1				47
334	64	43	250	19	-2.5	5.1	7.73	1				47
335	66	42	251	39	-2.7	4.8	7.47	1				47
336	67	34	252	09	-2.9	4.9	7.83	1				47
337	68	32	252	39	-3.1	6.9	7.92	1				47
338	66	19	252	43	-0.1	18.2	8.02	1				47
339	68	26	253	51	-0.6	10.2	7.60	1				47
340	39	41	182	21	-7.3	6.1	7.57	1	0	0	2.98	47
341	37	33	183	14	-3.1	17.2	8.89	1	0	0	3.12	47
342	36	57	184	29	-3.4	10.8	8.12	1	0	0	3.02	47
343	36	7	183	56	-3.7	11.0	7.84	1	0	0	2.94	47
344	34	21	183	30	-3.8	11.7	8.08	1	0	0	2.99	47
345	34	40	182	40	-3.8	9.2	7.73	1	0	0	2.93	47
346	33	58	183	18	-3.7	11.4	8.25	1	0	0	3.05	47
347	33	40	184	21	-3.7	12.0	7.98	1	0	0	2.95	47
348	37	15	183	37	-3.7	9.9	7.60	1	0	0	2.89	47
349	34	50	190	10	-3.7	18.8	8.41	1	0	0	2.96	47
350	76	6	285	25	-4.0	13.8	8.00	1	0	0	3.02	47

****** CONTINUE ******

NO	LAT. D	M	LONG. D	M	ELEV KM	TH. KM	PN KM/S	RR	RL	SW	RHO G/CC	REF.
351	78	29	283	49	-3.2	12.5	7.80	1	0	0	2.86	47
352	78	43	284	13	-2.8	12.5	8.10	1	0	0	2.94	47
353	78	31	282	18	-3.7	16.2	8.20	1	0	0	3.03	47
354	72	28	280	26	-1.4	18.4	7.60	1	0	0	2.83	47
355	70	44	282	22	-5.2	5.3	8.10	1	0	0	3.20	47
356	71	51	279	58	-3.9	9.4	8.30	1	0	0	3.19	47
357	71	22	280	21	-4.8	6.0	8.20	1	0	0	3.22	47
358	70	49	280	51	-6.9	5.2	8.20	1	0	0	3.22	47
359	70	20	283	49	-5.0	14.3	8.00	1				47
360	72	14	285	13	-1.9	20.0	8.20	1	0	0	2.97	47
361	72	39	287	4	-3.8	13.8	7.80	1	0	0	2.96	47
362	65	51	267	37	-3.8	12.9	8.30	1	0	0	3.00	47
363	64	50	267	8	-3.7	15.5	8.30	1	0	0	2.92	47
364	76	34	296	57	-3.5	11.6	8.32	1	0	0	3.01	47
365	76	37	298	15	-5.0	8.4	8.13	1	0	0	3.08	47
366	74	36	295	14	-3.9	13.1	8.31	1	0	0	3.07	47
367	73	40	293	33	-4.4	10.2	8.04	1	0	0	3.08	47
368	72	44	292	58	-5.1	10.9	7.78	1	0	0	2.99	47
369	70	19	297	30	-6.2	6.7	7.85	1	0	0	3.11	47
370	70	11	295	48	-6.8	9.4	8.05	1	0	0	3.09	47
371	70	5	294	6	-8.0	9.8	7.94	1	0	0	3.08	47
372	65	58	297	45	-5.9	7.4	8.21	1				47
373	67	32	298	6	-5.8	5.9	7.96	1	0	0	3.17	47
374	69	34	298	21	-5.5	6.9	8.44	1	0	0	3.30	47
375	71	10	299	40	-6.0	8.3	8.36	1	0	0	3.25	47
376	71	41	299	22	-6.4	9.8	8.64	1	0	0	3.23	47
377	71	50	298	57	-5.6	13.6	8.35	1	0	0	3.03	47
378	71	40	299	06	-5.9	14.6	8.42	1				47
379	70	55	297	41	-6.6	14.1	8.30	1				47
380	70	35	295	22	-6.0	15.8	8.43	1	0	0	3.08	47
381	75	29	295	17	-3.9	14.1	8.08	1				47
382	76	27	293	36	-5.0	7.8	8.23	1				47
383	74	54	293	1	-5.0	8.9	8.20	1	0	0	3.15	47
384	73	32	293	54	-4.5	10.6	7.92	1	0	0	3.05	47
385	53	48	288	27	-4.1	8.0	7.97	1	0	0	3.03	47
386	63	10	284	58	-4.6	7.9	7.87	1	0	0	3.04	47
387	61	16	286	42	-4.5	9.0	8.50	1	0	0	3.18	47
388	58	44	292	22	-5.1	5.9	8.05	1	0	0	3.16	47
389	55	40	291	50	-5.3	4.3	7.83	1	0	0	3.12	47
390	56	1	293	33	-5.1	4.2	7.80	1	0	0	3.09	47
391	66	45	295	56	-5.8	3.3	7.56	1	0	0	3.04	47
392	65	48	296	0	-5.8	4.8	8.09	1	0	0	3.21	47
393	73	57	295	59	-5.6	5.0	7.79	1	0	0	3.10	47
394	54	56	294	12	-5.1	4.8	8.21	1	0	0	3.22	47
395	54	7	293	21	-5.0	7.3	8.27	1	0	0	3.18	47
396	52	45	291	5	-4.5	6.3	7.43	1	0	0	2.90	47
397	61	9	298	13	-5.3	5.7	8.50	1	0	0	3.36	47
398	61	49	299	41	-5.7	4.4	8.08	1	0	0	3.23	47
399	54	28	284	52	-5.3	3.3	7.49	1	0	0	3.05	47
400	48	17	304	7	-4.6	8.3	7.76	1	0	0	2.96	47

****** CONTINUE ******

NO	LAT. D	M	LONG. D	M	ELEV KM	TH. KM	PN KM/S	RR	RL	SW	RHO G/CC	REF.
401	55	32	296	58	-5.0	5.2	7.84	1	0	0	3.09	47
402	66	31	301	15	-5.6	5.7	8.14	1	0	0	3.21	47
403	72	4	302	38	-5.5	7.4	8.23	1	0	0	3.21	47
404	64	14	292	25	-5.5	6.8	8.29	1	0	0	3.25	47
405	65	21	290	45	-5.8	6.0	8.04	1	0	0	3.16	47
406	63	52	289	51	-5.5	7.7	8.14	1	0	0	3.15	47
407	64	16	288	3	-5.4	7.6	8.32	1	0	0	3.20	47
408	57	8	306	34	-5.4	4.5	8.25	1	0	0	3.25	47
409	57	9	302	30	-4.9	5.9	8.06	1	0	0	3.15	47
410	51	39	293	50	-4.7	6.2	7.70	1	0	0	3.00	47
411	59	58	284	23	-4.6	10.2	8.12	1	0	0	3.05	47
412	48	44	300	23	-4.8	10.8	8.22	1	0	0	3.04	47
413	49	27	341	3	-5.5	5.2	7.68	1	0	0	3.05	47
414	48	36	343	58	-4.8	4.7	7.77	1	0	0	3.08	47
415	43	52	344	39	-4.4	4.5	7.65	1	0	0	3.05	47
416	43	7	350	9	-4.5	8.2	7.77	1	0	0	2.99	47
417	51	15	320	58	-5.1	5.1	8.11	1	0	0	3.20	47
418	50	53	322	53	-4.4	3.2	8.00	1	0	0	3.19	47
419	50	45	324	43	-3.9	3.1	7.90	1	0	0	3.16	47
420	54	43	333	58	-4.0	5.4	7.97	1				47
421	22	11	359	20	-3.4	3.7	8.04	1	0	0	3.19	47
422	93	55	329	26	-4.8	7.1	8.30	1				47
423	96	49	326	38	-4.6	8.8	8.20	1				47
424	125	52	307	4	-0.7	26.4	8.01	1	0	0	2.78	47
425	60	23	284	38	-4.5	6.7	7.85	1	0	0	3.02	47
426	68	16	292	30	-5.2	6.8	8.30	1				47
427	68	45	292	30	-5.2	5.3	8.10	1				47
428	69	08	292	29	-5.2	4.5	8.20	1				47
429	57	0	285	29	-4.4	11.9	8.43	1	0	0	3.08	47
430	69	41	293	36	-5.7	6.8	7.83	1	0	0	3.10	47
431	69	21	293	38	-5.5	6.4	7.99	1	0	0	3.15	47
432	69	30	293	36	-5.7	6.6	7.96	1				47
433	68	39	293	30	-5.4	5.0	8.29	1	0	0	3.26	47
434	69	11	293	24	-5.6	6.2	7.73	1	0	0	3.08	47
435	67	32	293	31	-5.8	6.0	7.95	1	0	0	3.16	47
436	67	8	293	31	-5.8	5.5	7.94	1	0	0	3.16	47
437	67	18	293	31	-5.8	6.4	7.91	1	0	0	3.14	47
438	69	17	294	13	-5.5	4.0	8.30	1				47
439	71	31	294	38	-0.0	11.8	8.20	1				47
440	68	33	292	46	-5.2	5.7	8.10	1				47
441	69	37	292	51	-5.3	9.2	8.10	1				47
442	60	5	285	25	-4.5	6.0	7.34	1	0	0	2.88	47
443	58	39	283	21	-2.7	11.5	7.42	1	0	0	2.77	47
444	58	26	284	19	-2.9	10.0	7.73	1	0	0	2.88	47
445	57	55	284	50	-3.7	8.9	7.54	1	0	0	2.87	47
446	65	57	269	8	-3.6	12.7	8.00	1	0	0	2.92	47
447	66	19	269	22	-3.6	15.4	8.20	1	0	0	2.95	47
448	54	27	291	27	-4.9	6.8	8.08	1	0	0	3.14	47
449	54	59	292	32	-5.2	5.5	8.04	1	0	0	3.17	47
450	62	17	297	8	-5.2	6.5	8.00	1	0	0	3.18	47

****** CONTINUE ******

NO	LAT. D	M	LONG. D	M	ELEV KM	TH. KM	PN KM/S	RR	RL	SW	RHO G/CC	REF.
451	67	26	297	3	-5.8	6.4	8.19	1	0	0	3.22	47
452	56	54	320	8	-2.8	1.5	8.36	1	0	0	3.38	47
453	57	0	321	38	-2.8	3.9	8.27	1	0	0	3.28	47
454	58	7	327	18	-4.3	7.0	8.30	1	0	0	3.26	47
455	58	9	328	52	-4.3	6.8	8.51	1	0	0	3.30	47
456	87	33	340	21	-5.1	4.7	7.99	1	0	0	3.18	47
457	89	50	337	19	-3.9	5.5	8.03	1	0	0	3.21	47
458	89	56	336	9	-3.5	4.8	8.49	1	0	0	3.35	47
459	91	16	333	20	-4.1	5.3	8.30	1	0	0	3.25	47
460	37	7	8	26	0.0	27.4	8.20	1	0	0	2.82	47
461	41	28	8	22	0.6	29.6	8.20	1				47
462	40	03	15	10	0.3	30.8	8.20	1				47
463	42	55	20	53	0.1	23.7	8.10	1				47
464	29	56	24	57	0.0	28.0	8.20	1				47
465	51	33	63	42	0.6	44.5	8.20	1				47
466	49	30	71	00	0.5	46.0	8.25	1				47
467	28	48	151	50	1.0	35.2	8.10	1				47
468	49	55	50	47	0.2	40.0	8.00	1				47
469	50	29	73	0	2.6	56.6	8.10	1	0	0	2.83	47
470	45	39	77	48	1.2	44.2	8.10	1				47
471	47	13	75	05	1.9	40.5	8.10	1				47
472	52	17	141	8	0.0	22.7	7.70	1	0	0	2.93	47
473	53	35	139	36	0.8	25.4	7.70	1				47
474	42	51	144	18	-1.5	27.5	8.00	1				47
475	54	39	135	16	0.5	31.8	7.70	1	0	0	2.79	47
476	54	49	135	50	0.5	26.5	7.70	1				47
477	38	39	246	23	0.9	43.0	8.20	1	0	0	2.77	47
478	42	58	246	38	1.7	40.8	7.90	1				47
479	43	37	253	13	0.9	53.8	8.10	1				47
480	44	33	269	51	0.3	40.0	8.00	1				47
481	60	39	263	40	0.1	33.0	8.20	1	0	0	2.62	47
482	39	30	248	08	0.9	47.5	8.30	1				47
483	53	19	238	14	0.1	23.0	8.00	1	0	0	2.87	47
484	55	7	240	19	0.1	26.1	8.20	1	0	0	2.91	47
485	50	27	242	44	1.8	26.0	7.82	1	0	0	2.92	47
486	54	58	243	20	0.1	27.8	7.80	1	0	0	2.88	47
487	53	50	244	53	1.4	27.0	7.77	1				47
488	52	52	249	45	1.6	41.5	7.80	1				47
489	53	46	244	55	0.7	41.0	7.80	1	0	0	2.69	47
490	40	00	15	00		35.0				1		67
491	35	00	27	00		37.5				1		67
492	44	00	42	00		37.5				1		67
493	34	00	46	00		37.5				1		67
494	42	00	58	00		42.5				1		67
495	54	00	56	00		30.0				1		67
496	60	00	55	00		40.0				1		67
497	43	00	66	00		37.5				1		67
498	55	00	68	00		45.0				1		67
499	48	00	73	00		45.0				1		67
500	41	00	79	00		37.5				1		67

****** CONTINUE ******

NO	LAT. D	M	LONG. D	M	ELEV KM	TH. KM	PN KM/S	RR	RL	SW	RHO G/CC	REF.
501	53	00	94	00		60.0				1		67
502	47	00	102	00		40.0				1		67
503	45	00	105	00		40.0				1		67
504	53	00	113	00		37.5				1		67
505	39	00	90	00		40.0				1		67
506	33	00	80	00		37.5				1		67
507	31	00	95	00		37.5				1		67
508	25	00	95	00		35.0				1		67
509	26	00	103	00		30.0				1		67
510	22	00	106	00		32.5				1		67
511	23	00	115	00		35.0				1		67
512	35	00	128	00		32.5				1		67
513	43	00	124	00		35.0				1		67
514	47	00	123	00		37.5				1		67
515	26	00	137	00		30.0				1		67
516	22	00	145	00		35.0				1		67
517	39	00	134	00		35.0				1		67
518	30	00	145	00		32.5				1		67
519	38	00	160	00		27.5				1		67
520	50	00	58	45		35.0		1				13
521	43	00	51	45		40.0		1				3
522	45	40	57	40		45.0		1				3
523	43	00	57	40		45.0		1				3
524	50	10	73	00		45.0		1				3
525	36	00	76	50		50.0		1				3
526	46	30	77	00		52.5		1				3
527	44	00	74	30		50.0		1				3
528	47	00	67	00		45.0		1				3
529	52	00	82	00		65.0				1		33
530	56	00	72	00		67.5				1		33
531	57	00	82	00		67.5				1		33
532	36	30	51	30		38.5						57
533	30	00	110	00		35.0				1		66
534	41	50	9	15		28.3			1			49
535	41	42	9	40		29.4			1			49
536	42	01	10	10		31.1			1			49
537	41	57	10	30		30.5			1			49
538	41	55	10	40		30.3			1			49
539	41	50	10	45		29.3			1			49
540	41	30	13	00		30.7			1			49
541	41	40	12	15		29.1			1			49
542	42	00	11	45		30.7			1			49
543	42	10	12	00		30.7			1			49
544	42	00	12	45		32.9			1			49
555	42	20	11	15		32.1			1			49
546	42	20	10	45		31.2			1			49
547	42	30	10	15		35.2			1			49
548	41	55	11	15		28.3			1			49

Table (2-2)

SPHERICAL HARMONIC COEFFICIENTS OF STTR, CRTH AND RHO

		STTR (SEC.)		CRTH (KM.)		RHO (G/CC)	
N	M	ANM	BNM	ANM	BNM	ANM	BNM
0	0	0.459	0.0	18.963	0.0	3.005	0.0
1	0	0.159	0.0	3.040	0.0	-0.039	0.0
1	1	-0.014	0.086	1.777	4.339	-0.015	-0.046
2	0	-0.149	0.0	4.060	0.0	-0.059	0.0
2	1	0.002	-0.159	0.650	1.647	-0.021	-0.018
2	2	-0.062	0.100	-0.508	-0.872	-0.004	0.022
3	0	-0.040	0.0	-0.726	0.0	0.011	0.0
3	1	-0.089	0.080	-1.093	-0.257	0.017	0.000
3	2	0.113	-0.053	-5.190	1.078	0.045	-0.021
3	3	-0.015	-0.013	0.627	2.781	-0.002	-0.050
4	0			1.455	0.0	-0.027	0.0
4	1			1.554	-2.205	-0.013	0.022
4	2			-2.908	0.575	0.034	-0.004
4	3			0.498	-1.857	-0.018	0.003
4	4			-0.053	2.392	0.014	-0.030
5	0			-3.209	0.0	0.037	0.0
5	1			-0.467	-0.612	0.003	0.001
5	2			0.256	0.775	0.006	-0.003
5	3			-0.452	1.050	0.004	-0.015
5	4			1.676	-1.675	-0.013	0.015
5	5			0.971	2.772	-0.020	-0.028
6	0			0.210	0.0	0.003	0.0
6	1			-1.104	-0.933	0.012	0.011
6	2			-0.460	-1.680	0.004	0.020
6	3			0.786	2.838	-0.008	-0.025
6	4			1.125	-0.322	-0.012	0.001
6	5			-0.630	-1.734	0.009	0.030
6	6			-0.329	2.346	-0.005	-0.035

Table (2-3)

GRAVITATIONAL POTENTIAL OF THE CRUST AND OBSERVED GEOPOTENTIAL(ERG $*10^{7}$)

		G1		G2		G3		GEOP	
N	M	ANM	BNM	ANM	BNM	ANM	BNM	ANM	BNM
1	1	2.441	1.735	-2.751	-6.718	-0.310	-4.983		
2	0	0.617	0.0	-3.757	0.0	-3.140	0.0		
2	1	0.701	0.709	-0.602	-1.524	-0.099	-0.815		
2	2	-1.070	-0.184	0.470	0.807	-0.600	0.623	0.150	-0.084
3	0	-0.152	0.0	0.478	0.0	0.326	0.0	0.057	0.0
3	1	-0.124	0.239	0.720	0.169	0.596	0.408	0.112	0.015
3	2	-0.774	0.737	3.417	-0.710	2.643	0.027	0.051	-0.046
3	3	-0.177	1.044	-0.413	-1.831	-0.590	-0.787	0.036	0.090
4	0	0.200	0.0	-0.742	0.0	-0.542	0.0	0.015	0.0
4	1	-0.202	-0.210	-0.793	1.125	-0.995	0.915	-0.035	-0.026
4	2	-0.535	0.134	1.483	-0.293	0.948	-0.159	0.022	0.034
4	3	0.477	-0.147	-0.254	0.947	0.223	0.800	0.058	-0.012
4	4	-0.114	0.714	0.032	-1.220	-0.082	-0.506	-0.002	0.019
5	0	-0.222	0.0	1.334	0.0	1.112	0.0	0.003	0.0
5	1	-0.046	-0.052	0.194	0.254	0.148	0.202	-0.003	0.0
5	2	-0.090	-0.115	-0.106	-0.322	-0.196	-0.437	0.029	-0.018
5	3	0.183	-0.050	0.188	-0.436	0.371	-0.486	-0.021	-0.001
5	4	0.573	-0.044	-0.697	0.697	-0.124	0.653	0.001	-0.008
5	5	-0.086	0.337	-0.404	-1.152	-0.490	-0.815	0.005	-0.030
6	0	0.058	0.0	-0.074	0.0	-0.016	0.0	-0.009	0.0
6	1	-0.021	-0.121	0.387	0.327	0.366	0.206	-0.006	0.011
6	2	-0.012	-0.085	0.161	0.554	0.149	0.469	0.000	-0.019
6	3	0.052	0.136	-0.275	-0.994	-0.223	-0.858	0.006	0.004
6	4	0.267	-0.167	-0.394	0.113	-0.127	-0.054	-0.010	-0.028
6	5	-0.112	-0.165	0.221	0.608	0.109	0.443	-0.008	-0.038
6	6	0.030	0.033	0.115	-0.822	0.145	-0.789	-0.002	-0.018

Table (2-4)

CORRELATION OF GEOPHYSICAL DATA

	N=2	N=3	N=4	N=5	N=6
		DEGREE POWER			
STTR(SEC.)	0.0613	0.0324			
CRTH(KM.)	20.6371	38.0130	27.6031	27.1080	23.8965
EQRT(KM.)	0.3071	0.5568	0.4685	0.3275	0.1565
G1(ERG $*10^{14}$)	2.5535	2.3591	1.2010	0.5626	0.1880
G2(ERG $*10^{14}$)	17.6721	16.4786	7.1809	4.6840	2.9341
GEOP(ERG $*10^{14}$)	0.0296	0.0301	0.0077	0.0026	0.0034
		DEGREE CROSS POWER			
STTR GEOP	-0.2828	-0.0717			
STTR CRTH	-0.9212	-0.5842			
STTR EQRT	-0.0539	-0.0513			
CRTH GEOP	-0.0507	-3.3595	1.2821	-1.1379	1.1143
CRTH EQRT	1.6762	3.8922	2.6850	1.8318	1.3707
GEOP EQRT	-0.8046	0.0607	0.5215	-0.1796	0.1378
GEOP G3	-0.1423	0.1339	0.0113	0.0149	-0.0151
G1 G2	-4.4720	-5.1280	-2.1922	-0.9990	-0.5233
		DEGREE CORRELATION			
STTR GEOP	-0.87	-0.14			
STTR CRTH	-0.82	-0.53			
STTR EQRT	-0.39	-0.38			
CRTH GEOP	-0.02	-0.20	0.17	-0.27	0.25
CRTH EQRT	0.66	0.85	0.75	0.61	0.71
GEOP EQRT	-0.78	0.03	0.54	-0.38	0.38
GEOP G3	-0.96	0.26	0.06	0.16	-0.18
G1 G2	-0.66	-0.82	-0.75	-0.62	-0.70

Table (2-5)

Correlation matrix

	Geopotential	Eq. Rock Top.	Crustal thickness	Travel time residuals
Geopotential	1	-.05	-.05	-.42
Eq. Rock Top.		1	+.75	-.11
Crustal Thickness			1	-.20
Travel time residuals				1

Table (2-6)

COMMON LOCATIONS OF CRUSTAL DATA AND P WAVE TRAVEL TIME RESIDUALS

LONG. DEG.	LAT. DEG.	CRTH KM	VCAV KM/S	PNVL KM/S	STTR S	STTR* S	CSTTR S	MSTTR S	
0- 5	45 50	20.00	5.90	7.65	0.768	0.828	-0.177	1.005	
5- 10	35- 40	27.40	5.46	8.20	0.958	1.018	0.212	0.806	
5- 10	40- 45	40.38	6.22	8.14	0.239	0.299	0.074	0.225	
5- 10	45- 50	9.19	4.38	8.10	-0.134	-0.074	-0.041	-0.033	
20- 25	20- 25	33.90	6.34	8.05	0.135	0.195	-0.208	0.403	
75- 80	60- 65	37.90	6.20	8.10	0.292	0.352	0.041	0.311	
90- 95	155-160	35.00	6.01	7.79	0.366	0.426	0.249	0.177	
110-115	45- 50	33.82	6.34	7.80	0.380	0.440	-0.159	0.599	
135-140	50- 55	31.80	6.00	7.60	0.422	0.482	0.194	0.288	
140-145	50- 55	22.70	6.20	7.58	0.442	0.502	-0.237	0.739	
200-205	65- 70	8.28	5.42	8.26	1.180	1.240	-0.740	1.980	
235-240	40- 45	15.80	5.73	8.00	0.640	0.700	-0.499	1.199	
235-240	45- 50	15.80	5.73	8.00	0.653	0.713	-0.499	1.212	
235-240	50- 55	22.00	5.75	7.95	0.616	0.676	-0.172	0.848	
240-245	35- 40	32.00	6.04	7.80	0.187	0.247	-0.089	0.336	
280-285	50- 55	3.34	5.09	7.49	0.394	0.454	-0.229	0.683	
290-295	70- 75	10.10	5.06	8.01	0.254	0.314	-0.158	0.472	
295-300	45- 50	33.90	6.01	8.11	0.719	0.779	0.076	0.703	
295-300	70- 75	10.21	4.92	8.25	0.200	0.260	-0.156	0.416	
295-300	75- 80	9.97	3.83	8.18	0.415	0.475	0.527	-0.052	
240-245	50- 55	33.74	6.15	7.82	-0.060	0.0	0.0	0.0	*
240-245	55- 60	26.12	5.80	8.20	0.226	0.286	-0.152	0.438	
245-250	40- 45	48.00	6.04	7.94	-0.046	0.014	0.649	-0.635	
245-250	50- 55	31.65	6.25	7.80	0.573	0.633	-0.097	0.730	
250-255	50- 55	56.00	6.34	7.90	-0.143	-0.083	0.363	-0.446	

FIGURE CAPTIONS FOR CHAPTER 2

Figure

(2-1) Distribution of data on crustal thickness

(2-2) Distribution of data on P wave travel time residuals

(2-3) Lateral variations of crustal thickness (in km.)

(2-4) Lateral variations of P wave travel time residuals (in sec.)

(2-5) Average density of the surface layer versus crustal thickness

(2-6) Lateral variations of the average density of the surface layer (g/cc). The zero degree harmonic of the density is excluded.

(2-7) Observed travel time residuals versus crustal residuals

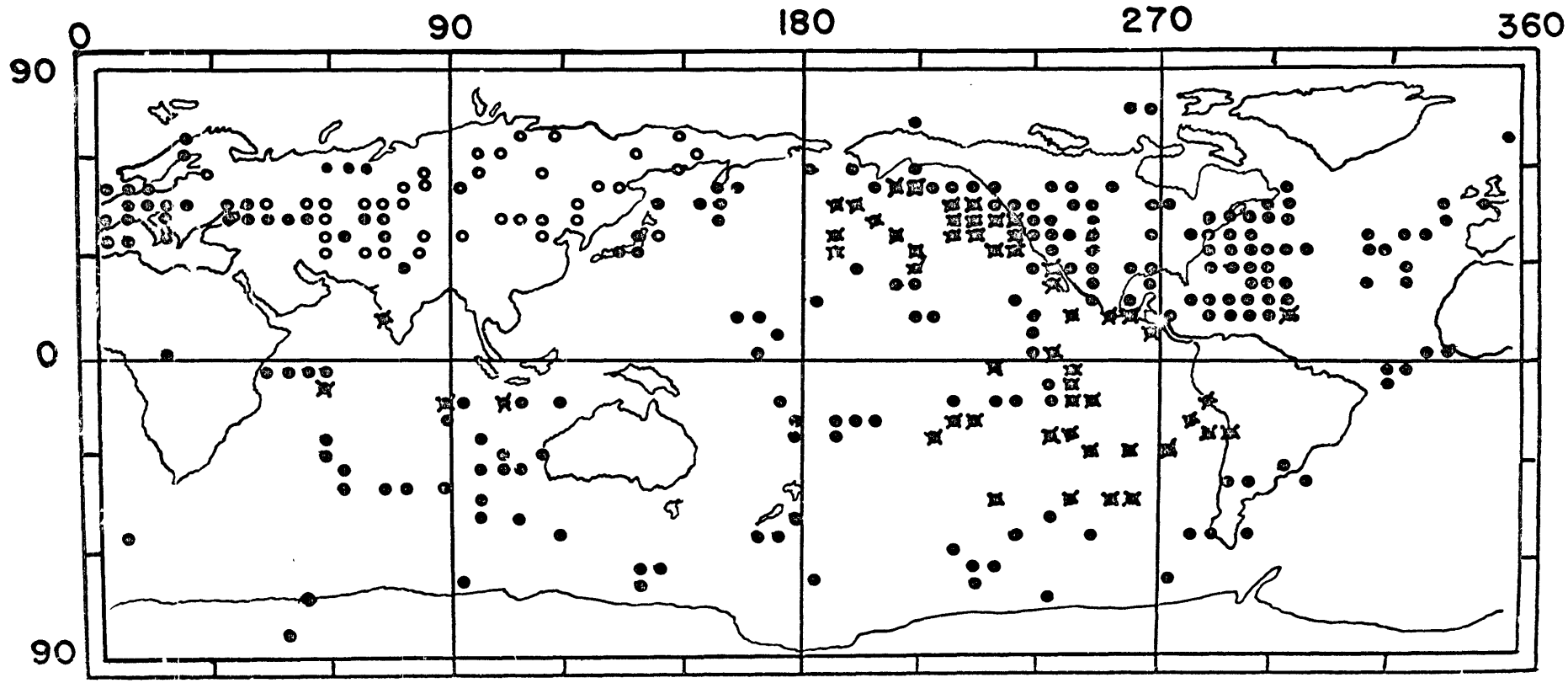

Fig. (2-1)

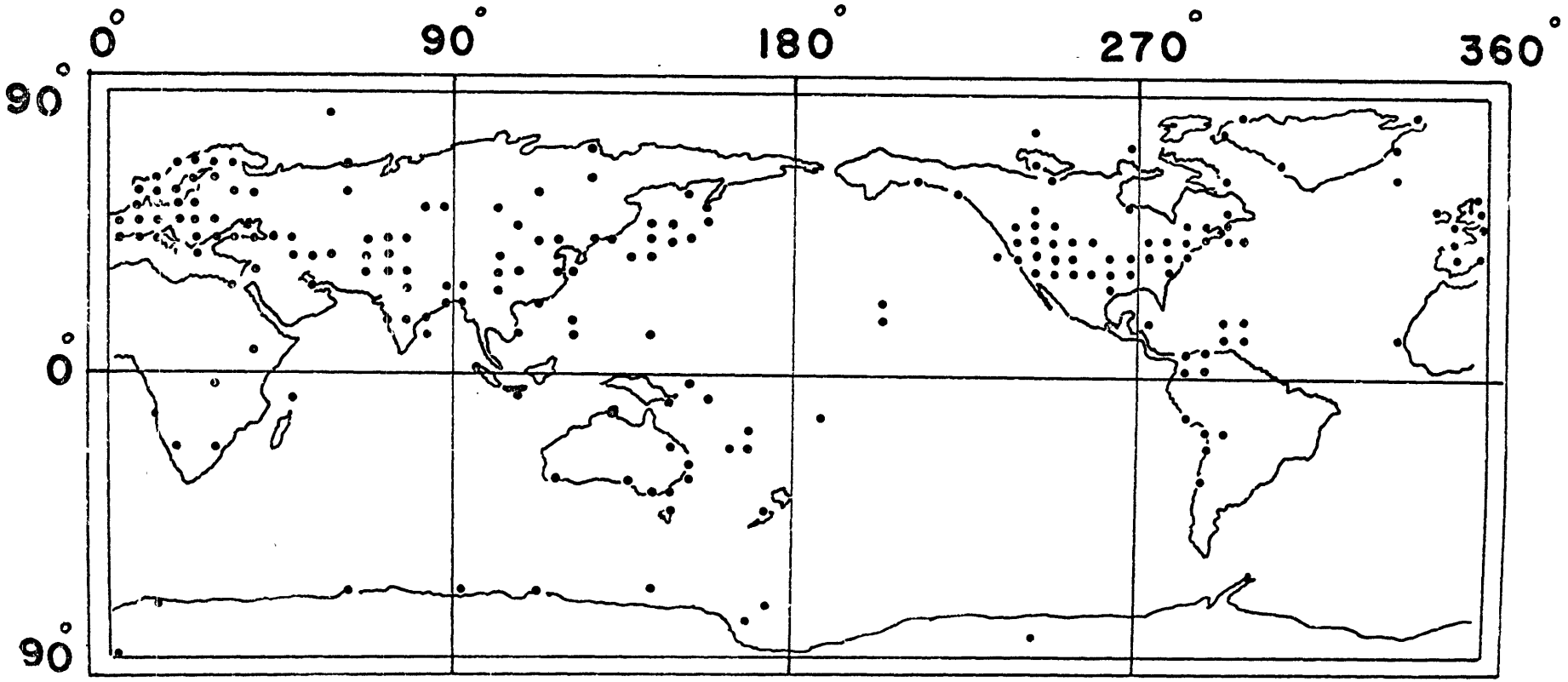

Fig.(2-2)

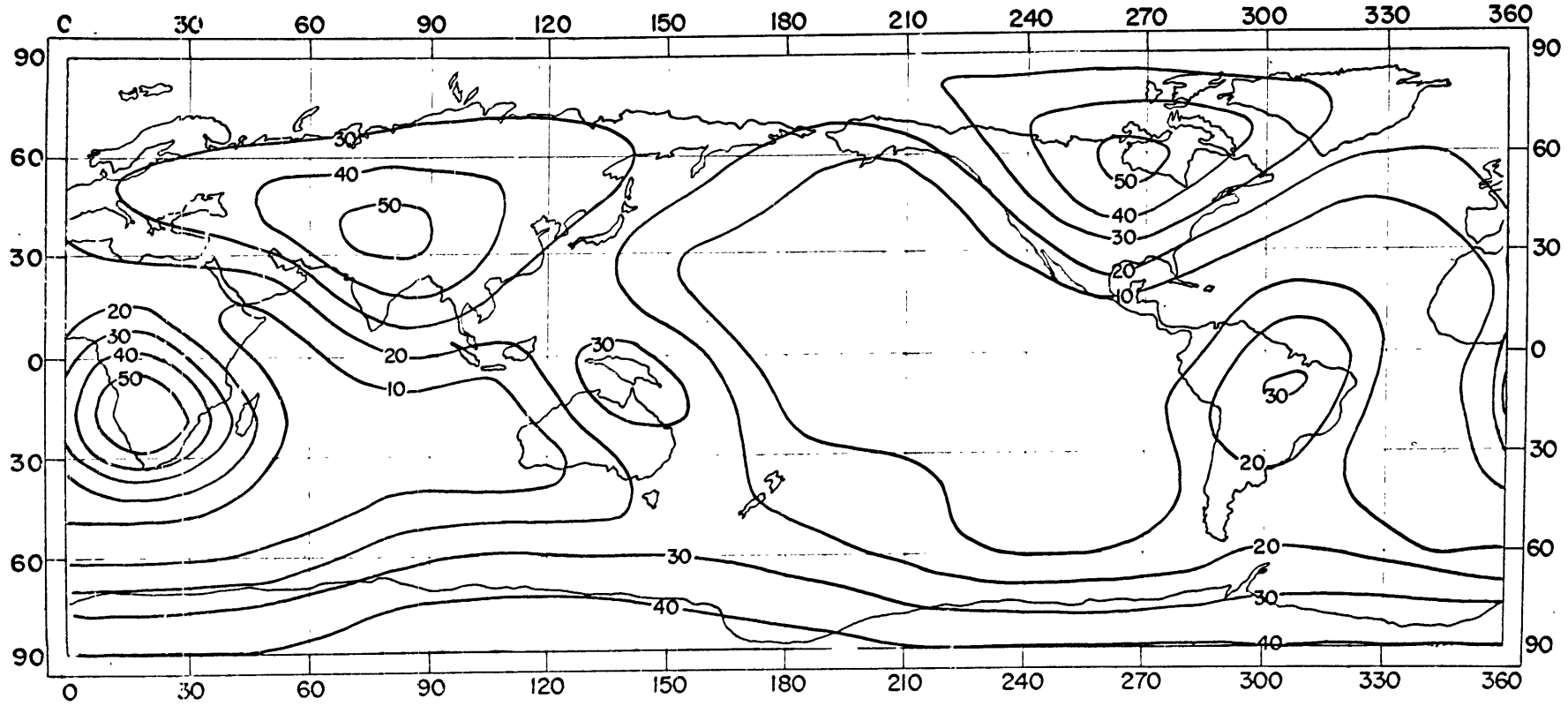
0
30
60
90
120
150
180
210
240
270
300
330
360
90
60
30
0
30
60
90
10
20
30
40
50

Fig.(2-3)

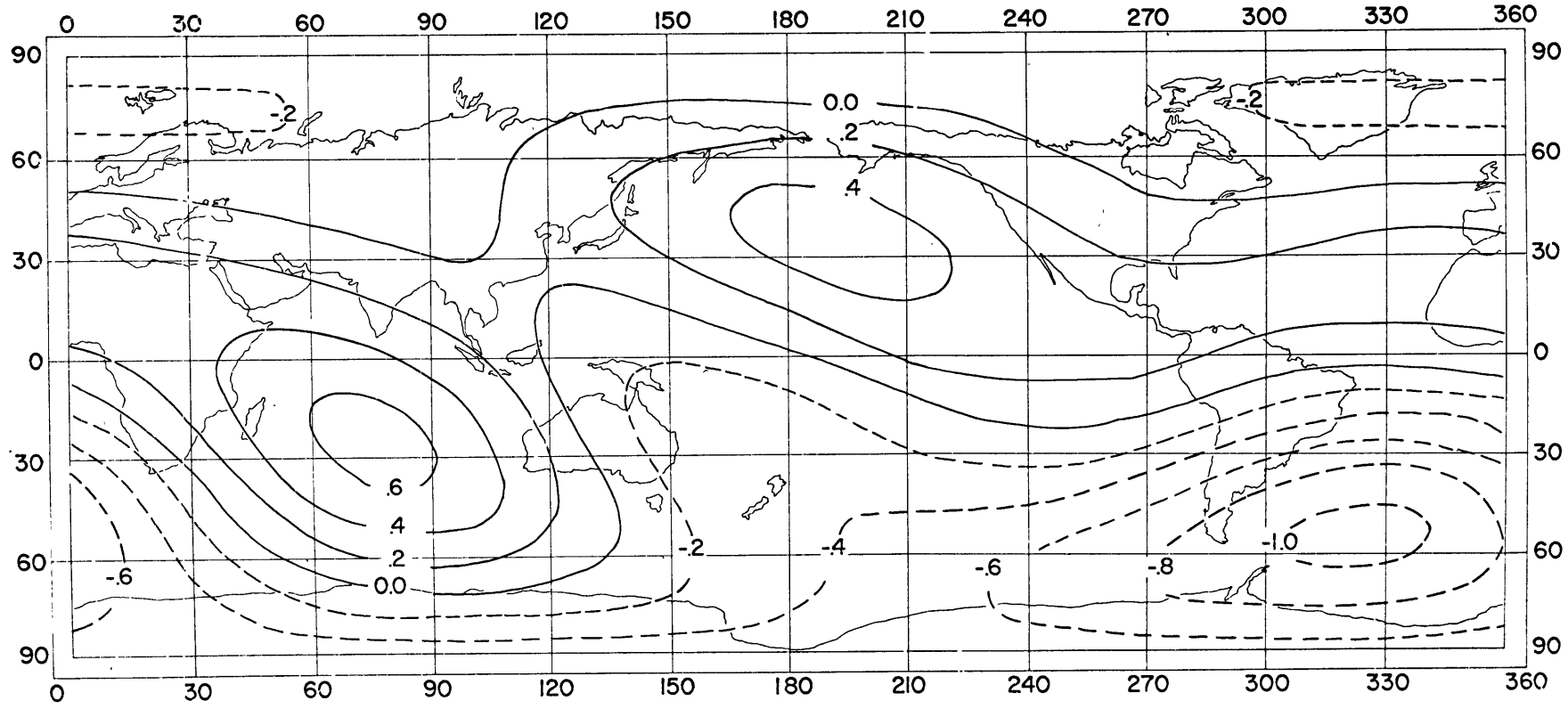
0
30
60
90
120
150
180
210
240
270
300
330
360
90
60
30
0
30
60
90
-.2
0.0
.2
.4
.6
.4
.2
0.0
-.6
-.2
-.4
-.6
-.8
-1.0

Fig. (2-4)

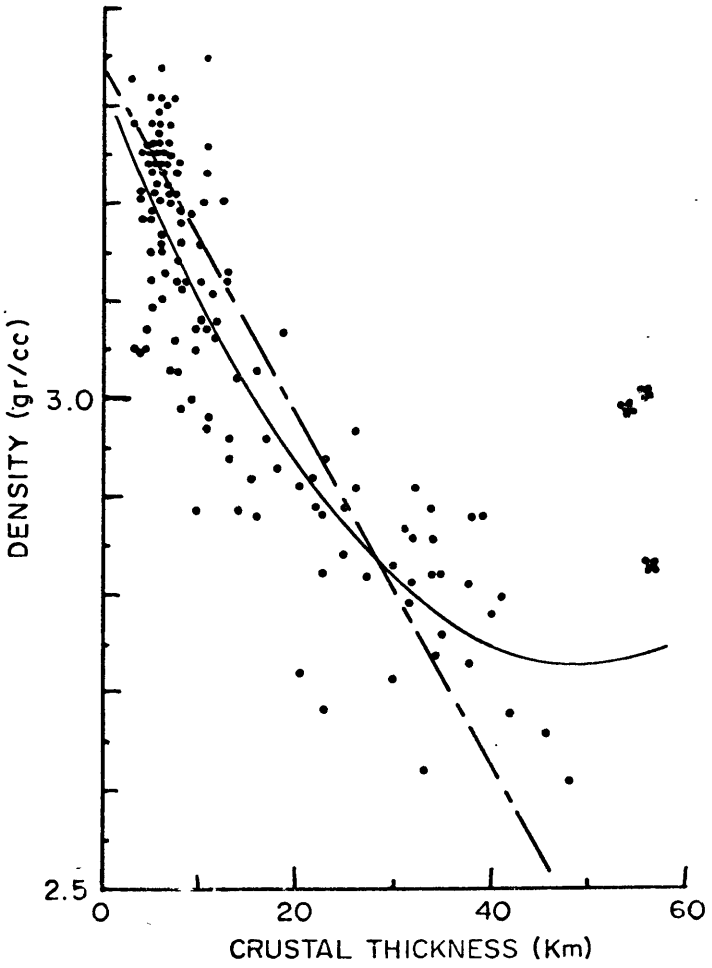

Fig. (2-5)

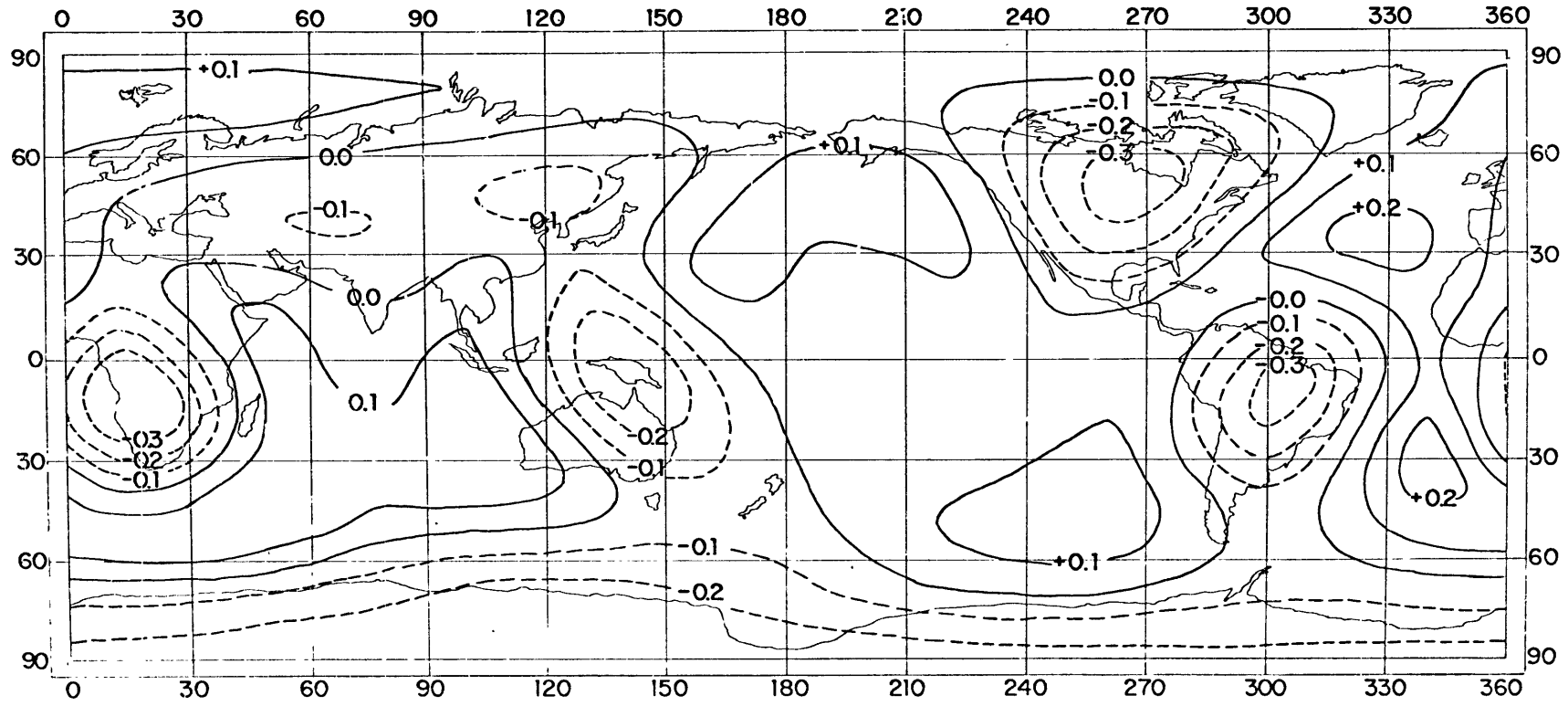
0 30 60 90 120 150 180 210 240 270 300 330 360
90 60 30 0 30 60 90
+0.1
0.0
-0.1
0.1
0.0
-0.1
0.1
0.3
0.2
0.1
0.2
0.1
0.0
-0.1
-0.2
-0.3
+0.1
+0.2
0.0
0.1
0.2
0.3
-0.2
-0.1
+0.2
-0.1
-0.2
+0.1

Fig.(2-6)

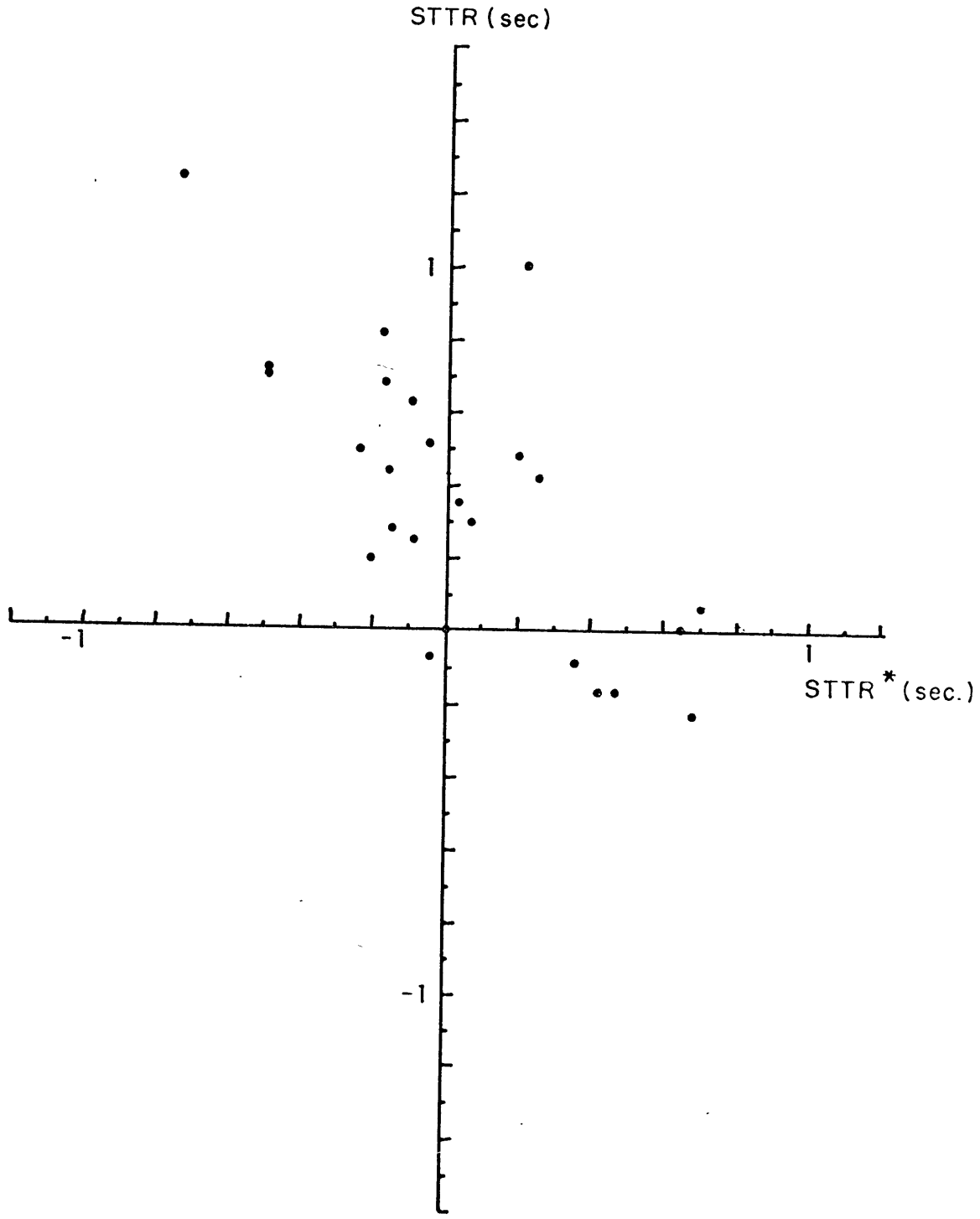

Fig. (2-7)

CHAPTER 3

Stress Analysis Inside the Earth

In Chapter 2 it was shown that the representation of the undulations of the earth's gravitational field, deduced from the artificial satellite data by different authors, using different techniques, agree very well (through 6th degree spherical harmonics). This indicates that the measurements and, hence, the representations are reliable and suggests the existence of density anomalies inside the earth. It was also shown in the previous chapter that the gravitational field due to the topography of the earth's surface and the lateral variation of the crustal density are an order of magnitude greater than the measured undulations of the field. This calls attention to the compensating density anomalies existing in the mantle. What we measure at the earth's surface is, in fact, the small imperfections of the compensation taking place within the earth.

In the present chapter we compute a special model of density variations in the mantle which not only takes into account surface topography, crustal thickness, P wave travel time residuals, and observed gravitational field but also minimizes the total shear-strain energy in the earth resulting from the density variations.

The chapter is divided into three sections. In the first part we start from the basic equations of elasticity and derive the final

formulas for calculating the density anomalies. The second part is devoted to computational and numerical analysis, and the third part presents the final density anomalies together with the corresponding displacements and stress differences in the mantle.

(3-1) - Theory

In deriving the equilibrium equations of the deformed earth subject to laterally inhomogeneous density distributions in the crust and mantle the following assumptions are made:

1 - The earth is considered to be a cold spherical body with a linearly elastic and isotropic mantle, a liquid core, and with no rotational motion.

2 - The elastic moduli of the earth are considered to vary only radially.

3 - The density anomalies are confined to the crust and the mantle.

These assumptions do not represent the conditions existing inside the real earth. The earth is hot with lateral and radial variations in temperature. It is close to a visco-elastic body for the static loading at low harmonics. The probable convection currents in the core and mantle contributes to the gravitational potential measured on the surface of the earth. In spite of these short comings, the mathematical simplification introduced by the assumptions makes the calculations feasible. Furthermore, it is shown in Chapter 5 that the

equilibrium equations of a thermo-visco-elastic mantle are analogous to those of an elastic model. Thus, studying an elastic model will yield useful information about the behavior of the actual density variations inside the real earth.

(3-1-1) - Basic Equations

The fundamental equations that formulate the problem are:

1 - Conservation of momentum

$$\nabla \cdot \bar{\bar{T}} + \bar{F} = \rho \frac{\partial^2}{\partial t^2} \bar{u} \tag{3-1}$$

where $\bar{\bar{T}}$ = stress tensor, $\bar{F}$ = body force acting on a unit volume, ∇ = gradient operator, ρ = density, and $\bar{u}$ = displacement vector.

2 - Density at a given point (Kaula, 1963)

$$\rho = \rho_o - \rho_o \Delta - u_r \frac{\partial}{\partial r} \rho_o + \delta\rho \tag{3-2}$$

where ρ_o = density inside the undisturbed, spherically symmetric earth, Δ = dilation, $\delta\rho$ = perturbation of the density, r = radial distance from the earth's center, and u_r = radial component of the displacement vector.

3 - General Infinitesimal Deformation Equation (Sokolikoff, 1956)

$$\bar{\bar{E}} = \frac{1}{2} \left[\nabla \bar{u} + (\nabla \bar{u})^T \right] \tag{3-3}$$

where $\bar{\bar{E}}$ = strain tensor, $\nabla \bar{u}$ = outer product of ∇ and $\bar{u}$, and $(\nabla \bar{u})^T$ = transpose of $\nabla \bar{u}$.

4 - Poisson's Equation:

$$\nabla^2 \Phi = -4\pi G \rho \tag{3-4}$$

where Φ = gravitational potential, G = gravitational constant, and ∇^2 = Laplacian operator.

5 - Stress-strain relationship in a linearly elastic and isotropic medium:

$$\bar{\bar{T}} = \lambda (\nabla \cdot \bar{u}) \bar{\bar{I}} + 2\mu \bar{\bar{E}} \tag{3-5}$$

where λ = lame constant, μ = rigidity, and $\bar{\bar{I}}$ = identity matrix.

Lord Rayleigh (1906) called attention to the application of equation (3-5) to a pre-stressed medium, such as the earth. He pointed out that equation (3-5), the ordinary stress-strain relationship, relates the strain to the excess stress measured from the pre-stressed condition. The pre-stressed condition inside the earth can well be approximated by a hydrostatic pressure, p_o, with negligible lateral variations. There is a change from the pre-stressed condition due to vertical displacements which can be approximated by: $u_r \frac{\partial}{\partial r} p_o$. Therefore, in equation (3-5), we should add the following terms to the diagonal elements of $\bar{\bar{T}}$ in order to include the effect of pre-stressed condition existing in the interior of the earth (Pekeris and Jarosh, 1958):

$$-P_o + U_r \frac{\partial}{\partial r} P_o$$

So equation (3-5) becomes:

$$\bar{\bar{T}} = \left[\lambda (\nabla \cdot \bar{u}) - P_o + U_r \frac{\partial}{\partial r} P_o \right] \bar{\bar{I}} + 2\mu \bar{\bar{E}} \qquad (3\text{-}5a)$$

(3-1-2) - Equations in the Mantle and the Core

The mantle (including the crust) is assumed to be an isotropic, cold, linearly elastic body with density anomalies $\delta\rho$ which vary laterally as well as radially. Adapting a spherical system of coordinates (r, θ, φ) with the origin at the center of the earth, and following Pekeris and Jarosh (1958), Alterman, et al. (1959), and Kaula (1963), equations (3-1) through (3-5) become

$$g_o \rho_o \Delta + \rho_o \frac{\partial}{\partial r} \Psi - g_o \delta\rho - \rho_o \frac{\partial}{\partial r}(g u_r) + \frac{\partial}{\partial r}(\lambda \Delta + 2\mu \frac{\partial}{\partial r} u_r) + \frac{2\mu}{r} e_{r\theta}$$
$$+ \frac{2\mu}{r \sin\theta} \cdot \frac{\partial}{\partial r} e_{r\varphi} + \frac{\mu}{r}(4 e_{rr} - 2 e_{\theta\theta} - 2 e_{\varphi\varphi} + 2 e_{r\theta} \operatorname{cotan} \theta) = 0, \qquad (3\text{-}6)$$

$$\frac{\rho_o}{r} \cdot \frac{\partial}{\partial \theta} \Psi + \frac{\partial}{\partial r}(\mu e_{r\theta}) + \frac{1}{r} \frac{\partial}{\partial \theta}(2\mu e_{\theta\theta} + \lambda \Delta - g_o \rho_o u_r)$$
$$+ \frac{2\mu}{r \sin\theta} \cdot \frac{\partial}{\partial \varphi} e_{\theta\varphi} + \frac{\mu}{r}[2 \operatorname{cotan} \theta (e_{\theta\theta} - e_{\varphi\varphi}) + 6 e_{r\theta}] = 0, \qquad (3\text{-}7)$$

$$\frac{\rho_o}{r \sin\theta} \cdot \frac{\partial}{\partial \varphi} \Psi + \frac{\partial}{\partial r}(\mu e_{r\theta}) + \frac{\mu}{r} \frac{\partial}{\partial \theta} e_{\theta\varphi} + \frac{1}{r \sin\theta} \cdot \frac{\partial}{\partial \varphi}(2\mu e_{\varphi\varphi} + \lambda \Delta - g \rho_o u_r)$$
$$+ \frac{6\mu}{r} e_{r\varphi} + \frac{4\mu}{r} \operatorname{cotan} \theta \, e_{\theta\varphi} = 0, \qquad (3\text{-}8)$$

and

$$\nabla^2 \gamma - 4\pi G(\rho_o \Delta + u_r \frac{\partial}{\partial r}\rho_o - \delta\rho) = 0 \quad , \tag{3-9}$$

where γ is the perturbation of the gravitational potential due to the density perturbations $(-\rho_o\Delta - u_r \frac{\partial}{\partial r}\rho_o + \delta\rho)$, e_{ij} is the $(i, j)^{th}$ element of the strain tensor. A zero subscript indicates the unperturbed state. The right hand side of equations (3-6) through (3-8) are set to zero since we are dealing with the static condition, i.e., $\frac{\partial^2}{\partial t^2}\bar{u} = 0$. In deriving these equations we have neglected the second order terms,

such as $$u_r \frac{\partial}{\partial r}\rho_o \cdot \frac{\partial}{\partial r}\gamma, \quad \delta\rho \frac{\partial}{\partial r}\gamma, \quad \rho_o \Delta \frac{\partial}{\partial r}\gamma \ .$$

These terms are smaller than the terms kept by about two orders of magnitude.

We represent the motions as:

$$u = \sum_{nm} U_{nm}(r) S_{nm}(\theta,\varphi) \ , \quad v = \sum_{nm} V(r)_{nm} \frac{\partial}{\partial\theta} S_{nm}(\theta,\varphi) \ , \quad w = \sum_{nm} \frac{V(r)_{nm}}{\sin\theta} \frac{\partial}{\partial\varphi} S_{nm}(\theta,\varphi) \tag{3-10}$$

where u, v and w denote the components of the displacement vector in r, θ, and φ directions respectively, and U(r) and V(r) are only radially dependent. This representation was first adopted by Hoskins (1910) and also used by Hoskins (1920), Pekeris and Jarosh (1958), Alterman, et al. (1959), Slichter and Caputo (1960), Longman (1962), and Kaula (1963). The dilatation has the following form:

$$\Delta = \sum_{nm} X_{nm}(r) \cdot S_{nm}(\theta, \varphi) \tag{3-11}$$

where

$$X_{nm}(r) = \frac{d}{dr} U_{nm}(r) - \frac{n(n+1) V_{nm}(r)}{r} + 2 \frac{U_{nm}(r)}{r} \tag{3-12}$$

Let

$$\delta\rho = \sum_{nm} \Delta\rho_{nm}(r) \cdot S_{nm}(\theta, \varphi) \tag{3-13}$$

then, using equations (3-9), (3-11), (3-12), (3-13) we obtain

$$\Psi = \sum_{nm} \Psi_{nm}(r) \cdot S_{nm}(\theta, \varphi) \tag{3-14}$$

where $\Delta\rho_{nm}(r)$ and $\Psi_{nm}(r)$ are only radially dependent. Substitution of equations (3-10) through (3-14) into equations (3-6) through (3-9) leads to the following equations:

$$\rho_o \frac{d}{dr}\Psi + g\rho_o X - g_o \Delta\rho - \rho_o \frac{d}{dr}(gU) + \frac{d}{dr}\left(\lambda X + 2\mu \frac{d}{dr} U\right) + \frac{\mu}{r^2}\left[4r \frac{d}{dr} U - 4U + n(n+1)\left(3V - U - r \frac{d}{dr} V\right)\right] = 0 \tag{3-6a}$$

$$\rho\Psi - g\rho_o U + \lambda X + r \frac{d}{dr}\left[\mu\left(\frac{d}{dr} V - \frac{V}{r} + \frac{U}{r}\right)\right] + \frac{\mu}{r}\left[5U + 3r \frac{dV}{dr} - V - 2n(n+1)V\right] = 0 \tag{3-7a}$$

$$\left[\frac{d^2}{dr^2} + \frac{2}{r}\frac{d}{dr} - \frac{n(n+1)}{r^2}\right]\psi - 4\pi G\left(\rho_o X + U\frac{d}{dr}\rho_o - \Delta\rho\right) = 0 \qquad (3\text{-}9a)$$

The subscripts n and m are omitted above in order to avoid complexity of the equations. Also we have considered a deformation specified by spherical harmonics of degree n and have utilized the following property of the harmonics

$$\left[\frac{\partial^2}{\partial\theta^2} + \operatorname{Cotan}\theta\,\frac{\partial}{\partial\theta} + \frac{1}{\sin^2\theta}\,\frac{\partial^2}{\partial\varphi^2} + n(n+1)\right] S_{nm}(\theta,\varphi) = 0 \qquad (3\text{-}15)$$

These equations differ from those of Alterman et al. (equations 23-25, 1959) by an additional term in equation (3-6a) and (3-9a) due to the density anomalies ($\Delta\rho$) included in the present studies, and omission of the frequency term in equations (3-6a) and (3-7a) because of the static case considered. Equations (3-6a), (3-7a), and (3-9a) represent three simultaneous differential equations of second order. To somilify this set of equations we follow Alterman, et al. (1959) and introduce the following dependent variables.

$$\bar{Y} = \begin{bmatrix} Y_1 \\ Y_2 \\ Y_3 \\ Y_4 \\ Y_5 \\ Y_6 \end{bmatrix} = \begin{bmatrix} U \\ \lambda X + 2\mu\frac{d}{dr}U \\ V \\ \mu\left(\frac{d}{dr}V - \frac{V}{r} + \frac{U}{r}\right) \\ \psi \\ \frac{d}{dr}\psi - 4\pi G\rho_o U \end{bmatrix} \qquad (3\text{-}16)$$

Using these variables, equations (3-6a), (3-7a) and (3-9a) are reduced to the following simultaneous ordinary first order differential equations:

$$\frac{d}{dr}\bar{Y} = \bar{\bar{M}} \cdot \bar{Y} + \bar{D} \tag{3-17}$$

where

$$\bar{\bar{M}} = \begin{pmatrix} M_{11} & M_{12} & M_{13} & 0 & 0 & 0 \\ M_{21} & M_{22} & M_{23} & M_{24} & 0 & M_{25} \\ M_{31} & 0 & M_{33} & M_{34} & 0 & 0 \\ M_{41} & M_{42} & M_{43} & M_{44} & M_{45} & 0 \\ M_{51} & 0 & 0 & 0 & 0 & M_{56} \\ 0 & 0 & M_{63} & 0 & M_{65} & M_{66} \end{pmatrix}, \tag{3-18}$$

with

$$M_{11} = -2\lambda/[r(\lambda+2\mu)],$$

$$M_{12} = 1/(\lambda+2\mu),$$

$$M_{13} = n(n+1)\lambda/[r(\lambda+2\mu)],$$

$$M_{21} = -4\rho_0 g_0/r + 4\mu(3\lambda+2\mu)/[r^2(\lambda+2\mu)],$$

$$M_{22} = -4\mu/[r(\lambda+2\mu)],$$

$$M_{23} = n(n+1)[\rho_0 g_0/r - 2\mu(3\lambda+2\mu)/[r^2(\lambda+2\mu)],$$

$$M_{24} = n(n+1)/r,$$

$$M_{26} = -\rho_0,$$

$$M_{31} = -1/r,$$

$$M_{33} = 1/r,$$

$$M_{34} = 1/\mu,$$

$$M_{41} = \rho_0 g_0/r - 2\mu(3\lambda+2\mu)/[r^2(\lambda+2\mu)],$$

$$M_{42} = -\lambda/[r(\lambda+2\mu)],$$

$$M_{43} = 2\mu[\lambda(2n^2+2n-1) + 2\mu(n^2+n-1)]/[r^2(\lambda+2\mu)],$$

$M_{44} = -3/r$,

$M_{45} = -\rho_o/r$,

$M_{51} = 4\pi G\rho_o$,

$M_{56} = 1$,

$M_{63} = -4\pi G\rho_o n(n+1)/r$,

$M_{65} = n(n+1)/r^2$, and

$M_{66} = -2/r$,

and

$$\bar{D} = (0 , g_o \Delta\rho , 0 , 0 , 0 , -4\pi G\Delta\rho) \qquad (3\text{-}19)$$

Notice that matrix $\bar{\bar{M}}$ depends on the properties of the unperturbed medium ($\rho_o, g_o, \lambda, \mu$) and the degree of the harmonics. The source vector $\bar{D}$ includes the perturbation of the density and the gravitational acceleration of the unperturbed condition, g_o .

In the case of the liquid core, $\mu = 0$, $\Delta\rho = 0$, Longman (1963) showed that equations (3-6) through (3-9) can be reduced to the two following equations.

$$\rho_o Y_5 - \rho_o g_o Y_1 + Y_2 = 0 \quad , \qquad (3\text{-}20)$$

and

$$\left[\frac{d^2}{dr^2} + \frac{2}{r}\frac{d}{dr} + \frac{4\pi G\rho_o^2}{\lambda} - \frac{n(n+1)}{r^2}\right] Y_5 = 0 \quad . \qquad (3\text{-}21)$$

Introducing a new dependent variable

$$Y_7 = \frac{d}{dr} Y_5 \quad , \qquad (3\text{-}22)$$

equation (3-21) is reduced to the two ordinary first order differential equations

$$\frac{d}{dr}\begin{bmatrix} Y_5 \\ Y_7 \end{bmatrix} = \begin{bmatrix} 0 & \frac{1}{r} \\ \frac{n(n+1)}{r^2} - \frac{4\pi G \rho_0^2}{\lambda} & \frac{-2}{r} \end{bmatrix} \begin{bmatrix} Y_5 \\ Y_7 \end{bmatrix} . \qquad (3\text{-}23)$$

(3-1-3) - Boundary Conditions

We solve equation (3-17) inside the mantle, and equations (3-20) and (3-23) inside the core, subject to the following boundary conditions:

I. At the earth's surface

i) stress-free boundary condition: all the stresses must vanish on the deformed surface of the earth.

$$Y_2 - g_0 \sigma_{nm} = 0 , \qquad (3\text{-}24)$$

and

$$Y_4 = 0 , \qquad (3\text{-}25)$$

where σ is the surface mass density due to the equivalent rock topography of the earth's surface before deformation.

ii) Dirichlet boundary condition: the external and internal gravitational potential should be equal.

$$Y_5 = \Phi'_{nm} \qquad (3\text{-}26)$$

where Φ' is the undulation of the earth's gravitational potential deduced from the artificial satellite data.

iii) Neumann boundary condition: the difference of the gradient of the external and the internal gravitational potentials is due to the surface mass distribution on the earth (topography and radial displacement at the surface of the earth).

$$\frac{d}{dr} Y_5 - \frac{d}{dr} \Phi'_{nm} = 4\pi G (\sigma_{nm} + \rho_o Y_1) \quad . \tag{3-27}$$

Equation (3-27) can be written in the following form (Pekeris and Jarosh, 1958):

$$Y_6 + \frac{n+1}{a} Y_5 = 4\pi G \sigma_{nm} \quad , \tag{3-27a}$$

where a is the mean radius of the earth.

II. At the center of the earth all the y's should be regular (Kaula, 1963); that is,

$$Y_i = 0 \quad , \quad i = 1, \ldots, 6 \tag{3-28}$$

and

$$\frac{d}{dr} Y_i = 0 \quad , \quad i = 1, 3, 5 \quad . \tag{3-29}$$

III. At the core-mantle boundary all the y's are continuous except y_3 which is arbitrary because of the liquidity of the core.

In Kaula's studies the present topography is assumed to be the surface mass on the undeformed earth while the present gravitational undulations are considered to be due to the deformed earth (equations 11 and 11' of Kaula, 1963). These two equations are incompatible, because if the earth today is the deformed one its topography will be the sum of the initial topography and the displacements at the earth's surface after deformation. On the other hand, if the present earth is the undeformed state and it is assumed to be deformed under the present surface topography and internal density perturbations, then the present gravitational potential is not the potential after deformation. This incompatibility did not affect his results for the elastic mantle model significantly because of small deformations compared with the topography. For his second mantle model, however, it might have a very pronounced effect since the deformations are very large, about 1600 meters at the earth's surface.

(3.1-4) - Strain and Gravitational Energies

Once we know y_1, y_3, and y_5 at the core-mantle boundary we can determine the other y's there. This will be discussed in part 2 of the present chapter. Therefore, we can integrate equation (3-17)

through the mantle if $\Delta\rho$ is known. At the earth's surface we have four equations relating the three unknowns y_1, y_3 and y_5 of the core-mantle boundary. Thus, we have an over determined system. In reality, however, $\Delta\rho$ is unknown throughout the mantle and we are dealing with an under determined system (four equations and infinite unknowns). To overcome this difficulty we must introduce other constraints. One possible constraint is to minimize the total shear strain and gravitational energy of the mantle. In order for the mantle model to represent a static or quasi-static condition under the surface and body loads it is necessary to make the stress differences inside the mantle less than the creep strengths of the mantle materials. Although the minimization of the total shear strain energy does not guarantee local minimum stress difference, it will tend to reduce the stress differences in the mantle, On the other hand, the minimization of the total gravitational energy of the deformation of the mantle reduces the amplitude of the density perturbations.

In this section we formulate the strain and the gravitational energy in terms of the variables used in the previous sections.

The total strain energy is (Sokolnikoff, 1956):

$$E = \int_{V^e} \frac{1}{2} T_{ij} e_{ij} \, dv \tag{3-30}$$

Using the strain stress relationship and the definition of the compressibility,

$$K = \lambda + \frac{2}{3}\mu \tag{3-31}$$

we obtain

$$E = \int_V \left[\frac{1}{2} K \Delta^2 + \mu \left(e_{ij} e_{ij} - \frac{1}{3}\Delta^2 \right) + \frac{1}{2} \left(U_r \frac{d}{dr} P_o - P_o \right) \Delta \right] dv. \tag{3-32}$$

Here

$\mathcal{E}_{cm} = \frac{1}{2} K \Delta^2$; Compressional strain energy density,

$\mathcal{E}_{sh} = \mu \left(e_{ij} e_{ij} - \frac{1}{3}\Delta^2 \right)$; Shear strain energy density, and

$\mathcal{E}_{hd} = \frac{1}{2} \left(U_r \frac{d}{dr} P_o - P_o \right) \Delta$; Energy density of the work done by hydrostatic pressure .

Burridge and Knopoff (1966) do not recommend calling E the strain energy since it includes work done by the pre-stresses, but this is a matter of definition.

Using equations (3-3), (3-10), (3-11), (3-12) and (3-16), the shear strain energy density is expressed in terms of y's by the following:

$$\mathcal{E}_{sh} = \mu \left[\bar{y}^T \cdot \bar{\bar{P}} \cdot \bar{y} \right] S^2_{nm}(\theta, \varphi) \tag{3-33}$$

with

$$\bar{\bar{P}} = \begin{bmatrix} P_{11} & P_{12} & P_{13} & 0 & 0 & 0 \\ P_{12} & P_{22} & P_{23} & & & \\ P_{13} & P_{23} & P_{33} & & & \\ 0 & & & P_{44} & & \\ 0 & & & & & \\ 0 & & & & & \end{bmatrix} \tag{3-34}$$

with

$$P_{11} = 2(3\lambda+2\mu)^2/[3r^2(\lambda+2\mu)^2]\,, \qquad P_{23} = -n(n+1)P_{12}/2\,,$$

$$P_{12} = -2(3\lambda+2\mu)/[3r(\lambda+2\mu)^2]\,, \qquad P_{33} = 2n^2(n+1)^2(3\lambda^2+4\mu^2+6\mu\lambda)/[r^2(\lambda+2\mu)^2]$$

$$P_{13} = -n(n+1)P_{11}/2\,, \qquad -n(n+1)/r\,,$$

$$P_{22} = 2/[3(\lambda+2\mu)^2]\,, \qquad P_{44} = n(n+1)/2\mu^2\,. \tag{3-35}$$

The total shear-strain energy in the mantle is, therefore, given by

$$E_{sh} = \int_v \varepsilon_{sh}\, dv = \int_b^a r^2\mu\, dr\, \bar{y}^T \cdot \left(\int_0^{2\pi}\int_0^{\pi} \sin\theta\, d\theta\, d\varphi\, \bar{\bar{P}}\, S^2_{nm}(\theta,\varphi) \right) \cdot \bar{y} \tag{3-36}$$

where b is the radius of the core-mantle boundary.

Using the orthogonality condition of spherical harmonics, equation (3-36) is then reduced to

$$E_{sh} = 4\pi \int_b^a r^2\mu\, dr\, \bar{y}^T \cdot \bar{\bar{P}} \cdot \bar{y} \quad . \tag{3-36a}$$

Notice that matrix $\bar{\bar{P}}$ is symmetric and depends on the elastic properties of the unperturbed condition and on the degree of the spherical harmonic representation of the displacement.

The gravitational force at a given point in the earth is (Hoskins, 1920; Kovach and Anderson, 1967):

$$\bar{f} = \hat{r} f_r + \hat{\theta} f_\theta + \hat{\varphi} f_\varphi \quad . \tag{3-37}$$

Following the procedure adopted for the shear-strain energy we express the gravitational energy of the deformation of the mantle by:

$$E_{gr} = \int_{v} (\bar{f} \cdot \bar{U})\, dv = 4\pi \int_{r=b}^{\alpha} r^2 \rho_o\, dr\, \bar{y}^T \cdot \bar{\bar{Q}} \cdot \bar{y} \qquad (3\text{-}38)$$

where

$$\bar{\bar{Q}} = \begin{bmatrix} Q_{11} & 0 & Q_{13} & 0 & 0 & Q_{16} \\ 0 & 0 & 0 & 0 & 0 & 0 \\ Q_{13} & 0 & 0 & 0 & Q_{35} & 0 \\ 0 & 0 & 0 & 0 & 0 & 0 \\ 0 & 0 & Q_{35} & 0 & 0 & 0 \\ Q_{16} & 0 & 0 & 0 & 0 & 0 \end{bmatrix},$$

with

$$Q_{11} = -4g_o/r\,, \qquad Q_{16} = -1/2\,, \quad \text{and}$$

$$Q_{13} = n(n+1)g_o/r\,, \qquad Q_{35} = -n(n+1)/2r\,.$$

Here again the matrix $\bar{\bar{Q}}$ is symmetric and depends on the gravitational acceleration of the unperturbed medium and the degree of the harmonics

(3-1-5) - Maximum Shear Stress

Laboratory measurements show that the rate of strain of materials subject to stresses smaller than their creep strengths is negligible (Orowan, 1960). Therefore, we should compute the

maximum shear stresses in the mantle due to the surface and body loads discussed above and then compare them with the creep strength of the mantle.

Love (1911) studied the maximum shear stress inside an incompressible earth due to a surface load (the surface topography) which was expressed in terms of the zonal spherical harmonics. In this section we extend his studies to the case of surface and body loads given in terms of tesseral as well as zonal harmonics. The maximum shear stress at a point is (Sokolnikoff, 1956):

$$|S| = \frac{1}{2}(\tau_1 - \tau_3) \tag{3-39}$$

where τ_1 and τ_3 are, respecively, the maximum and the minimum principle stresses at that point which are the roots of the following cubic equation:

$$\tau^3 - \Theta_1 \tau^2 + \Theta_2 \tau - \Theta_3 = 0 \tag{3-40}$$

where Θ_1, Θ_2 and Θ_3 are the stress invariants,

$$\Theta_1 = T_{rr} + T_{\theta\theta} + T_{\varphi\varphi} ,$$

$$\Theta_2 = \begin{vmatrix} T_{rr} & T_{r\theta} \\ T_{r\theta} & T_{\theta\theta} \end{vmatrix} + \begin{vmatrix} T_{rr} & T_{r\varphi} \\ T_{r\varphi} & T_{\varphi\varphi} \end{vmatrix} + \begin{vmatrix} T_{\theta\theta} & T_{\varphi\theta} \\ T_{\varphi\theta} & T_{\varphi\varphi} \end{vmatrix} , \qquad (3-41)$$

$$\Theta_3 = \begin{vmatrix} T_{rr} & T_{r\theta} & T_{r\varphi} \\ T_{r\theta} & T_{\theta\theta} & T_{\theta\varphi} \\ T_{r\varphi} & T_{\theta\varphi} & T_{\varphi\varphi} \end{vmatrix} ,$$

and

$$\begin{Bmatrix} T_{rr} \\ T_{\theta\theta} \\ T_{\varphi\varphi} \\ T_{r\theta} \\ T_{r\varphi} \\ T_{\theta\varphi} \end{Bmatrix} = \begin{bmatrix} 0 & R_{12} & 0 & 0 \\ R_{21} & R_{22} & R_{23} & 0 \\ R_{31} & R_{32} & R_{33} & 0 \\ 0 & 0 & 0 & R_{44} \\ 0 & 0 & 0 & R_{54} \\ 0 & 0 & R_{63} & 0 \end{bmatrix} \begin{Bmatrix} Y_1 \\ Y_2 \\ Y_3 \\ Y_4 \end{Bmatrix} , \qquad (3-42)$$

with

$$R_{21} = \frac{2\mu(3\lambda+2\mu)}{(\lambda+2\mu)r} S_{nm}(\theta,\varphi),$$

$$R_{31} = R_{21} ,$$

$$R_{12} = S_{nm}(\theta,\varphi) ,$$

$$R_{22} = \frac{\lambda}{\lambda+2\mu} S_{nm}(\theta,\varphi) ,$$

$$R_{32} = R_{22} ,$$

$$R_{23} = \frac{2\mu}{r}\left(\frac{\partial^2}{\partial\theta^2} - \frac{n(n+1)\lambda}{\lambda+2\mu}\right) S_{nm}(\theta,\varphi) ,$$

$$R_{33} = \frac{-2\mu}{r}\left(\frac{\partial^2}{\partial\theta^2} + \frac{2n(n+1)(\lambda+\mu)}{\lambda+2\mu}\right) S_{nm}(\theta,\varphi) ,$$

$$R_{44} = \frac{\partial}{\partial\theta} S_{nm}(\theta,\varphi) ,$$

$$R_{54} = \frac{1}{\sin\theta}\cdot\frac{\partial}{\partial\varphi} S_{nm}(\theta,\varphi), \quad \text{and}$$

$$R_{63} = \frac{2\mu}{r\sin\theta}\left(\frac{\partial^2}{\partial\theta\partial\varphi} - \cot\theta\cdot\frac{\partial}{\partial\varphi}\right) S_{nm}(\theta,\varphi).$$

(3-2) - Computational Procedure

In the calculations of density perturbations of the mantle a spherically layered model is used for the earth in which it is assumed that the density perturbations inside a layer do not change with depth. The unknown density anomalies in the layers of the mantle together with the parameters of the core-mantle boundary (y_1, y_3, and y_5) are determined by satisfying the imposed boundary conditions at the earth's surface and minimizing the total shear-strain and gravitational energies. For the integration of equations (3-17) and (3-23) matricant method is adopted. This method is discussed in Appendix 2.

(3-2-1) - Normalization Process

Before integrating the equations we normalize the variables by the following transformations (Longman, 1963):

$$
\begin{array}{lll}
\lambda_1 = \lambda/\lambda^* & d = \Delta\rho/\rho_0^* & Z_3 = Y_3/a \\
\mu_1 = \mu/\lambda^* & C = a\rho_0^* g_0^*/\lambda^* & Z_4 = Y_4/\mu \\
\rho_1 = \rho_0/\rho_0^* & B = 4\pi G a \rho_0^*/g_0^* & Z_5 = Y_5/a g_0^* \\
g_1 = g_0/g_0^* & Z_1 = Y_1/a & Z_6 = Y_6/g_0^* \\
r_1 = r/a & Z_2 = Y_2/\lambda^* & Z_7 = Y_7/g_0^*
\end{array}
\qquad (3\text{-}43)
$$

where the asterisk denotes the values at the earth's surface. These transformations change the foregoing equations into the following forms:

$$\frac{d}{dr_1}\bar{Z} = \bar{\bar{M}}' \cdot \bar{Z} + \Delta\rho_1 \bar{D}_1 \quad , \tag{3-17a}$$

$$Z_2 = C\rho_1 (g_1 Z_1 - Z_5) \quad , \tag{3-20a}$$

and

$$\frac{d}{dr}\begin{bmatrix} Z_5 \\ Z_7 \end{bmatrix} = \begin{bmatrix} 0 & 1 \\ \frac{n(n+1)}{r^2} - BC\frac{\rho_1^2}{\lambda_1} & -\frac{2}{r_1} \end{bmatrix}\begin{bmatrix} Z_5 \\ Z_7 \end{bmatrix} . \tag{3-23a}$$

where

$$\bar{D}_1 = (0, Cg_1, 0, 0, 0, B)$$

and

$$\bar{\bar{M}}' = \begin{bmatrix} M'_{11} & M'_{12} & M'_{13} & 0 & 0 & 0 \\ M'_{21} & M'_{22} & M'_{23} & M'_{24} & 0 & M'_{26} \\ M'_{31} & 0 & M'_{33} & M'_{34} & 0 & 0 \\ M'_{41} & M'_{42} & M'_{43} & M'_{44} & M'_{45} & 0 \\ M'_{51} & 0 & 0 & 0 & 0 & M'_{56} \\ 0 & 0 & M'_{63} & 0 & M'_{65} & M'_{66} \end{bmatrix}$$

with

$$M'_{11} = -2\lambda_1/[r_1(\lambda_1+2\mu_1)],$$

$$M'_{12} = 1/[\lambda_1+2\mu_1],$$

$$M'_{13} = n(n+1)\lambda_1/[r_1(\lambda_1+2\mu_1)],$$

$$M'_{21} = [-4c\rho_1 g_1 r_1 + \frac{4\mu_1(3\lambda_1+2\mu_1)}{(\lambda_1+2\mu_1)}]/r_1^2,$$

$$M'_{22} = -4\mu_1/[r_1(\lambda_1+2\mu_1)].$$

$$M'_{23} = n(n+1)[c\rho_1 g_1 r_1 - \frac{2\mu_1(3\lambda_1+2\mu_1)}{(\lambda_1+2\mu_1)}]/r_1^2,$$

$$M'_{24} = n(n+1)/r_1,$$

$$M'_{26} = -c\rho_1,$$

$$M'_{31} = -1/r_1,$$

$$M'_{33} = 1/r_1,$$

$$M'_{34} = 1/\mu_1,$$

$$M_{41} = [c\rho_1 g_1 r_1 - \frac{2\mu_1(3\lambda_1+2\mu_1)}{(\lambda_1+2\mu_1)}]/r_1^2,$$

$$M_{42} = -\lambda_1/[r_1(\lambda_1+2\mu_1)],$$

$$M_{43} = 2\mu_1[\lambda_1(2n^2+2n-1) + 2\mu_1(n^2+n-1)]/[r_1^2(\lambda_1+2\mu_1)],$$

$$M_{44} = -3/r_1,$$

$$M_{45} = -c\rho_1 r_1,$$

$$M_{51} = B\rho_1,$$

$$M_{56} = 1,$$

$$M_{63} = -n(n+1)B\rho_1/r_1,$$

$$M_{65} = n(n+1)/r_1^2, \text{ and}$$

$$M_{66} = -2/r_1.$$

The boundary conditions are changed to

I) At the earth's surface $r_1 = 1$

$$\bar{S} = \begin{bmatrix} Z_2 \\ Z_4 \\ Z_5 \\ Z_6 \end{bmatrix} = \begin{vmatrix} -g_o^* \sigma_{nm}/\lambda_1^* \\ 0 \\ \Phi'_{nm}/\alpha g^* \\ 4\pi G\sigma_{nm}/g_o^* - (n+1)Z_5 \end{vmatrix} \qquad (3\text{-}24a\text{-}27a)$$

II) At the center of the earth, $r_1 = 0$

$$Z_i = 0 \quad , \quad i = 1, \cdots, 6 \tag{3-28a}$$

$$\frac{d}{dr_1} = 0 \quad , \quad i = 1, 3, 5 \tag{3-29a}$$

III) At the core-mantle boundary, $r_1 = b/a$

core		mantle
Z_1	$\longleftrightarrow$	$Z_1 = \alpha$
Z_2	$\longleftrightarrow$	Z_2
arbitrary		$Z_3 = \beta$
$Z_4 = 0$	$\longleftrightarrow$	Z_4
Z_5	$\longleftrightarrow$	Z_5
$Z_7 - B\rho_1 Z_1$	$\longleftrightarrow$	Z_6

and the energy terms are now given as:

$$E_{sh} = 4\pi \int_{r_1 = b/a}^{1} \mu_1 r_1^2 dr_1 \; \bar{Z}^T \cdot \bar{\bar{P}}_1 \cdot \bar{Z} \tag{3-36b}$$

$$E_{gr.} = 4\pi \int_{r_1 = b/a}^{1} \rho_1 r_1^2 dr_1 \; \bar{Z}^T \cdot \bar{\bar{Q}} \cdot \bar{Z} \tag{3-38b}$$

where

$$\bar{Z} = (Z_1, Z_2, Z_3, Z_4, Z_5, Z_6) \tag{3-44}$$

and $\overline{\overline{P}}_1$ and $\overline{\overline{Q}}_1$ have, respectively, the same expression as $\overline{\overline{P}}$ and $\overline{\overline{Q}}$ with all the parameters having subscripts 1.

(3-2-2) - Integration Inside the Earth

At the center of the earth Z_5 and Z_7 vanish while some of the coefficients appearing in equation (3-23a) are infinite. Thus, the integration is difficult. To start with non-zero values of Z_5 and Z_7 and finite values of the coefficients we follow Longman (1963) and introduce a homogeneous sphere of radius ϵ (200 km) at the earth's center (central sphere). On the surface of this sphere Z_5 is expressed in terms of the power series of ϵ_1 ($\epsilon_1 = \epsilon/\alpha$) as:

$$Z_5 = q_0 \epsilon_1^n + q_2 \epsilon_1^{n+2} + \cdots \qquad (3\text{-}45)$$

substituting this expression in equation (3-23a) a recurrence formula, for determining the coefficients q_i is found to be

$$q_{i+2} = -BC\, q_i / [i^2 + (2n-5)i + 4n + 6] \qquad (3\text{-}46)$$

Therefore, Z_5 and Z_7 are obtained on the central sphere within an unknown factor, q_0. Using the matricant method (see Appendix III) the integration inside the core is carried out. The values of Z_5 and Z_7, at the core-mantle boundary, in terms of their values on the central sphere and the matricant of the core are, therefore, found to be

$$\bar{Z}'_{r_1 = b/\alpha} = \bigcap_{\epsilon_1}^{= b/\alpha} \cdot \bar{Z}'_{r_1 = \epsilon_1} \tag{3-47}$$

where

$$\bar{Z}' = \frac{1}{q_o} \begin{bmatrix} Z_5 \\ Z_7 \end{bmatrix} \tag{3-48}$$

Once Z_5 is found at the core-mantle boundary equation (3-20a) yields a relationship between Z_1 and Z_2. So at the core-mantle boundary, inside the mantle, we have:

$$\bar{Z} = \begin{bmatrix} 1 & 0 & 0 \\ c\rho_1 g_1 & 0 & -c\rho_1 z'_5 \\ 0 & 1 & 0 \\ 0 & 0 & 0 \\ 0 & 0 & z'_5 \\ -B\rho_1 & 0 & z'_7 \end{bmatrix} \begin{Bmatrix} \alpha \\ \beta \\ q_o \end{Bmatrix} \tag{3-49}$$

which can be written as

$$\bar{Z} = \bar{\bar{J}} \cdot \bar{X}' \tag{3-49a}$$

where the elements of vector $\bar{X}'$ are unknown.

Since equation (3-17a) includes a radially dependent source term

we divide the mantle into K layers, Figure (3-1), thin enough so that the density perturbation as well as the elastic properties in a layer can be considered constant. The value of $\bar{Z}$ at the top of the i^{th} layer $\bar{Z}_i$, is expressed in terms of its value at the core-mantle boundary, $\bar{Z}_o$, the matricant of the medium located between the core-mantle boundary and the top of the i^{th} layer, $\bar{\bar{\Omega}}_o^i$, and the source term, $\bar{\Omega}_J'^i$ (see Appendix III), by

$$\bar{Z}_i = \bar{\bar{\Omega}}_o^i \cdot \bar{Z}_o + \sum_{J=1}^{i} \bar{\Omega}_J'^i \quad . \tag{3-50}$$

We make the following assumptions in order to obtain a general form of the solution in the mantle:

1) All the layers from $i = 1, \ldots, n_1$ have no density anomalies.

2) The layers from $i = n_1 + 1, \ldots, n_2$ have some unknown density anomalies.

3) The rest of the layers, $i = n_2 + 1, \ldots, K$, have some known density anomalies.

The known density anomalies are due to the crustal and upper mantle structure (see Chapter 2).

Let

$$\bar{\eta} = \left([\Delta\rho_1]_{n_1+1}, \ldots, [\Delta\rho_1]_{n_2} \right) \quad , \tag{3-51}$$

$$\bar{D} = \left([\Delta\rho_1]_{n_2+1}, \ldots, [\Delta\rho_1]_{K} \right) \quad , \tag{3-52}$$

$$\bar{X} = (\bar{X}' , \bar{\eta}) \quad , \tag{3-53}$$

$$\bar{\bar{\Gamma}}^{i}_{j} = \left[\bar{\bar{\Omega}}^{i}_{o} \cdot \bar{J} \;\middle|\; \bar{\Omega}^{\prime i}_{n_1+1} \;\middle|\; \cdots \;\middle|\; \bar{\Omega}^{\prime i}_{j} \right] , \tag{3-54}$$

where $j \leq n_2$,

and

$$\bar{\bar{\Gamma}}^{\prime i}_{j} = \left[\bar{\Omega}^{\prime i}_{n_2+1} \;\middle|\; \cdots \;\middle|\; \bar{\Omega}^{\prime i}_{j} \right] , \tag{3-55}$$

where $j > n_2$. Using these definitions, together with equation (3-49a) equation (3-50) becomes:

$$\bar{Z}_i = \begin{cases} \bar{\bar{\Gamma}}^{i} \cdot \bar{X} & , \; i \leq n_2 \qquad (3\text{-}50a) \\ \bar{\bar{\Gamma}}^{i} \cdot \bar{X} + \bar{\bar{\Gamma}}^{\prime i} \cdot \bar{D} & i > n_2 \qquad (3\text{-}50b) \end{cases}$$

and the boundary conditions at the earth's surface are:

$$\bar{S} = \bar{\bar{\mathcal{K}}} \cdot \bar{X} + \bar{\bar{\mathcal{K}}}' \cdot \bar{D} \tag{3-56}$$

Here $\bar{S}$, $\bar{\bar{\mathcal{K}}}$ and $\bar{\bar{\mathcal{K}}}'$ are found by omitting the first and third rows of $\bar{Z}$, $\bar{\bar{\Gamma}}$ and $\bar{\bar{\Gamma}}'$ respectively.

(3-2-3) - Minimization of the Energies and the Final Solution

To parameterize the problem we apply different weighting factors to the shear-strain and gravitational energies, ω_{sh} and ω_{gr}, respectively. Using equation (3-50b) and keeping in mind that the second term in the right hand side vanishes when $i \leq n_2$ we combine the two energy terms into a single expression.

$$E = \omega_{sh} E_{sh} + \omega_{gr} E_{gr} \tag{3-57}$$

or

$$E = \bar{X}^T \cdot \bar{\bar{W}}_1 \cdot \bar{X} + \bar{X}^T \cdot \bar{\bar{W}}_2 \cdot \bar{D} + \bar{D} \cdot \bar{\bar{W}}_2^T \cdot \bar{X} + \bar{D}^T \cdot \bar{\bar{W}}_3 \cdot \bar{D} \ . \tag{3-57a}$$

Here

$$\begin{bmatrix} \bar{\bar{W}}_1 \\ \bar{\bar{W}}_2 \\ \bar{\bar{W}}_3 \end{bmatrix} = \sum_{i=1}^{K} \frac{1}{3} \left(r_{1(i)}^3 - r_1^3{}_{(i-1)} \right) \begin{bmatrix} \bar{\bar{\Gamma}}^T \cdot \bar{\bar{S}} \cdot \bar{\bar{\Gamma}} \\ \bar{\bar{\Gamma}}^T \cdot \bar{\bar{S}} \cdot \bar{\bar{\Gamma}}' \\ \bar{\bar{\Gamma}}'^T \cdot \bar{\bar{S}} \cdot \bar{\bar{\Gamma}}' \end{bmatrix} \tag{3-58}$$

where

$$\bar{\bar{S}} = 4\pi\left[\omega_{sh}\,\mu_1(i)\cdot\tilde{\tilde{P}}_1(i) + \omega_{gr}\,\rho_1(i)\,\tilde{\tilde{Q}}_1(i)\right] \tag{3-59}$$

and

$$\begin{bmatrix}\tilde{\tilde{P}}(i)\\ \tilde{\tilde{Q}}(i)\end{bmatrix} = \frac{1}{2}\begin{bmatrix}\bar{\bar{P}}(i)+\bar{\bar{P}}(i-1)\\ \bar{\bar{Q}}(i)+\bar{\bar{Q}}(i-1)\end{bmatrix}$$

Minimization of E subject to the constraints given by equation (3-56) is a generalized least-squares problem. Adopting the method of Lagrangian multipliers, this leads to the following simultaneous first order linear equations:

$$\begin{bmatrix}\bar{\bar{W}}_1 & \bar{\bar{\mathcal{K}}}^T\\ \bar{\bar{\mathcal{K}}} & 0\end{bmatrix}\begin{bmatrix}\bar{X}\\ \bar{\Lambda}\end{bmatrix} = \begin{bmatrix}-\bar{\bar{W}}_2\cdot\bar{D}\\ \bar{S}-\bar{\bar{\mathcal{K}}}'\cdot\bar{D}\end{bmatrix} = \begin{bmatrix}\bar{V}_1\\ \bar{V}_2\end{bmatrix} \tag{3-60}$$

The solution vector, $\bar{X}$, is given by (Arley and Buch, 1950):

$$\bar{X} = \bar{\bar{W}}_1^{-1}\cdot\bar{V}_1 - \bar{\bar{W}}_1^{-1}\cdot\bar{\bar{\mathcal{K}}}^T\cdot\left(\bar{\bar{\mathcal{K}}}\cdot\bar{\bar{W}}_1^{-1}\cdot\bar{\bar{\mathcal{K}}}^T\right)^{-1}\cdot\bar{\bar{\mathcal{K}}}\cdot\bar{\bar{W}}_1^{-1}\cdot\bar{V}_1$$
$$+\ \bar{\bar{W}}_1^{-1}\cdot\bar{\bar{\mathcal{K}}}^T\cdot\left(\bar{\bar{\mathcal{K}}}\cdot\bar{\bar{W}}_1^{-1}\cdot\bar{\bar{\mathcal{K}}}^T\right)^{-1}\cdot\bar{V}_2 \qquad . \tag{3-61}$$

(3-2-4) - Test of the Numerical Calculations

The following examples were computed in order to check the computer programs utilized.

A) - Surface loading of an earth model:

The deformations of an earth model whose parameters are given in Table (3-1) were determined for a surface mass of $1 \times S_{3,0}(\theta,\varphi)\ g/cm^2$. Figures (3-2a) and (3-2b) show the resulting values of y_1, y_3 and y_5. The values of y_1 and y_3 agree with the plotted results of Takeuchi, et al. (1962) while y_5 is greater than theirs by a constant factor. Notice that the visible mass at the surface after deformation is about .78 times the initial one which indicates an imperfect compensation of the load.

B) - An elastic layer overlying an incompressible liquid sphere

The deformation of an elastic layer overlying a liquid half-space and subject to a surface loading has been studied by Jeffreys (1959). We computed, however, the deformation of an elastic layer, 50 km. thick, 2.74 g/cc density and 3.45×10^{11} dyn./cm^2 rigidity and Lame constant, which overlies an incompressible liquid sphere with 6321 km. radius and 2×2.74 g/cc density. The following loads were considered:

1 - Surface loading. For an initial topography on the layer, $.365 \times S_{3,0}(\theta,\varphi)$cm, the radial displacement at the mid-surface of the layer is found to be $-.186 \times S_{3,0}(\theta,\varphi)$cm which agrees with Jeffreys' result and, moreover, shows that the compensation process is quite perfect.

2 - Body loading (a). A mass equivalent to that of the initial surface topography of example (1) was distributed uniformly

throughout the thickness of the layer. The resulting displacements at the mid-surface equal those of example (1). This result is expected since the lateral dimensions of the loads (about 5000 km.) are very large compared to the thickness of the layer and, thus, the layer deforms as a thin shell when it is subjected to this load.

3 - Body loading (b). In the foregoing examples three boundary conditions at the surface, equations (3-24a), (3-25a) and (3-27a) were used to calculate the deformations. For the present example, however, we added another boundary condition, namely, the perturbations of the gravitational potential at the surface obtained in example (a), and then determined the density anomalies in the layer. This is just the inverse problem of example (a) and the resulting density perturbations are identical to those of example (a).

C) - Kaula's problem

As a final example we determined the lateral density perturbations of the lower mantle of the earth model (Table 3-1), specified by the spherical harmonic with n = 3 and m = 2. In the calculation, the corresponding gravitational potential and topography at the earth's surface and the density perturbations of the first two layers of the model were taken from Kaula's model 1 (1963). The density perturbations of the region between 38 and 350 km depths were set to zero (this was due to the lack of storage in the computer). The lower mantle was divided into L layers with radially independent

density perturbations. These perturbations were then obtained by satisfying the boundary conditions at the surface, equations (3-24a to 3-27a), and also minimizing the total shear-strain energy of thc earth.

Figure (3-3) shows the totla shear-strain energy for seven models. The energy decreases very rapidly as the single layer model, L = 1, is replaced by the two layer model, L = 2. Thereafter the energy decreases very slowly as a function of L. Shear-strain energies associated with L values of 2, 3, 4, 6 and 9 are 1/3 of that given by Kaula. Thus, Kaula's model should be somewhere between the models with L = 1 and L = 2.

Figure (3-4) displays the radial variations of the lower mantle density perturbations for different L values. It is evident from the figure that the radial dependence of the density anomalies has an oscillatory behavior. Kaula also found this kind of behavior in his layered model approach and rejected it since he considered it to be implausible. For this reason he adopted a third order polynomial model for the radial variations of the anomalies (personal communication, 1968). The polynomial model differs from a layered one in that it yields smoothly varying density perturbations. Considering a vector whose components are the density perturbations in each layer (the density vector) the polynomial model has the effect of minimizing the length of this vector. Thus, to make our results comparable with the polynomial model of Kaula, we minimized the total shear-strain energy together with the square of the length of the

density vector. Two density models, L = 3 and L = 18, were computed where we used a weighting factor of unity for the energy term and weights of .005 and .01 for the density vector term respectively. The results are included in Figures (3-3) and (3-4). Minimizing both the amplitude of the density perturbations and the total shear-strain energy increases the latter by about 7 per cent for L = 3 and several hundred per cent for L = 18. But, in this case, the density perturbations decrease somewhat continuously with depth. Their maximum amplitudes are less than twice that of Kaula's results. This discrepancy is probably due partly to the zero density anomalies assumed for the region between 38 and 350 km. depths and partly to the difference between the layered models considered and Kaula's polynomial model.

(3-3) - Density Anomalies in the Mantle

As a final model of the density anomalies in the mantle we present the density perturbations, specified by the spherical harmonics with n = 2,....,6 and m = 0,....n. These perturbations were calculated for Gutenberg's earth model (Table 3-1) by satisfying the following boundary conditions and constraints:

1 - The gravitational potential of the deformed earth is assumed to be equal to the geopotential presented by Kaula (1967).

2 - Lee and Kaula's (1967) spherical harmonic representation of

the equivalent rock topography is assumed to be the topography on the surface of the earth after the deformation.

3 - The surface layer density model proposed in Chapter 2 is used for all the harmonics considered.

4 - For harmonics with degrees smaller than four, the upper mantle density anomalies determined in Chapter 2 are used. For harmonics with degrees greater than three it is assumed that the lower mantle is spherically symmetric and the density anomalies are confined to the upper mantle and the crust.

5 - Both the total shear-strain energy of the mantle and the amplitude of the density perturbations, associated with two different weighting factors, are minimized. The final model is selected by a trial and error variation of the weighting factor of density perturbations.

In order to achieve a minimum total gravitational energy associated with the density anomalies and, thus, eliminate the oscillatory feature of the radial dependence of the density perturbations it is found that the minimization of the amplitude of the perturbations is more effective than the minimization of the gravitational energy given by equation (3-38b). This is because the gravitational energy of the accretion process of the density anomalies computed by (Kellogg, 1953)

$$E = \frac{1}{2} \int_{v} \Phi . \Delta \rho . dv \qquad (3\text{-}62)$$

is an order of magnitude greater than the gravitational energy associated with the deformation of the earth subject to the density perturbations (equation (3-38b)). Therefore, following the procedure adopted in the case of Kaula's problem we divide the region with unknown density into L layers with radially independent density perturbations. The minimization of the amplitude of those perturbations is easily taken into account by adding $2 \times \omega_d$ to the diagonal terms of matrix W_1 in equation (3-60), starting from the fourth row. Here ω_d is the weighting factor for the density vector defined in the previous section. Table (3-2) is the list of the density models constructed for different values of L and ω_d. The variations of the total shear-strain energy with L and ω_d are illustrated in Figures (3-5) and (3-6). Included in the figures are the perturbations specified by zonal harmonics. The energy values are normalized to the energy associated with L = 3 and $\omega_d = 0$, respectively.

Models (2) and (8) are selected as the final density model of the mantle because: 1) they produce nearly a minimum total shear-strain energy, 2) they just cease to show oscillatory features with depth, and 3) they happen to divide the mantle into regions in agreement with other geophysical investigations (Chinnery and Toksöz, 1967; Toksöz, et al., 1967; Press, 1968). The spherical harmonic coefficients of the density perturbations of the mantle deduced from these models are tabulated in Table (3-3). Using these values the lateral variations of the final density anomalies are contoured at different depths (Figures (3-7 to 12)).

Figure (3-13) shows their radial variations under shield ($\theta = 40^{\circ}$, $\varphi = 200^{\circ}$), tectonic ($\theta = 100^{\circ}$, $\varphi = 180^{\circ}$), and oceanic ($\theta - 50^{\circ}$, $\varphi = 200^{\circ}$) areas. The upper mantle is characterized by positive density anomalies under the shields and negative ones under the oceans. The large density anomaly under southwestern Africa may not be realistic and is probably due to the unrealistic harmonic representation of the seismic travel time residuals which were used as an input in the analysis. The large change at 400 km. depth is due to the modeling effect. Using different values for ω_d and/or L it is possible to obtain smaller changes there. In general, the density anomalies decrease with depth. In the crust they are on the order of 0.3 g/cc, in the upper mantle 0.1 g/cc and in the lower mantle 0.04 g/cc.

Figures (3-14 to 19) display the lateral variations of the radial displacements and the perturbations of the gravitational potential at the surface of the earth, at 800 km. depth, and at the core-mantle boundary. The radial variations at specified latitudes and longitudes are illustrated in Figure (3-20). It is evident from the figures that the shield areas are lifted up and the oceanic areas are depressed. But, the maximum displacements occuring at about 800 km. depth indicates that, down to 800 km. the shield areas are contracted while the oceanic areas are expanded, and from 800 km. to the core-mantle boundary the materials beneath the shield areas are expanded while those under the oceanic areas are contracted.

The maximum shear-stresses associated with the final density model were determined. Figures (3-21 to 23) show their lateral variations at depths of 30, 163 and 426 km., and Figure (3-24) shows their radial variations at specified latitudes and longitudes. These figures illustrate the correlations between the surface features of the earth with maximum shear-stresses existing at shallow depths. In general shield areas and oceanic basins are characterized by small stress differences while tectonic areas appear to have large stress differences. In the deep mantle, however, the effect of the surface features on the stress differences disappear. The radial dependence of the stress differences is not a smoothly varying function but, rather, exhibits three maxima and minima. The largest stress difference, about 1 Kbar occurs at about 400 km. and the other maxima are at about 30 and 2100 km. depths. The maxima at 400 km. are most likely due to the assumption that the lower mantle density perturbations are specified by spherical harmonics through only the third degree. Including higher harmonics may reduce this value significantly. Figure (3-24) also contains the stress differences associated with Kaula's density model 1 (1963). These are about four times smaller than the results of the present studies. This difference is due to: a) the large density anomalies in the crust and upper mantle inferred from seismic data which requires large density perturbations in the lower mantle in order to obtain a gravitational field similar to the observed

one, and b) the higher harmonics, n = 5 and 6, included for the density variations in the present studies.

LIST OF TABLES FOR CHAPTER 3

Table

Table (3-1)

GUTENBERG'S EARTH MODEL

NO	DEPTH KM	RHO G/CC	VP KM/S	VS KM/S	MU (10^{11} DYN/CM2)	LAMBDA DYN/CM2)	G CM/S2
1	0	2.74	6.14	3.55	3.45	3.42	982
2	19	3.00	6.58	3.80	4.33	4.32	983
3	38	3.32	8.20	4.65	7.18	7.97	984
4	50	3.34	8.17	4.62	7.13	8.04	985
5	60	3.35	8.14	4.57	7.00	8.20	985
6	70	3.36	8.10	4.51	6.83	8.38	986
7	80	3.37	8.07	4.46	6.70	8.54	986
8	90	3.38	8.02	4.41	6.57	8.59	986
9	100	3.39	7.93	4.37	6.47	8.37	986
10	125	3.41	7.85	4.35	6.45	8.11	987
11	150	3.43	7.89	4.36	6.52	8.31	988
12	175	3.46	7.98	4.38	6.64	8.76	989
13	200	3.48	8.10	4.42	6.80	9.23	989
14	225	3.50	8.21	4.46	6.96	9.67	990
15	250	3.53	8.38	4.54	7.28	10.24	991
16	300	3.58	8.62	4.68	7.84	10.92	992
17	350	3.62	8.87	4.85	8.52	11.45	993
18	400	3.69	9.15	5.04	9.37	12.15	995
19	450	3.82	9.45	5.21	10.37	13.38	996
20	500	4.01	9.88	5.45	11.91	15.32	997
21	600	4.21	10.30	5.76	13.97	16.73	998
22	700	4.40	10.71	6.03	16.00	18.47	998
23	800	4.56	11.10	6.23	17.70	20.79	997
24	900	4.63	11.35	6.32	18.49	22.66	995
25	1000	4.74	11.60	6.42	19.54	24.71	993
26	1200	4.85	11.93	6.55	20.81	27.41	990
27	1400	4.96	12.17	6.69	22.20	29.06	986
28	1600	5.07	12.43	6.80	23.44	31.45	983
29	1800	5.19	12.67	6.90	24.71	33.90	982
30	2000	5.29	12.90	6.97	25.70	36.63	981
31	2200	5.39	13.10	7.05	26.79	38.92	984
32	2400	5.49	13.32	7.15	28.07	41.27	989
33	2600	5.59	13.59	7.23	29.22	44.80	997
34	2800	5.69	13.70	7.20	29.50	47.80	1011
35	2898	9.40	8.10			61.71	1037
36	3000	9.55	8.23			64.72	1015
37	3500	10.15	8.90			80.42	908
38	4000	10.70	9.50			96.58	800
39	4500	11.20	9.97			111.39	631
40	4982	11.50	10.44			125.34	469
41	5121	12.00	10.75			138.66	422
42	6371	12.30	11.31			157.34	000

Table (3-2)

DENSITY MODELS

MODEL	N	L	WD	
1	1 - 3	3	0.0	
2	1 - 3	3	0.001	*
3	1 - 3	3	0.01	
4	1 - 3	4	0.01	
5	1 - 3	6	0.01	
6	1 - 3	8	0.01	
7	4 - 6	3	0.0	
8	4 - 6	3	10^{-5}	*
9	4 - 6	3	10^{-4}	
10	4 - 6	3	$5*10^{-3}$	
11	4 - 6	3	0.1	
12	4 - 6	1	10^{-5}	
13	4 - 6	2	10^{-5}	
14	4 - 6	5	10^{-5}	
15	4 - 6	7	10	

* Final models

Table (3-3)

SPHERICAL HARMONIC COEFFICIENTS OF THE DENSITY ANOMALIES IN THE MANTLE (10^{-2} G/CC)

UPPER MANTLE

		DEPTH(KM) 50 - 125		DEPTH(KM) 125 - 225		DEPTH(KM) 225 - 400	
N	M	ANM	BNM	ANM	BNM	ANM	BNM
2	0	2.175	0.0	2.175	0.0	2.175	0.0
2	1	.377	1.483	.377	1.483	.377	1.483
2	2	.522	-1.132	.522	-1.132	.522	-1.132
3	0	.084	0.0	.084	0.0	.084	0.0
3	1	.326	-0.599	.326	-0.599	.326	-0.599
3	2	-1.654	.774	-1.654	.774	-1.654	.774
3	3	.146	1.007	.146	1.007	.146	1.007
4	0	1.027	0.0	.410	0.0	-0.036	0.0
4	1	.925	-0.786	.368	-0.314	-0.019	.033
4	2	-0.698	.040	-0.279	.017	-0.005	-0.015
4	3	.186	.082	.076	.032	-0.021	-0.001
4	4	-0.503	.276	-0.201	.111	.014	.003
5	0	-1.391	0.0	-0.546	0.0	.044	0.0
5	1	-0.060	.066	-0.024	.026	.002	-0.005
5	2	-0.024	.361	-0.011	.141	-0.018	-0.009
5	3	-0.672	.878	-0.262	.343	.045	-0.036
5	4	-0.612	-0.689	-0.237	-0.270	.047	.029
5	5	1.231	.598	.481	.237	-0.054	.006
6	0	-0.345	0.0	-0.131	0.0	.024	0.0
6	1	-0.593	-0.212	-0.227	-0.084	.030	-0.003
6	2	-0.230	-0.883	-0.088	-0.337	.010	.005
6	3	.247	.959	.095	.369	-0.012	-0.040
6	4	-0.131	.311	-0.046	.120	.026	-0.007
6	5	-0.195	-1.256	-0.075	-0.480	.008	.071
6	6	.173	1.694	.067	.652	-0.005	-0.067

LOWER MANTLE

		DEPTH(KM) 400 - 1000		DEPTH(KM) 1000 - 2000		DEPTH(KM) 2000 - 2898	
N	M	ANM	BNM	ANM	BNM	ANM	BNM
2	0	-1.332	0.0	-0.012	0.0	.331	0.0
2	1	-0.222	-1.273	-0.004	-0.003	.052	.324
2	2	-0.030	.702	-0.026	.017	-0.019	-0.162
3	0	-0.172	0.0	.011	0.0	.039	0.0
3	1	-0.504	.487	.034	-0.027	.114	-0.108
3	2	1.237	-0.770	-0.066	.055	-0.272	.180
3	3	-0.174	-0.580	.011	.013	.039	.114

FIGURE CAPTIONS FOR CHAPTER 3

Figure

(3-1) Layers for the integration process

(3-2a) y_1 and y_3 versus depth for the surface laoding of the earth model

(3-2b) y_5 versus depth for the surface loading of the earth model

(3-3) Total shear-strain energy of the earth versus L for Kaula's model

(3-4) Radial variations of the lower mantle density perturbations with different values of L for Kaula's model

(3-5) Total shear-strain energy of the earth versus L. Normalized for the energy corresponding to the case when L = 3.

(3-6) Total shear-strain energy of the earth versus ω_d. Normalized for the energy corresponding to the case when $\omega_d = 0$.

(3-7 to 3-12) Lateral variations of density in the regions between 50-125, 125-225, 225-400, 400-1000, 1000-2000, 2000-2898, respectively. Units are in g/cc.

(3-13) Radial variations of the density perturbations under shield, tectonic and oceanic areas. Units are in g/cc.

(3-14 to 3-16) Lateral variations of the radial displacements at the surface of the earth, at 800 km. depth, and at the core-mantle boundary. Units are in meters.

(3-17 to 3-19) Lateral variations of the gravitational perturbations at the surface of the earth, at 800 km. depth and at the core-mantle boundary. Units are in 10^6 ergs.

(3-20) Radial variations of the radial displacements and the perturbations of the gravitational potential.

(3-21 to 3-23) Lateral variations of the maximum shear stresses at 30, 163 and 426 km. depths. Units are in bars.

(3-24) Radial variations of the maximum shear stresses at given latitudes and longitudes. The figure also includes Kaula's results.

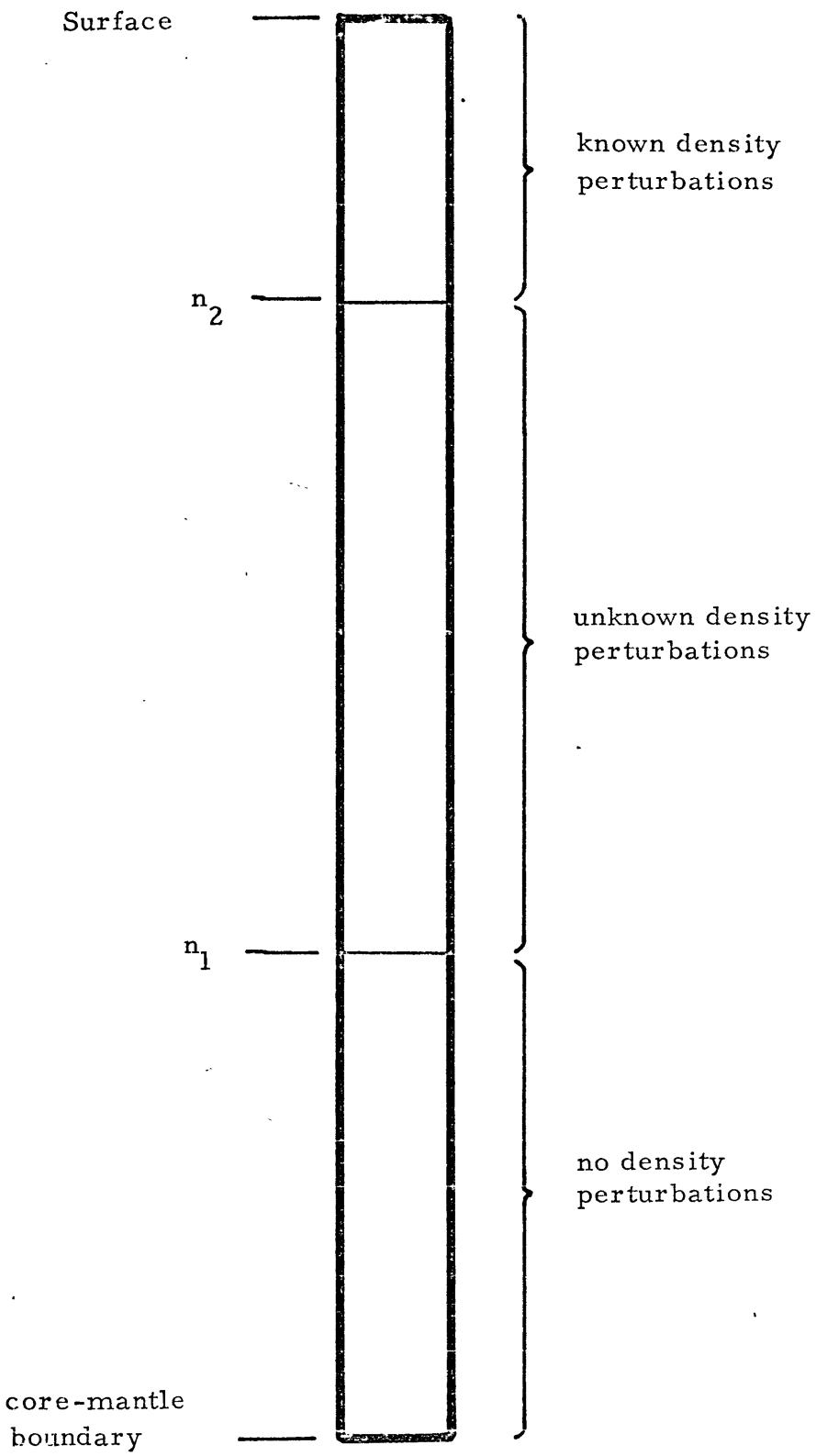
Surface
known density perturbations
n_2
unknown density perturbations
n_1
no density perturbations
core-mantle boundary

Fig. (3-1)

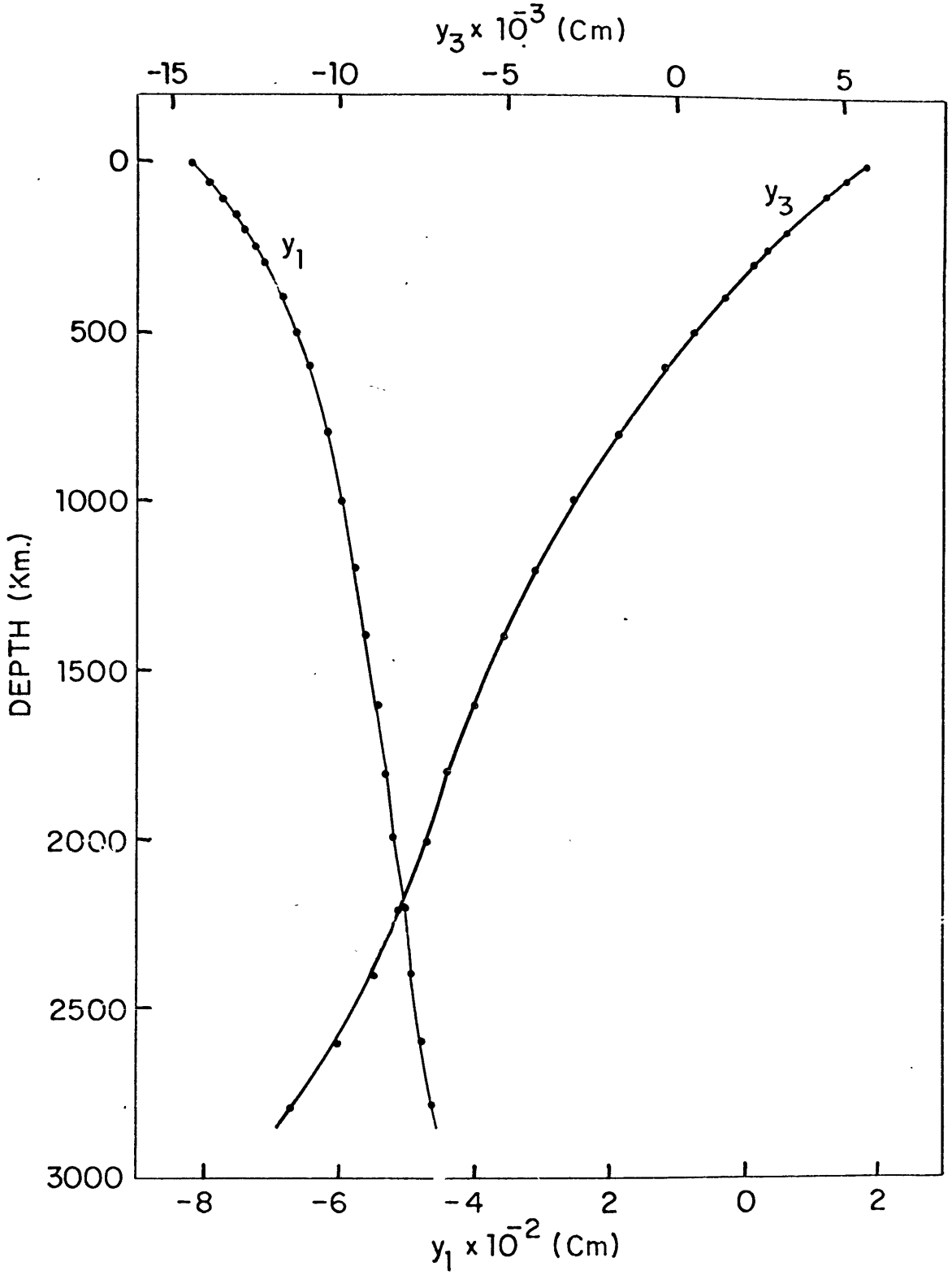
$y_3 \times 10^{-3}$ (Cm)
-15
-10
-5
0
5
0
500
1000
1500
2000
2500
3000
DEPTH (Km.)
y_1
y_3
-8
-6
-4
2
0
2
$y_1 \times 10^{-2}$ (Cm)

Fig. (3-2α)

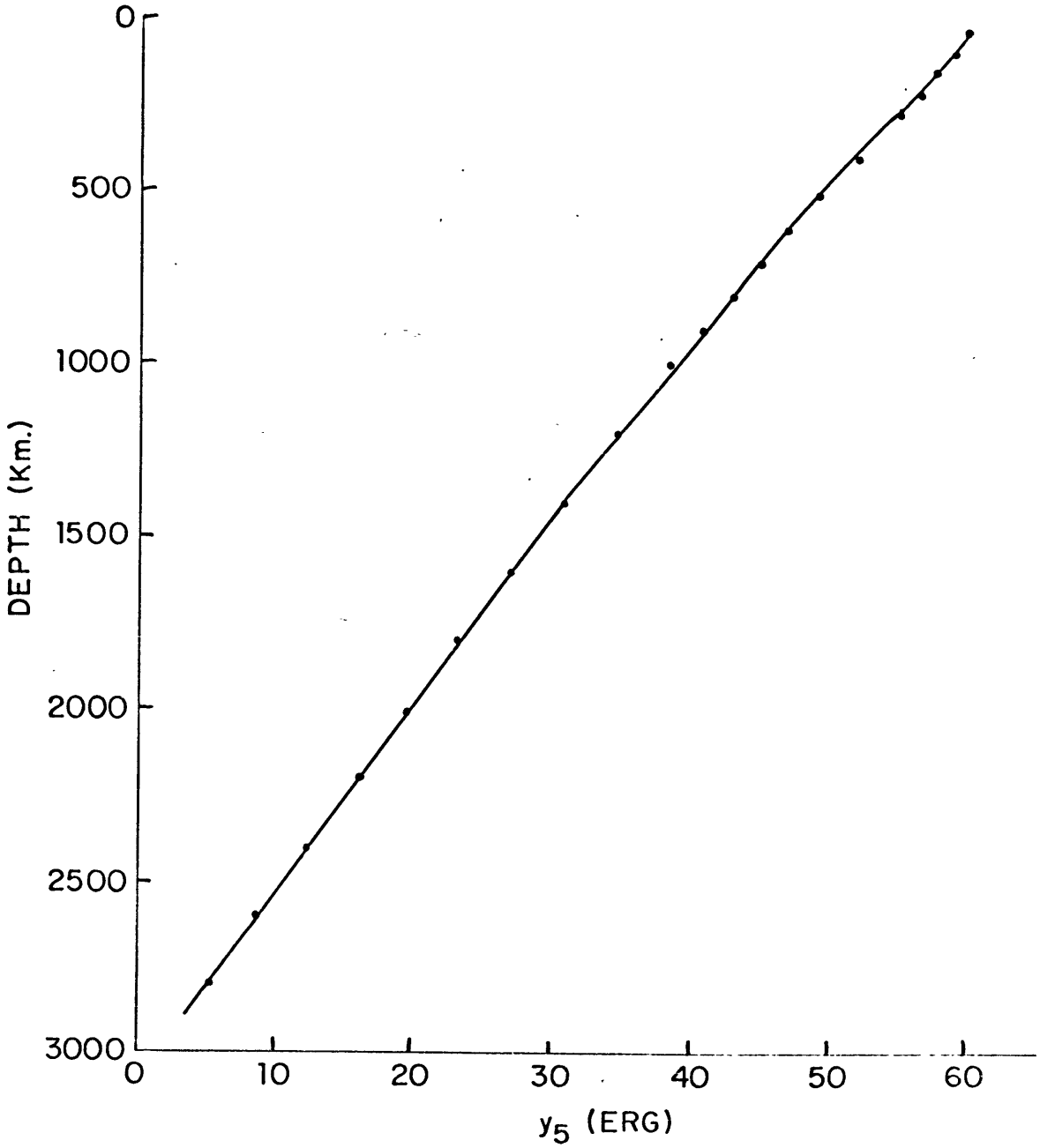

Fig. (3-2b)

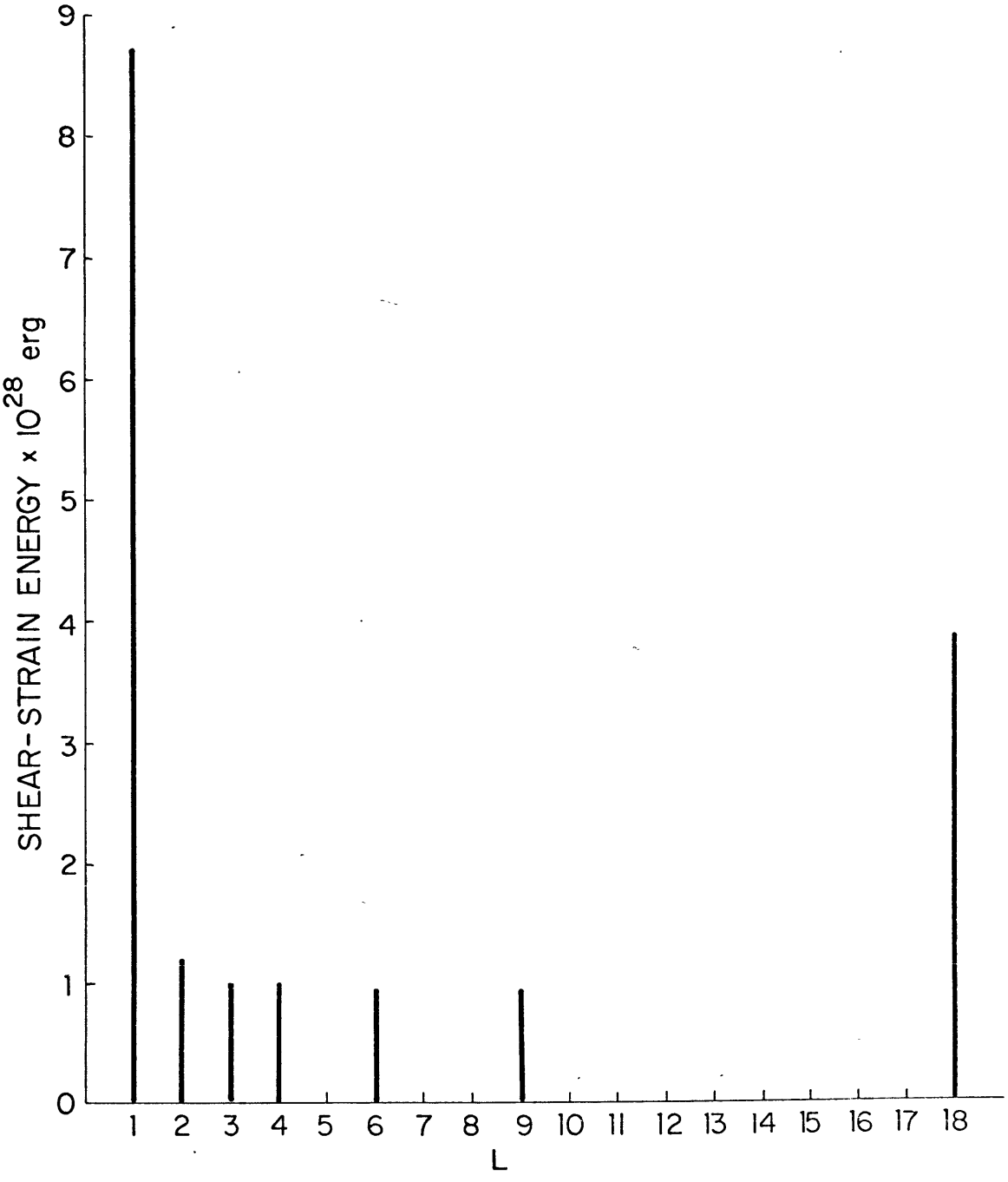
SHEAR-STRAIN ENERGY x 10^{28} erg
0
1
2
3
4
5
6
7
8
9
1 2 3 4 5 6 7 8 9 10 11 12 13 14 15 16 17 18
L

Fig. (3-3)

Fig.(3-4)

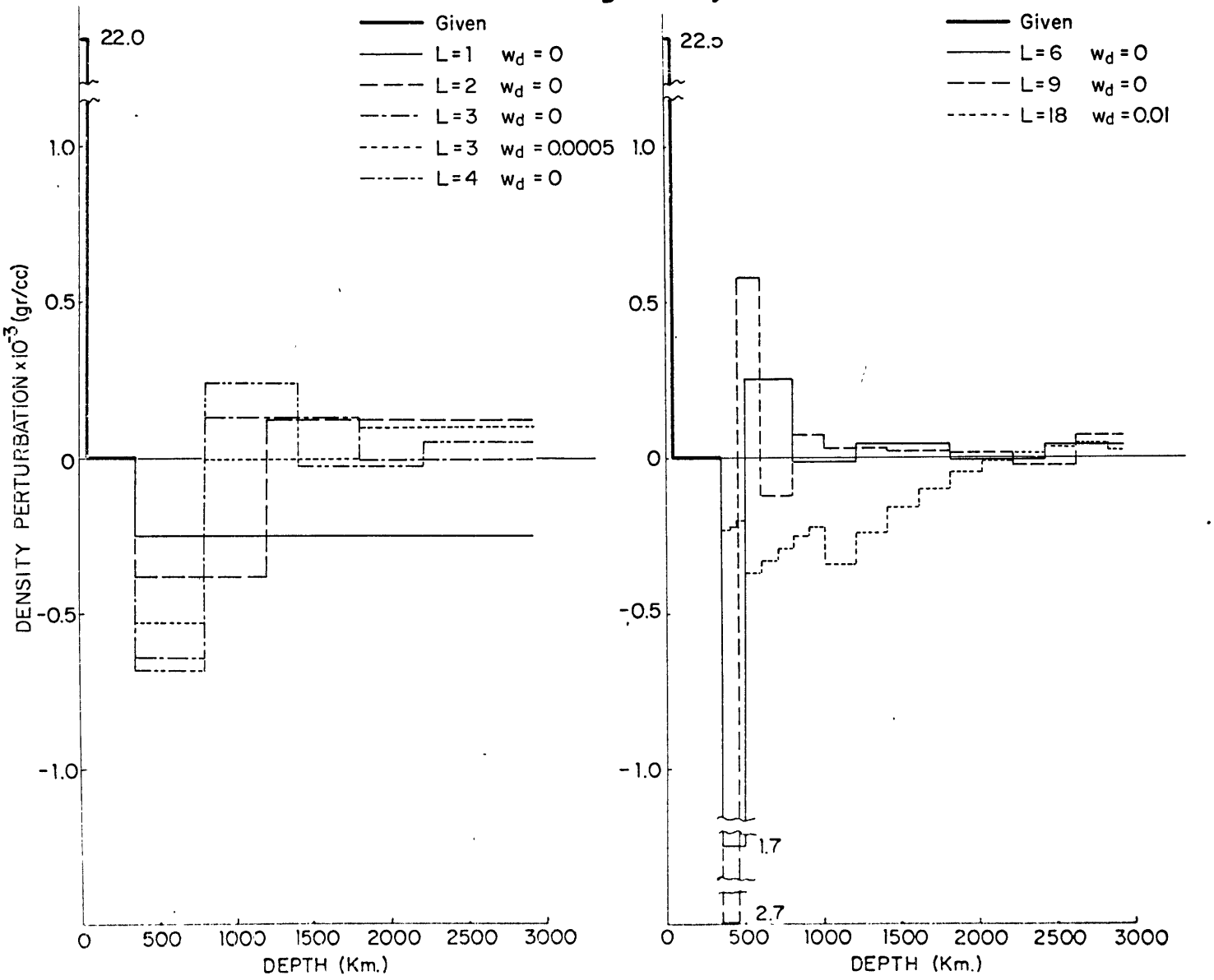
Given
L=1 w_d = 0
L=2 w_d = 0
L=3 w_d = 0
L=3 w_d = 0.0005
L=4 w_d = 0
22.0
1.0
0.5
0
-0.5
-1.0
DENSITY PERTURBATION x10^{-3}(gr/cc)
0 500 1000 1500 2000 2500 3000
DEPTH (Km.)
Given
L=6 w_d = 0
L=9 w_d = 0
L=18 w_d = 0.01
22.5
1.7
2.7

SHEAR-STRAIN ENERGY

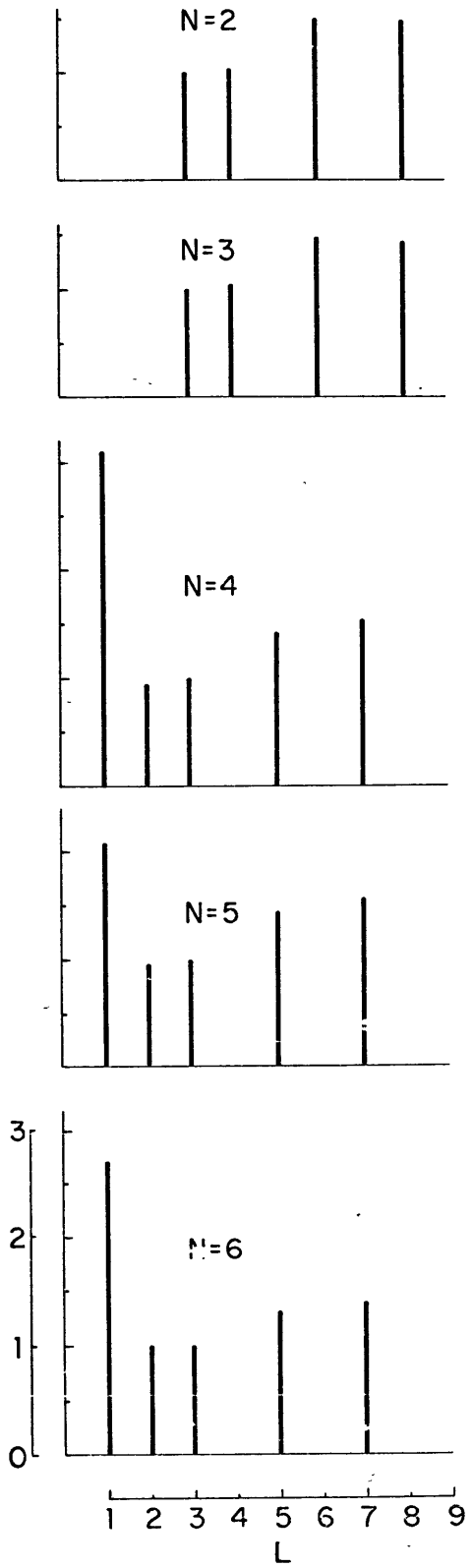

Fig. (3-5)

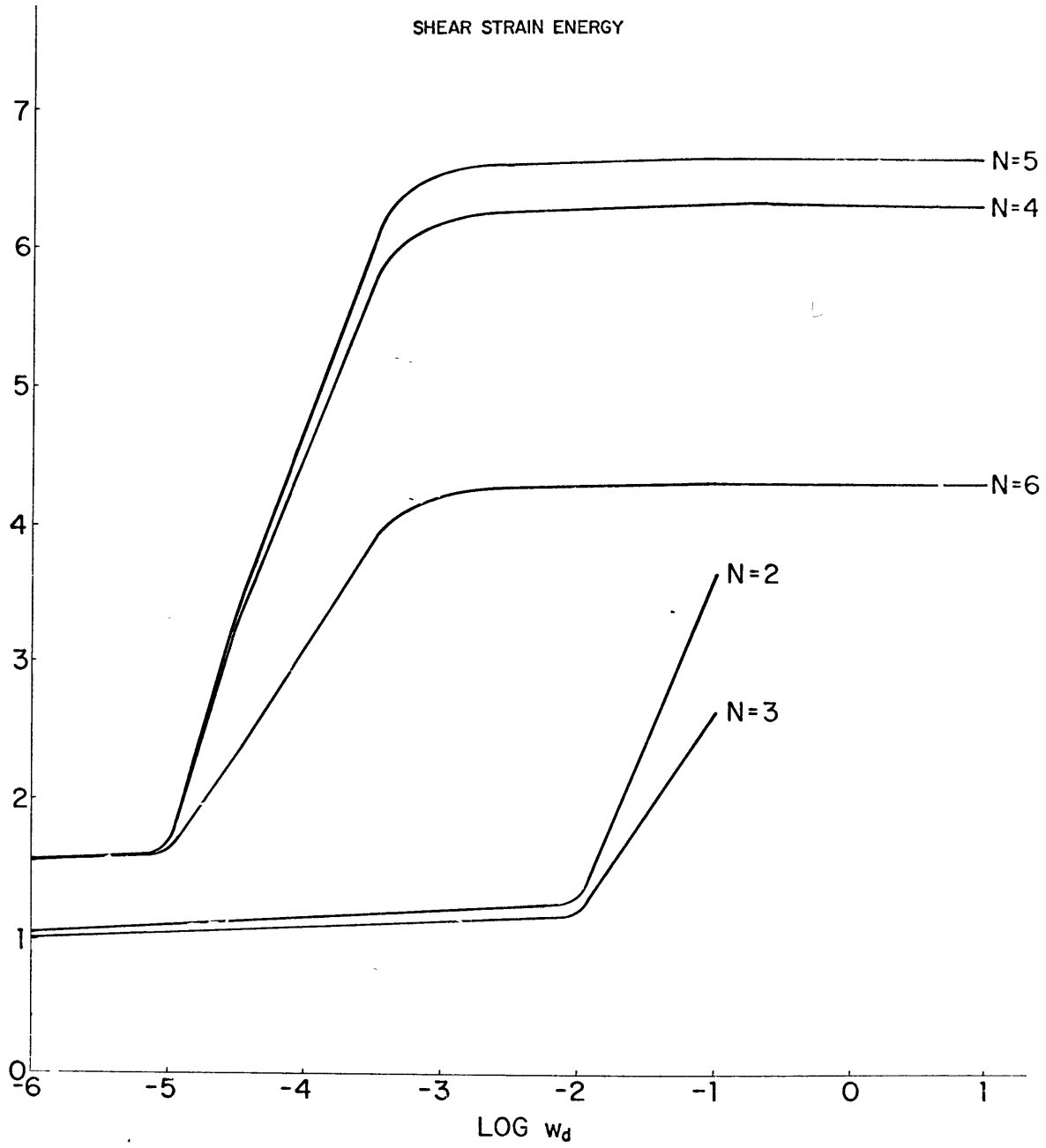

Fig. (3-6)

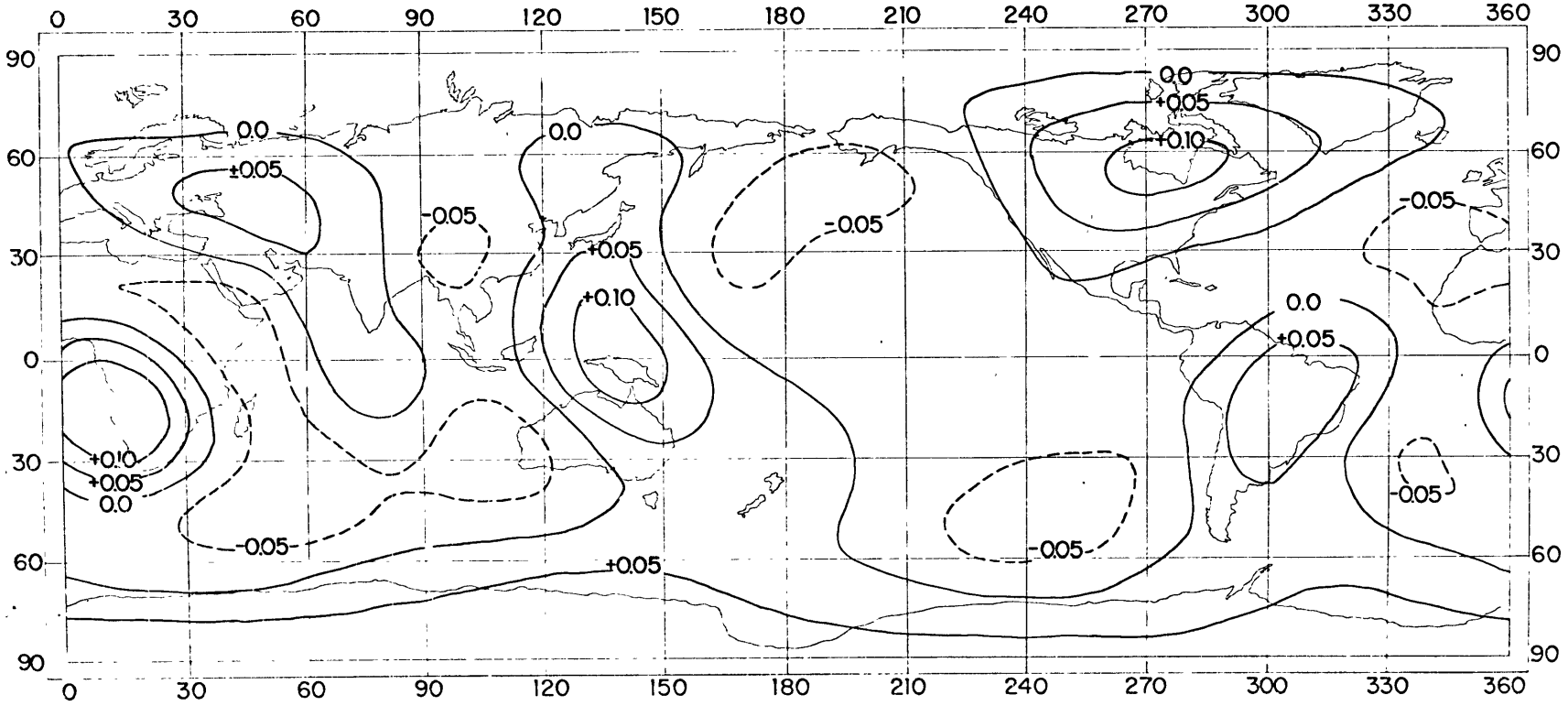
0
30
60
90
120
150
180
210
240
270
300
330
360
90
60
30
0
30
60
90
0.0
±0.05
-0.05
0.0
+0.05
+0.10
-0.05
0.0
+0.05
+0.10
-0.05
0.0
+0.05
+0.10
+0.05
0.0
-0.05
-0.05
-0.05
+0.05

Fig.(3-7)

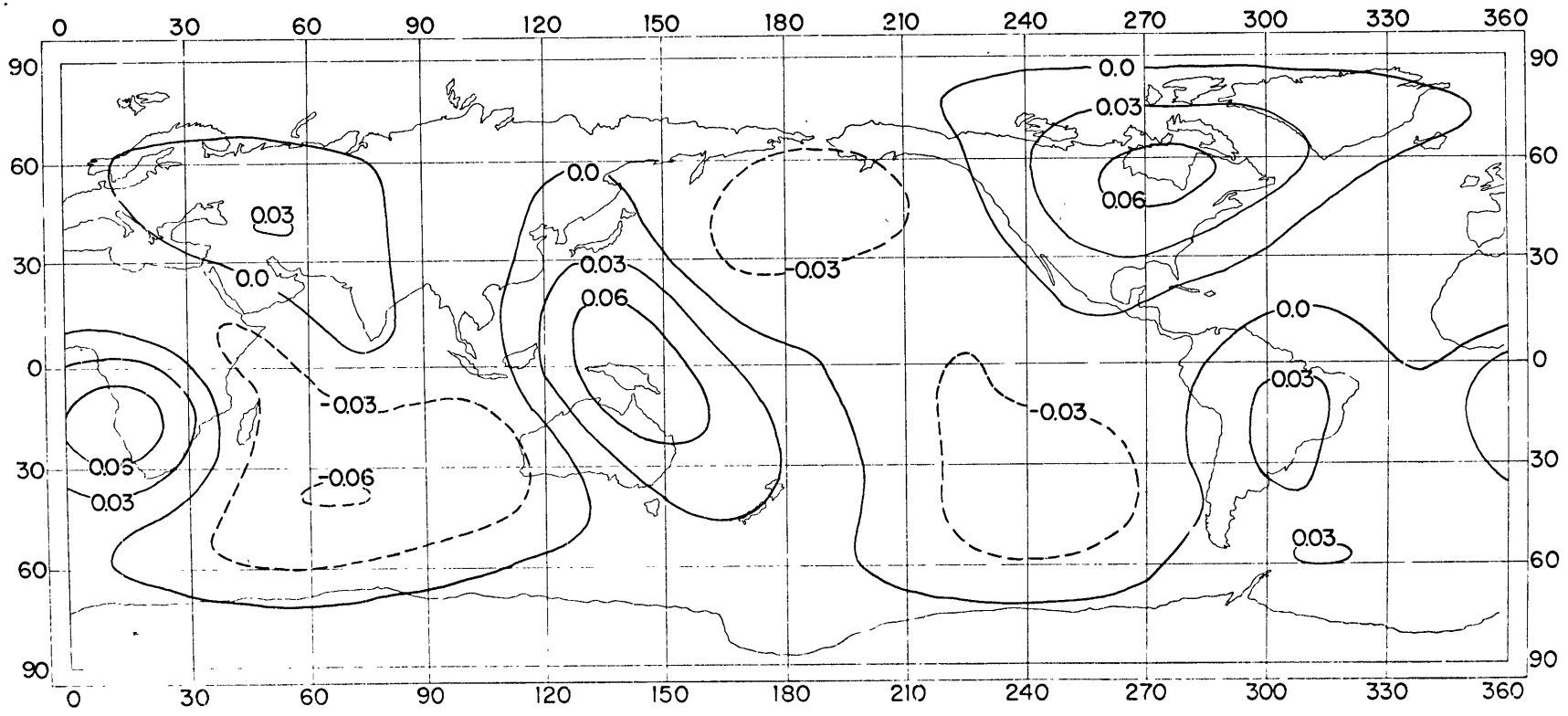
0
30
60
90
120
150
180
210
240
270
300
330
360
90
60
30
0
30
60
90
0.0
0.03
0.06
-0.03
-0.06

Fig. (3-8)

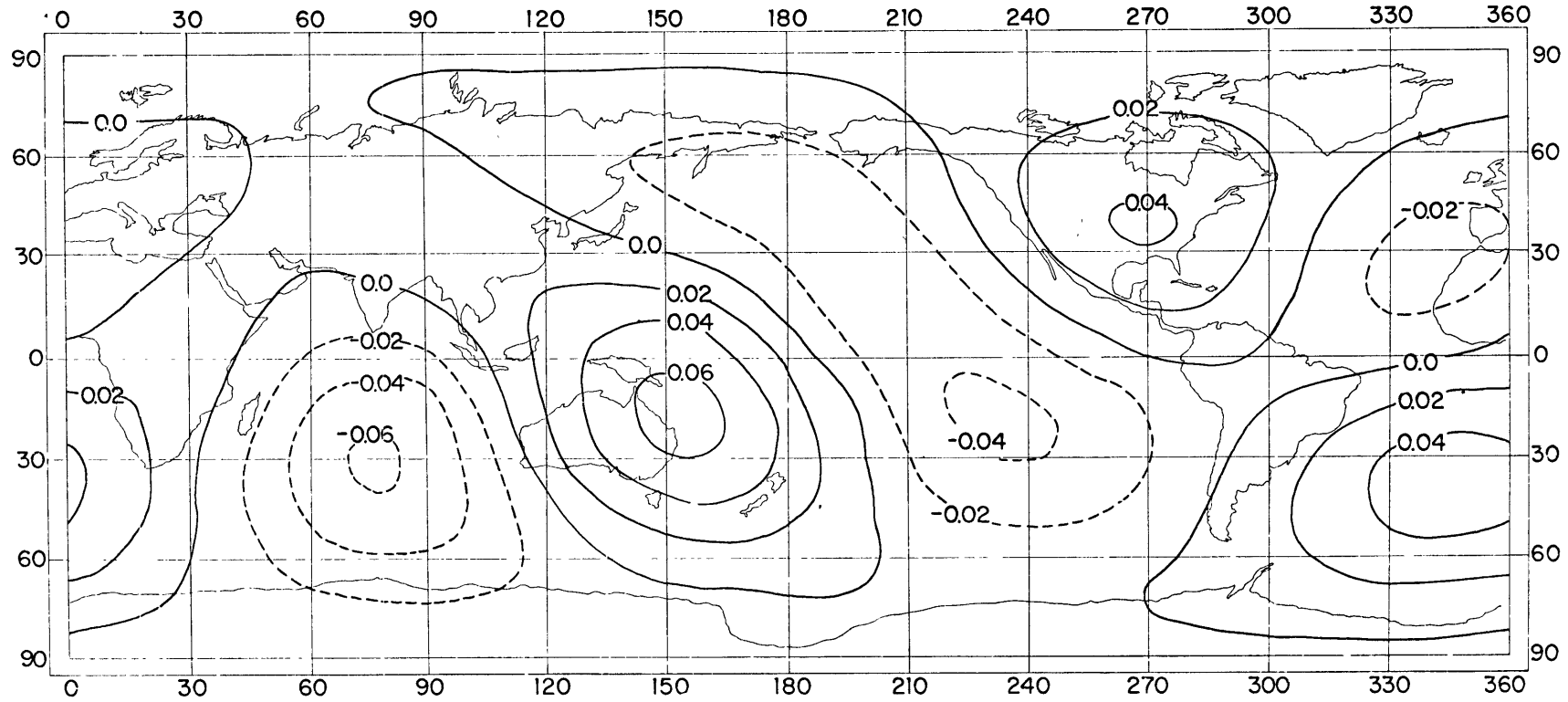
0 30 60 90 120 150 180 210 240 270 300 330 360
90 60 30 0 30 60 90
0.0
0.0
0.0
0.02
0.04
0.06
-0.02
-0.04
-0.06
0.02
0.04
-0.02
-0.04
-0.02
0.0
0.02
0.04

Fig.(3-9)

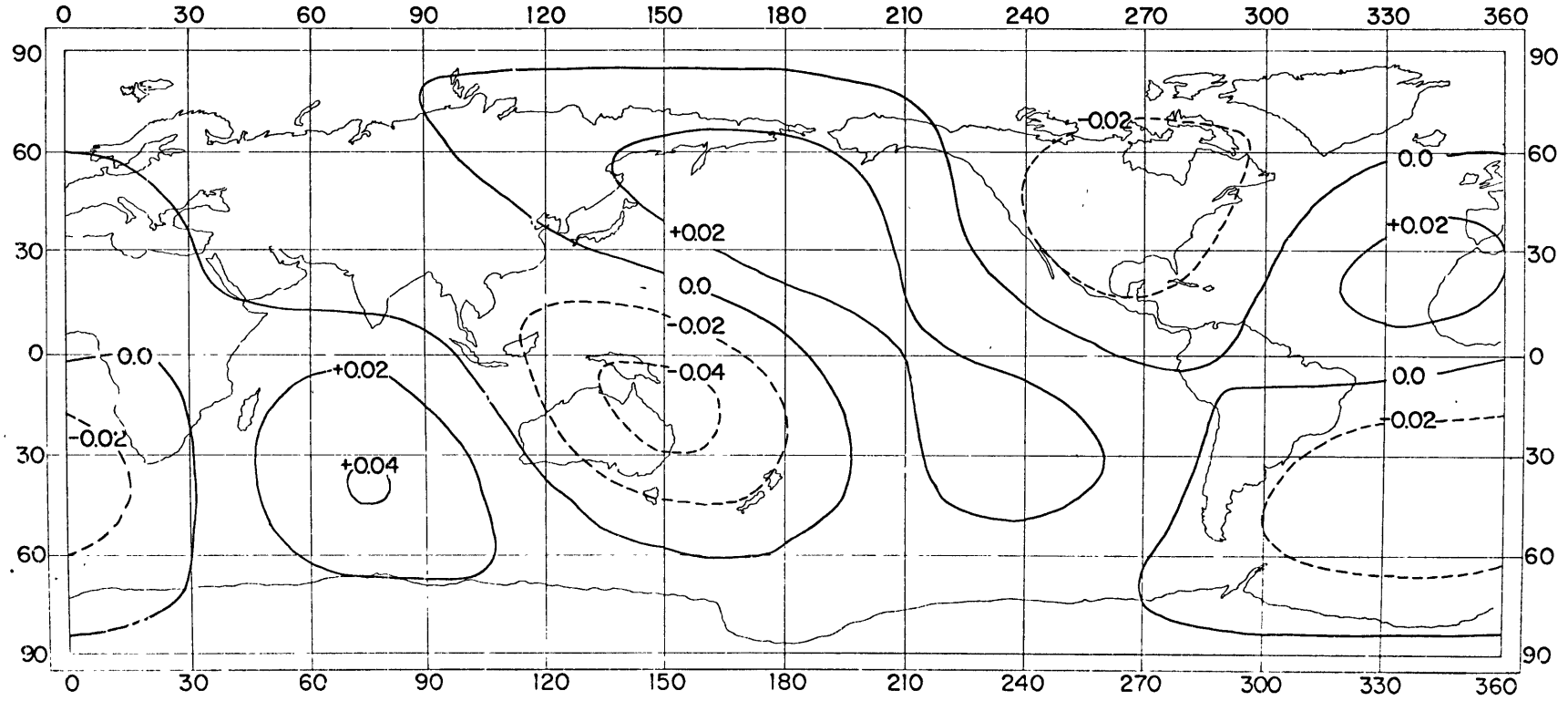
0
30
60
90
120
150
180
210
240
270
300
330
360
90
60
30
0
30
60
90
+0.02
0.0
-0.02
-0.04
-0.02
0.0
+0.02
+0.04
-0.02
0.0
+0.02
0.0
-0.02

Fig. (3-10)

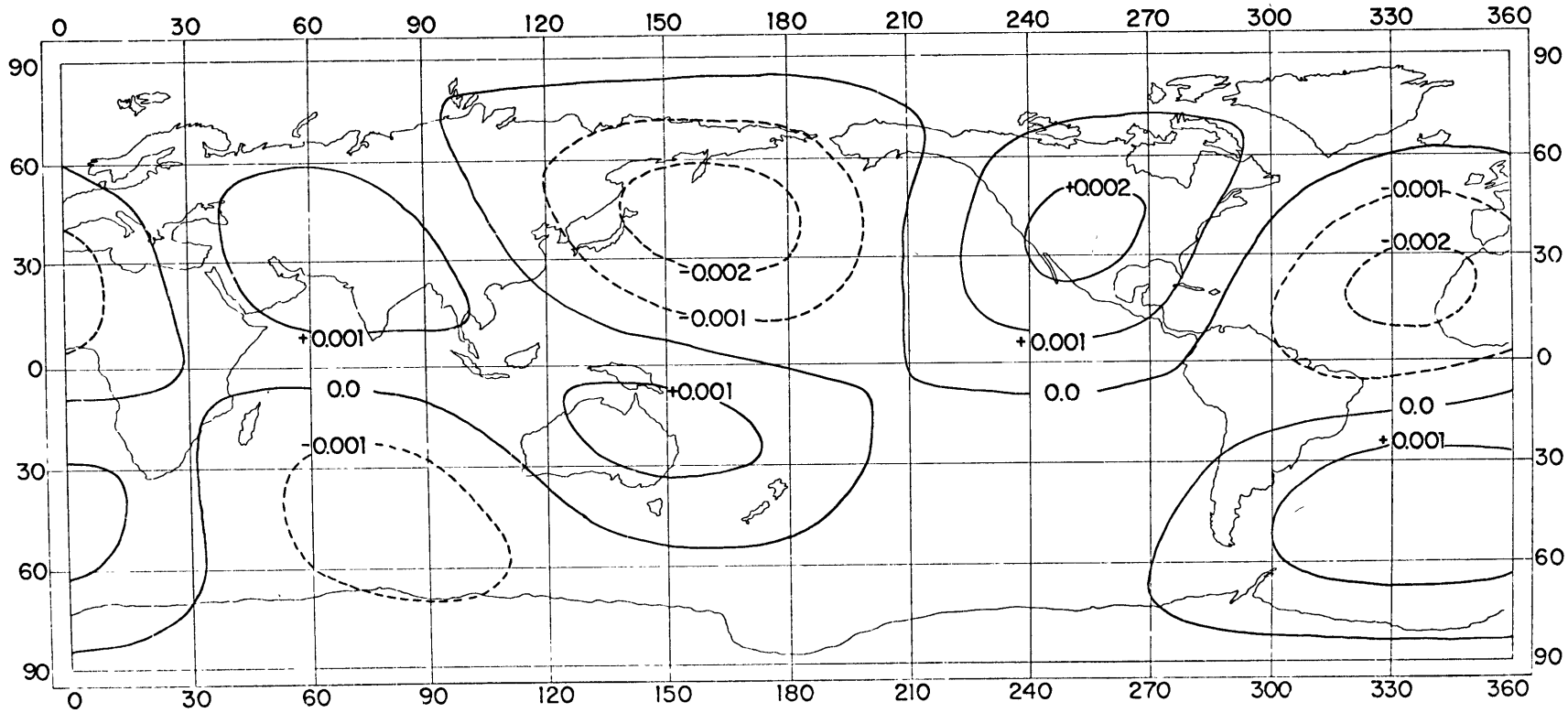
0
30
60
90
120
150
180
210
240
270
300
330
360
90
60
30
0
30
60
90
+0.001
0.0
-0.001
-0.002
-0.001
+0.001
+0.002
+0.001
0.0
-0.001
-0.002
0.0
+0.001

Fig. (3-11)

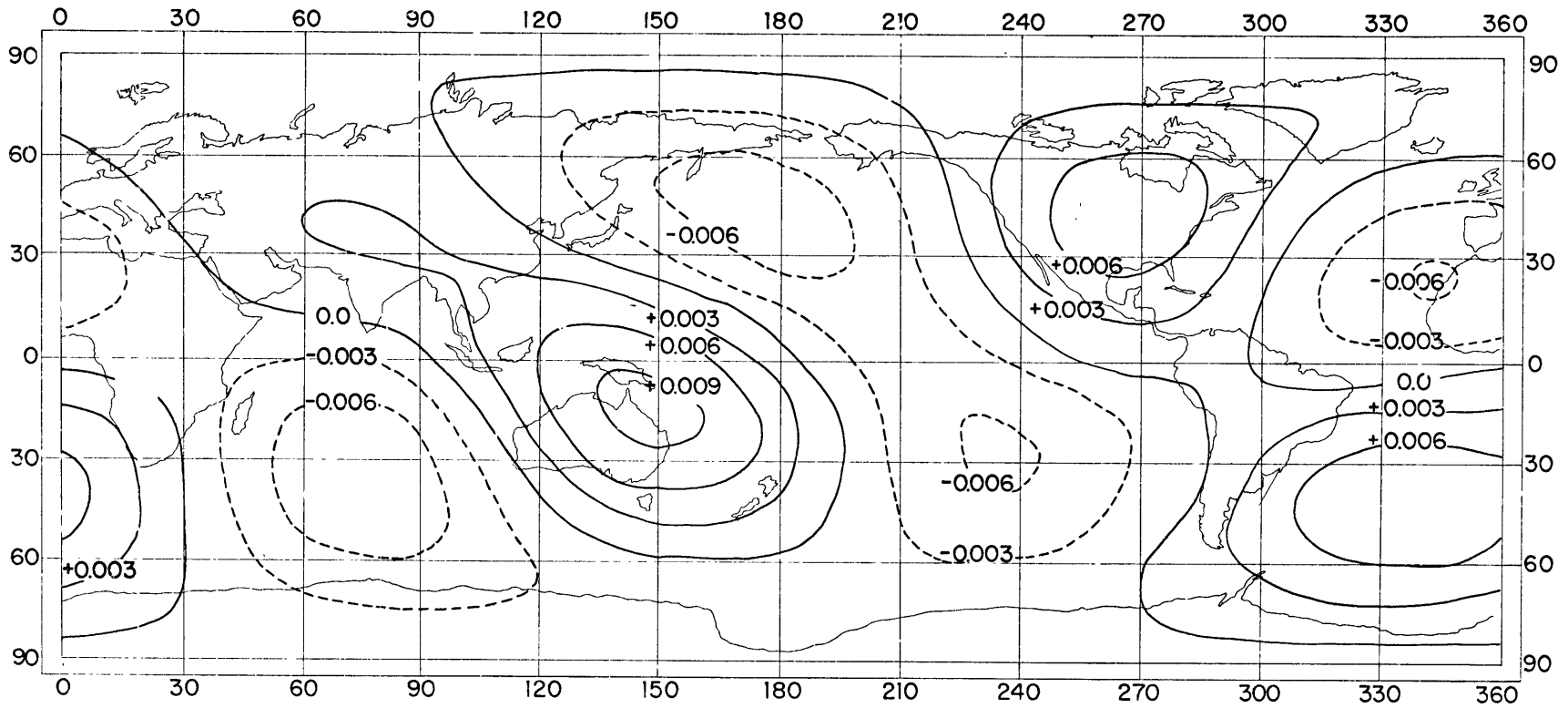
0
30
60
90
120
150
180
210
240
270
300
330
360
90
60
30
0
30
60
90
-0.006
+0.006
+0.003
-0.006
0.0
+0.003
+0.006
-0.003
+0.009
-0.006
+0.003
-0.006
-0.003
-0.006
-0.003
0.0
+0.003
+0.006

Fig.(3-12)

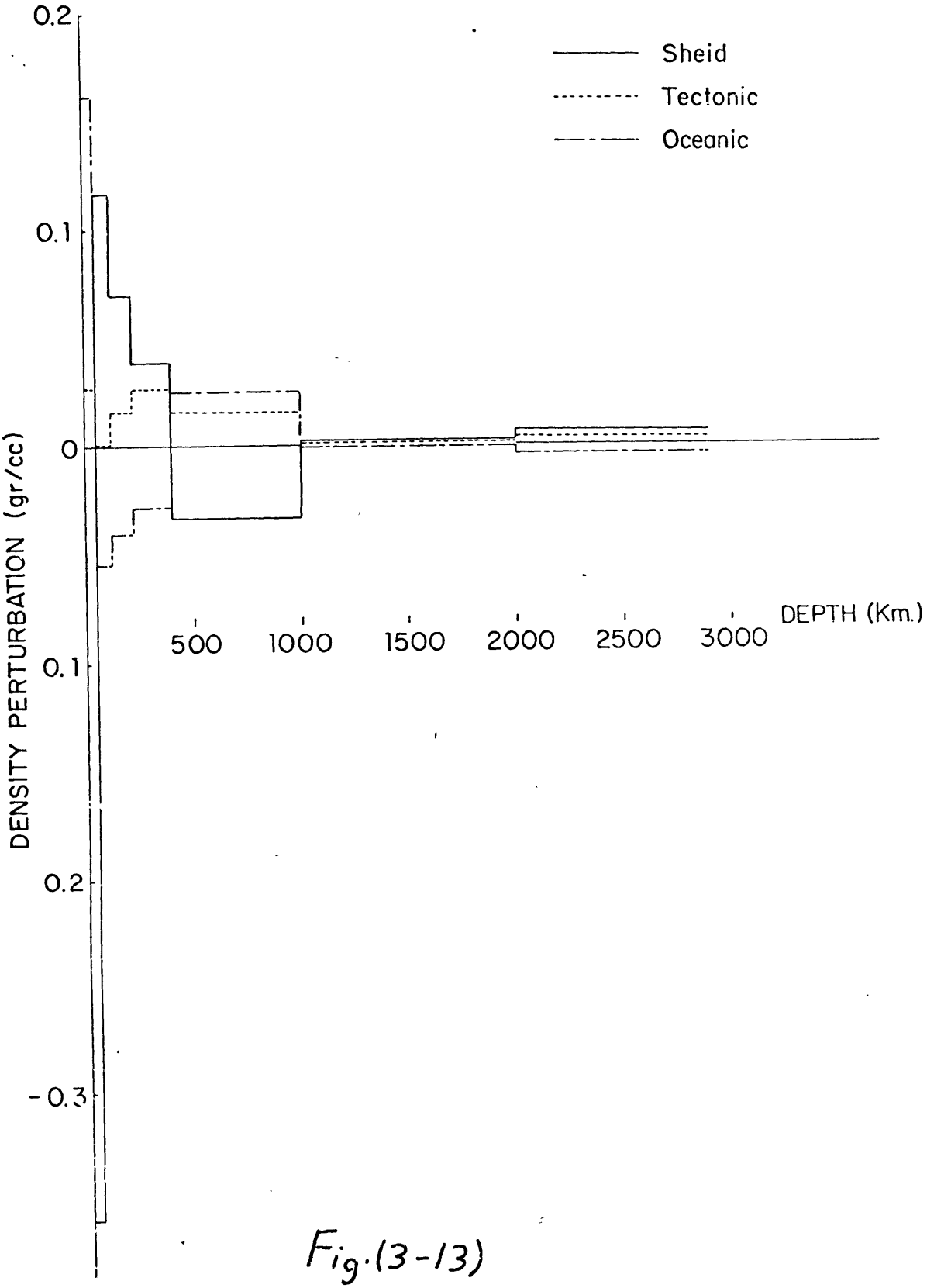
0.2
0.1
0
0.1
0.2
-0.3
DENSITY PERTURBATION (gr/cc)
Sheid
Tectonic
Oceanic
500
1000
1500
2000
2500
3000
DEPTH (Km.)

Fig. (3-13)

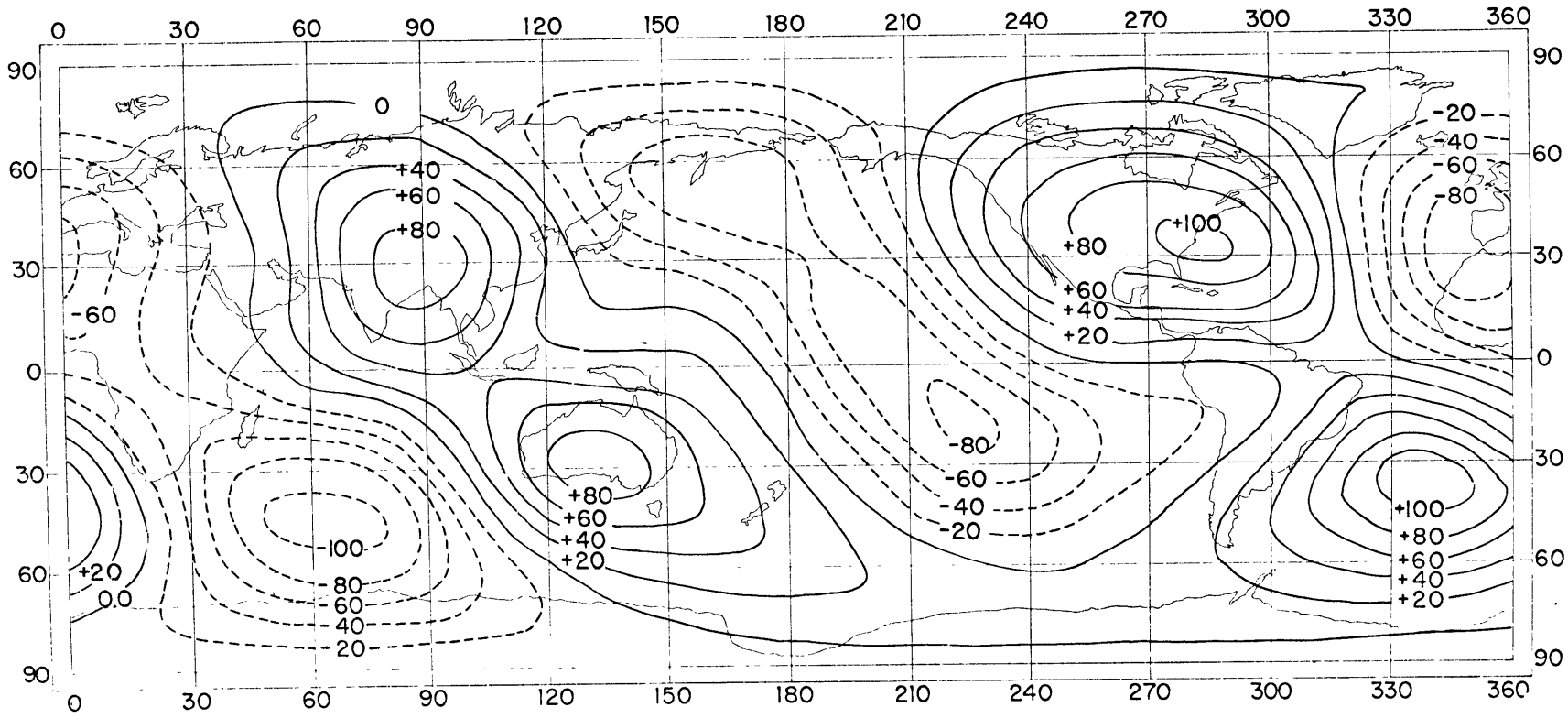
0 30 60 90 120 150 180 210 240 270 300 330 360
90 60 30 0 30 60 90
0
+40
+60
+80
-60
-100
-80
-60
-40
-20
+20
0.0
+80
+60
+40
+20
-80
-60
-40
-20
+80
+60
+40
+20
+100
-20
-40
-60
-80
+100
+80
+60
+40
+20

Fig. (3-14)

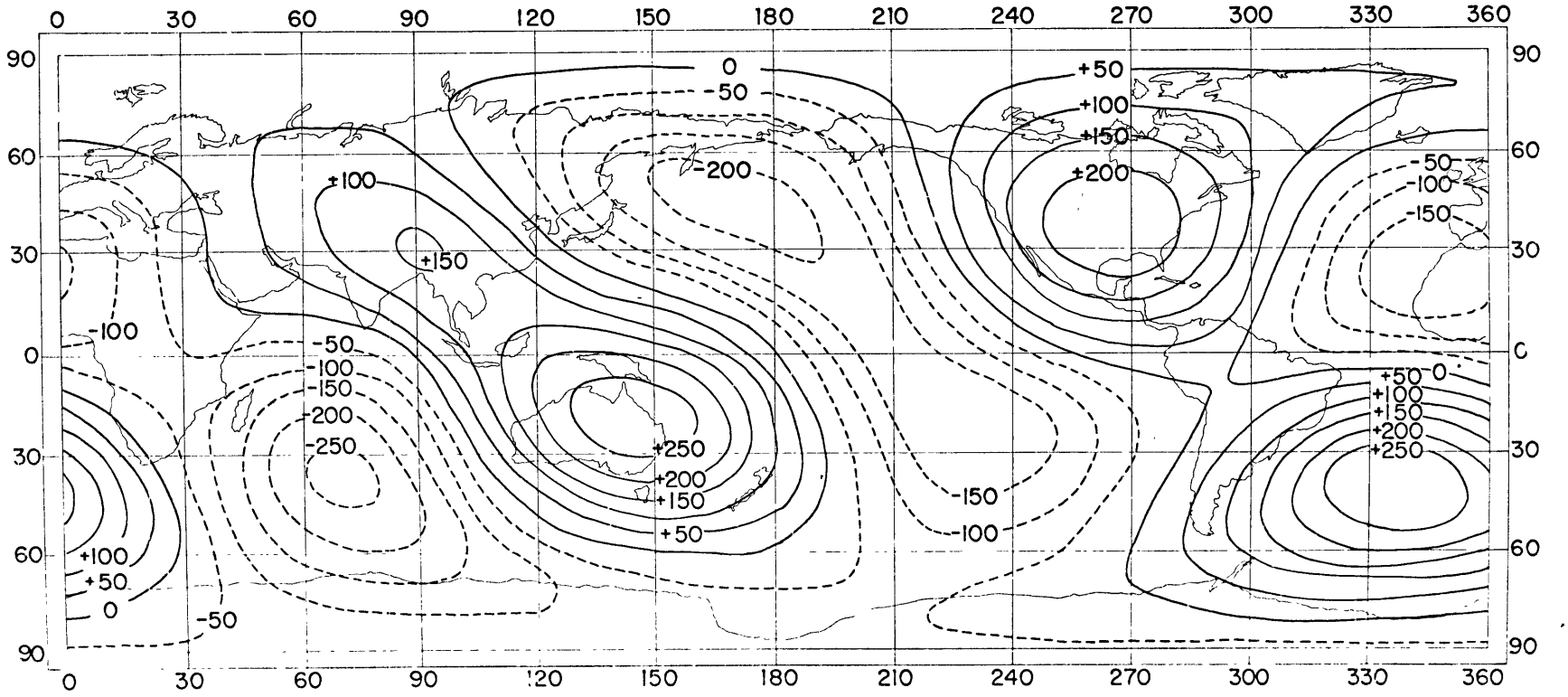
0 30 60 90 120 150 180 210 240 270 300 330 360
90 60 30 0 30 60 90
0
-50
+50
+100
+150
+200
-200
+100
+150
-100
-50
-100
-150
-200
-250
+250
+200
+150
+50
-150
-100
-50
-100
-150
+50
0
+100
+150
+200
+250
+100
+50
0
-50

Fig. (3-15)

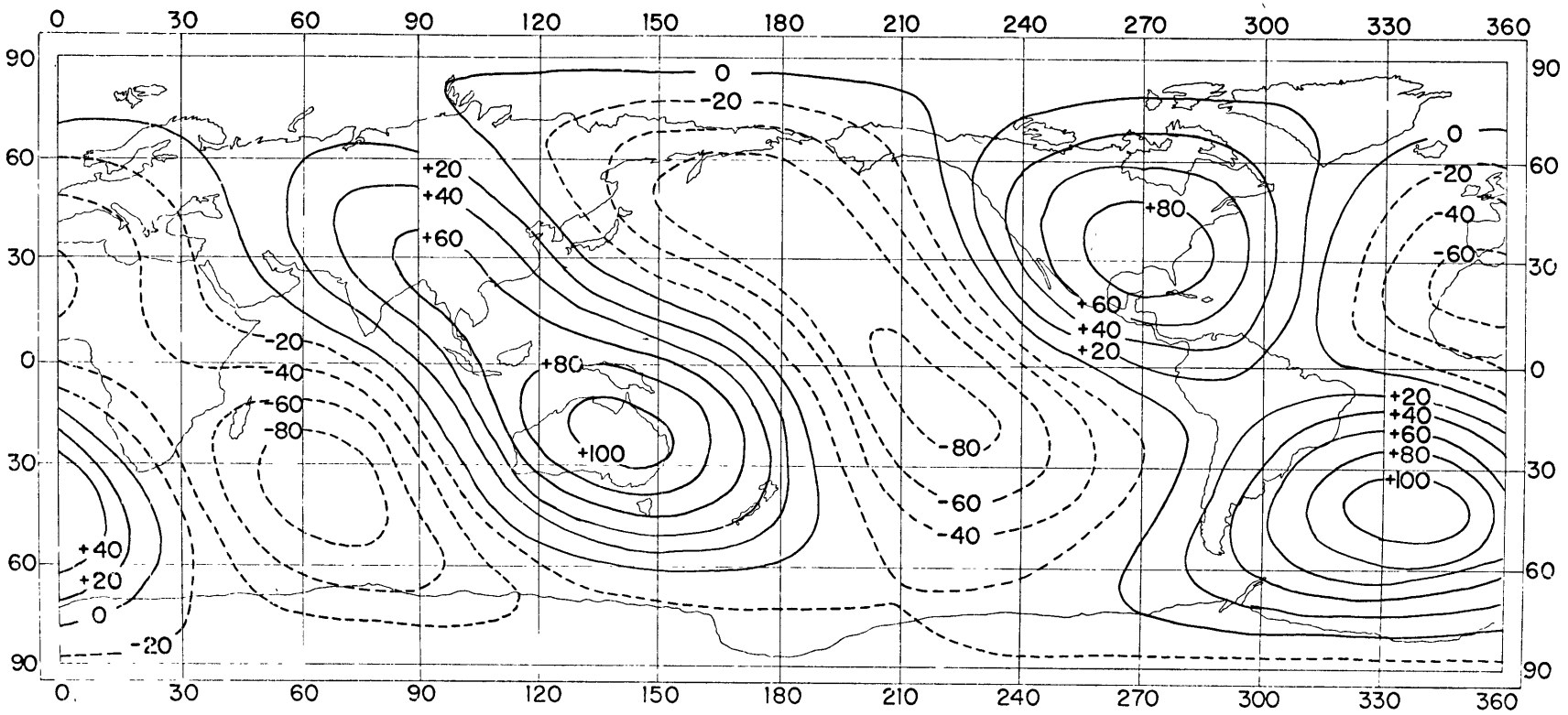
0 30 60 90 120 150 180 210 240 270 300 330 360
90 60 30 0 30 60 90
0
-20
+20
+40
+60
-20
-40
-60
-80
+80
+100
+40
+20
0
-20
+80
+60
+40
+20
0
-20
-40
-60
-80
-60
-40
+20
+40
+60
+80
+100

Fig.(3-16)

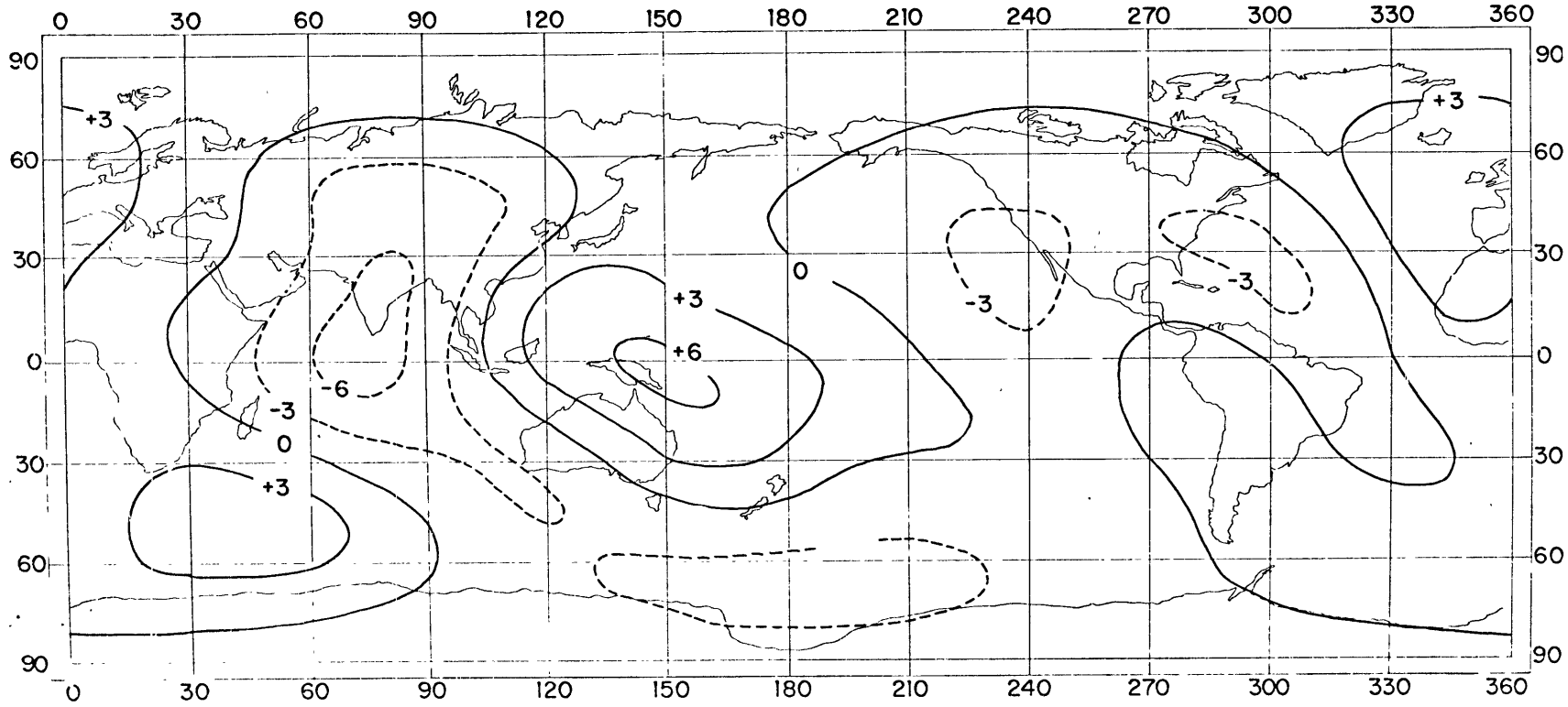
0
30
60
90
120
150
180
210
240
270
300
330
360
90
60
30
0
30
60
90
+3
+3
+6
0
-3
-3
-6
-3
0
+3

Fig. (3-17)

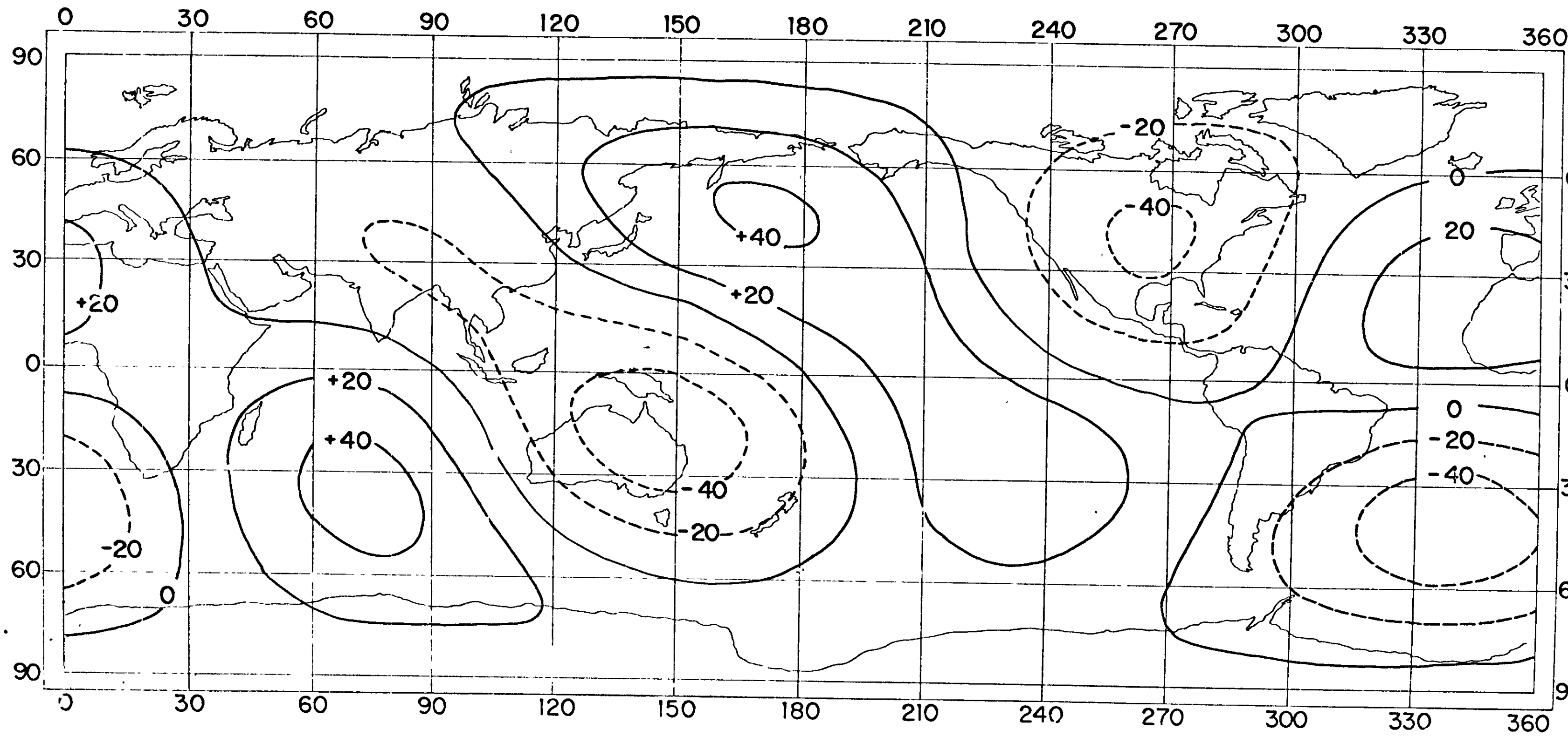

0
30
60
90
120
150
180
210
240
270
300
330
360
90
60
30
0
30
60
90
+40
+20
-20
-40
0
20

Fig. (3-18)

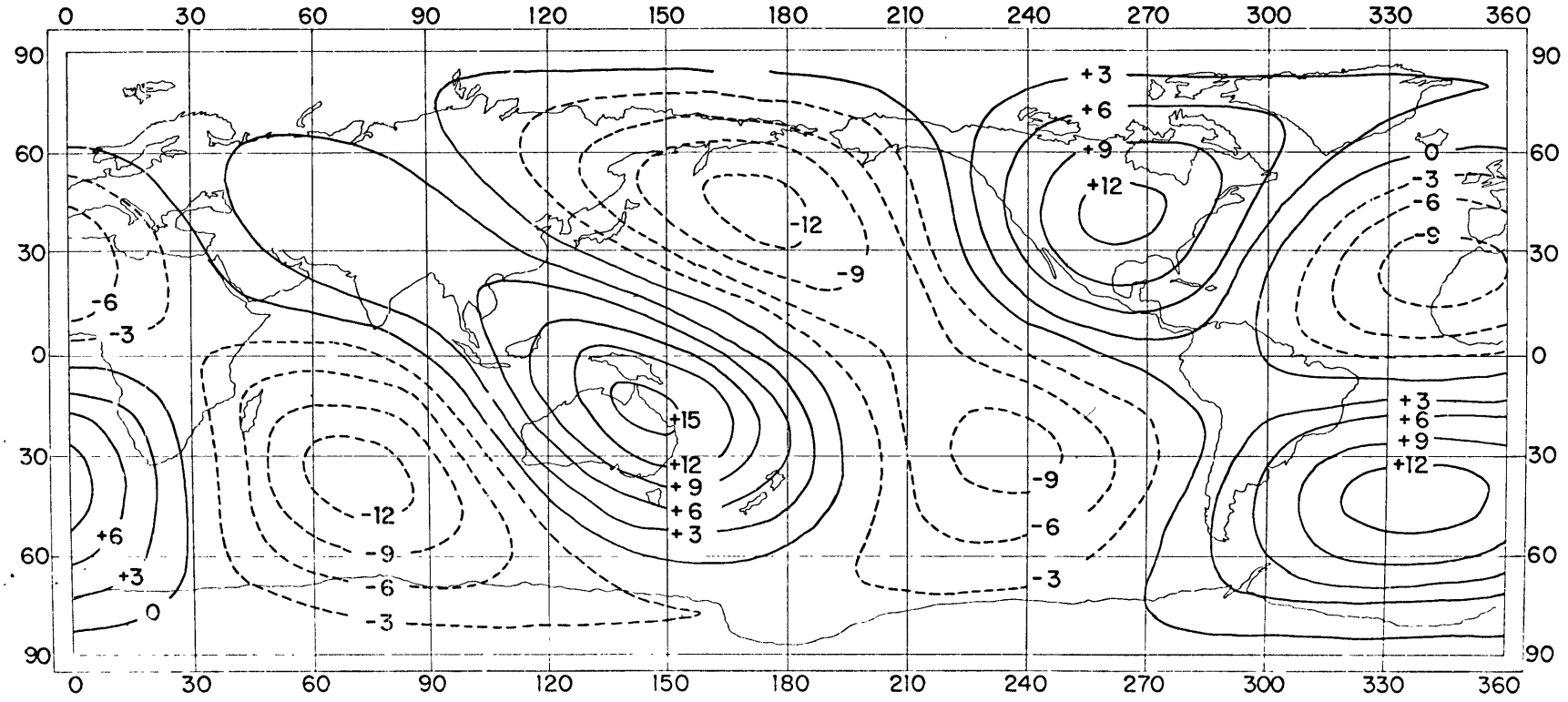
0
30
60
90
120
150
180
210
240
270
300
330
360
90
60
30
0
30
60
90
+3
+6
+9
+12
0
-3
-6
-9
-12
-9
-6
-3
+15
+12
+9
+6
+3
-12
-9
-6
-3
+6
+3
0
-9
-6
-3
+3
+6
+9
+12

Fig.(3-19)

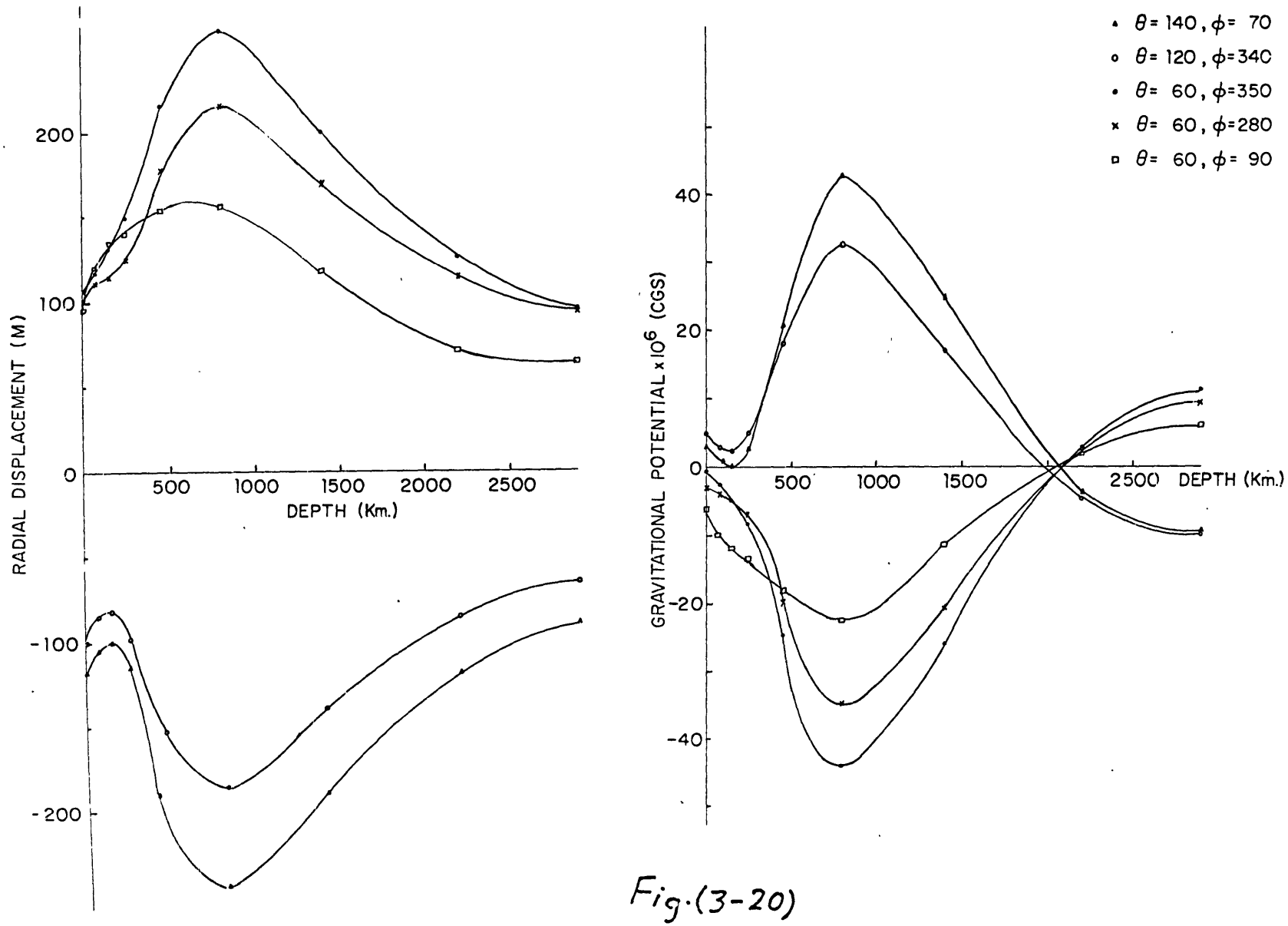
RADIAL DISPLACEMENT (M)
200
100
0
-100
-200
500
1000
1500
2000
2500
DEPTH (Km.)
GRAVITATIONAL POTENTIAL x 10^6 (CGS)
40
20
0
-20
-40
500
1000
1500
2500
DEPTH (Km.)
θ = 140, φ = 70
θ = 120, φ = 340
θ = 60, φ = 350
θ = 60, φ = 280
θ = 60, φ = 90

Fig.(3-20)

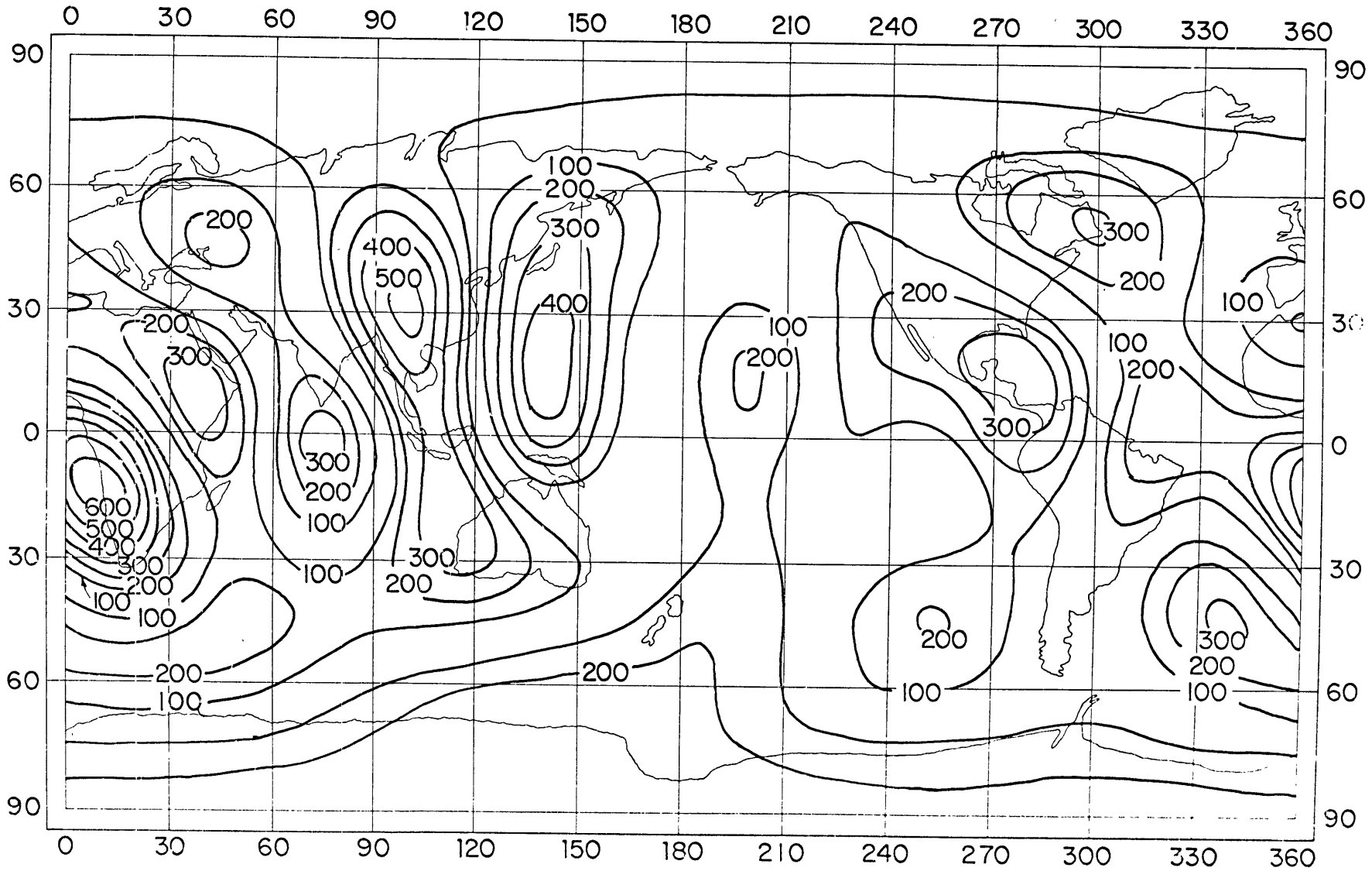
0 30 60 90 120 150 180 210 240 270 300 330 360
90 60 30 0 30 60 90
100 200 300 400 500 600

Fig. (3-21)

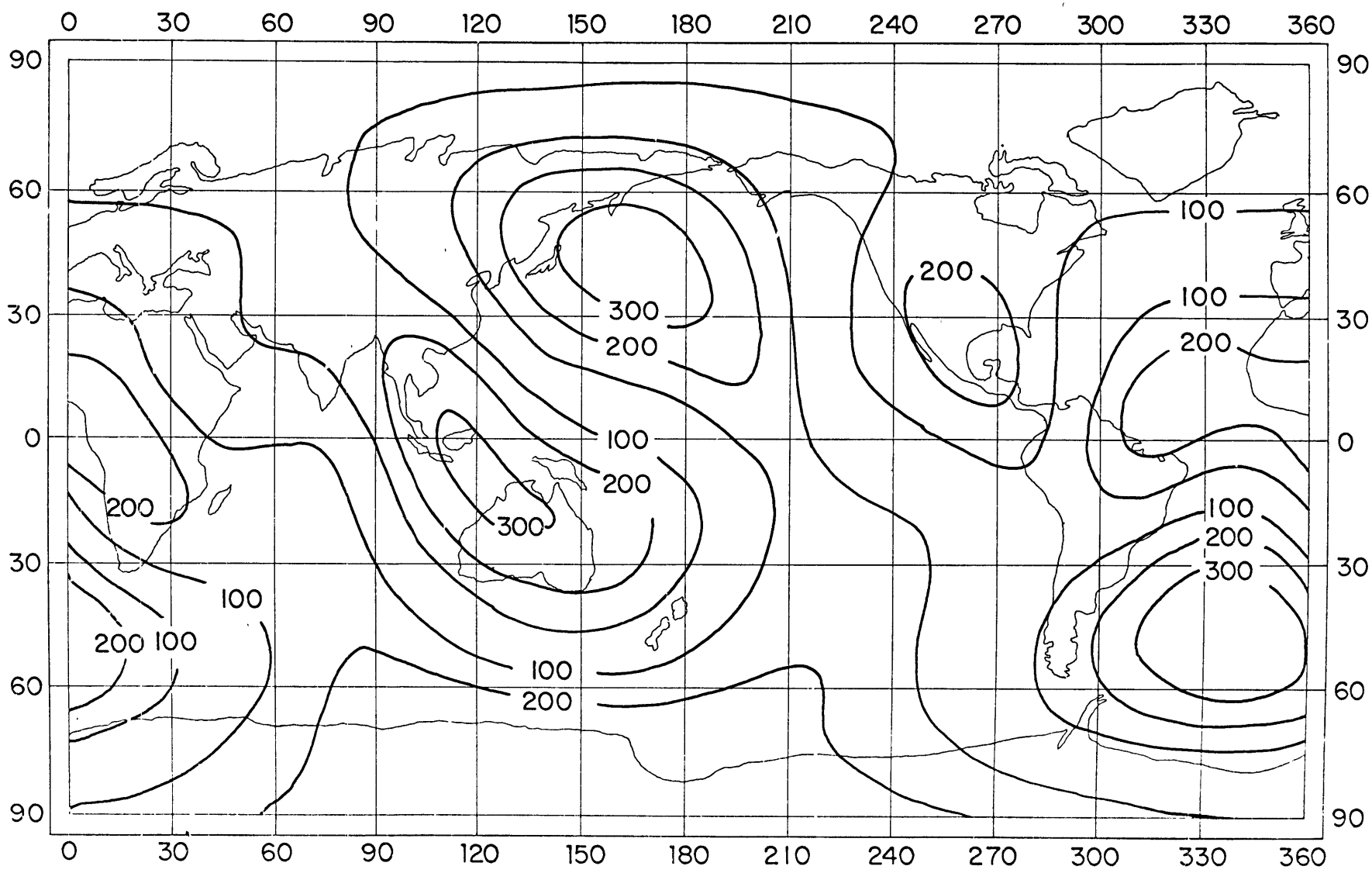
0 30 60 90 120 150 180 210 240 270 300 330 360
90 60 30 0 30 60 90
300
200
100
200
100
200
100
200
300
100
200
100
200
100
200
300

Fig.(3-22)

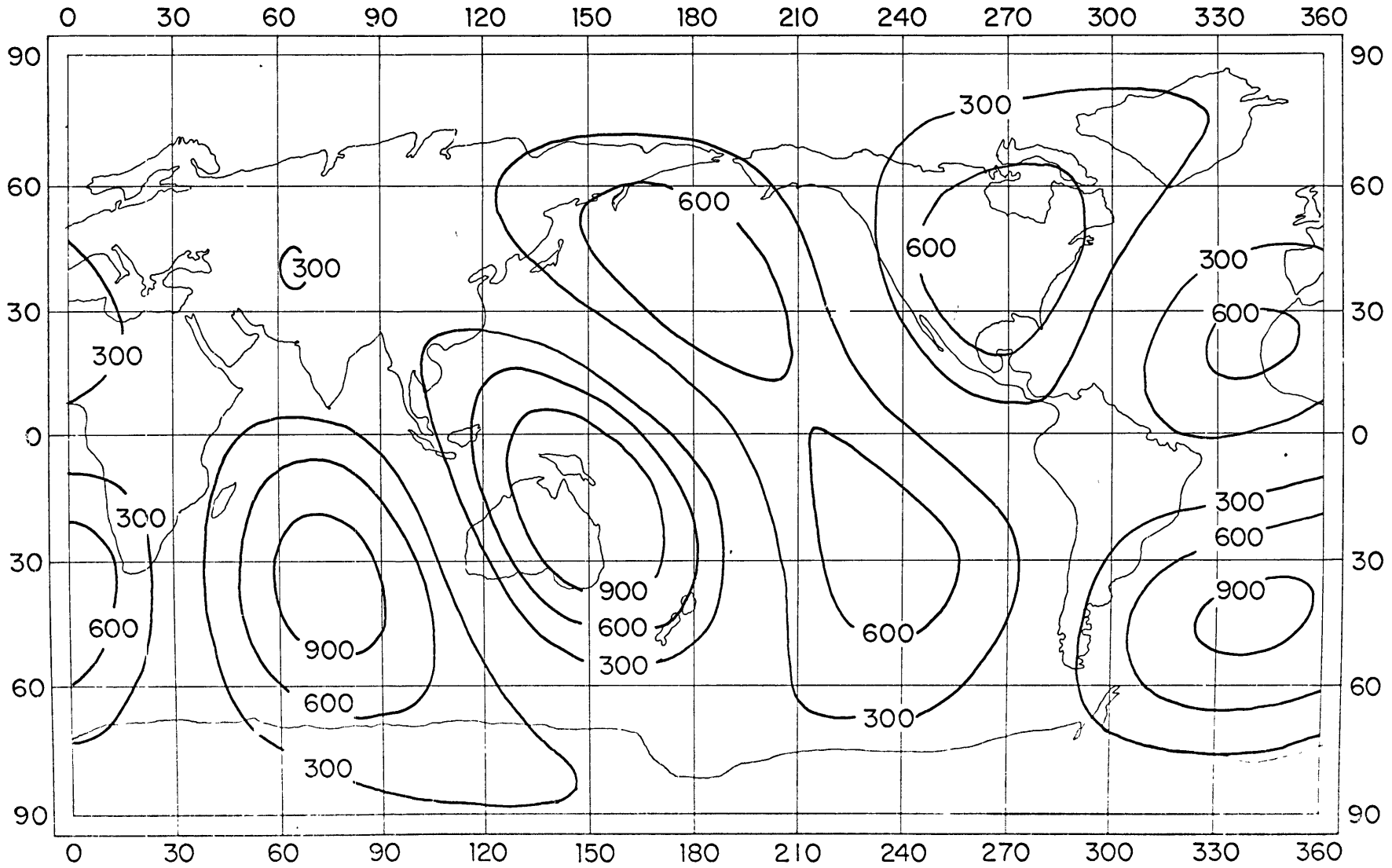
0 30 60 90 120 150 180 210 240 270 300 330 360
90 60 30 0 30 60 90
300
600
900

Fig.(3-23)

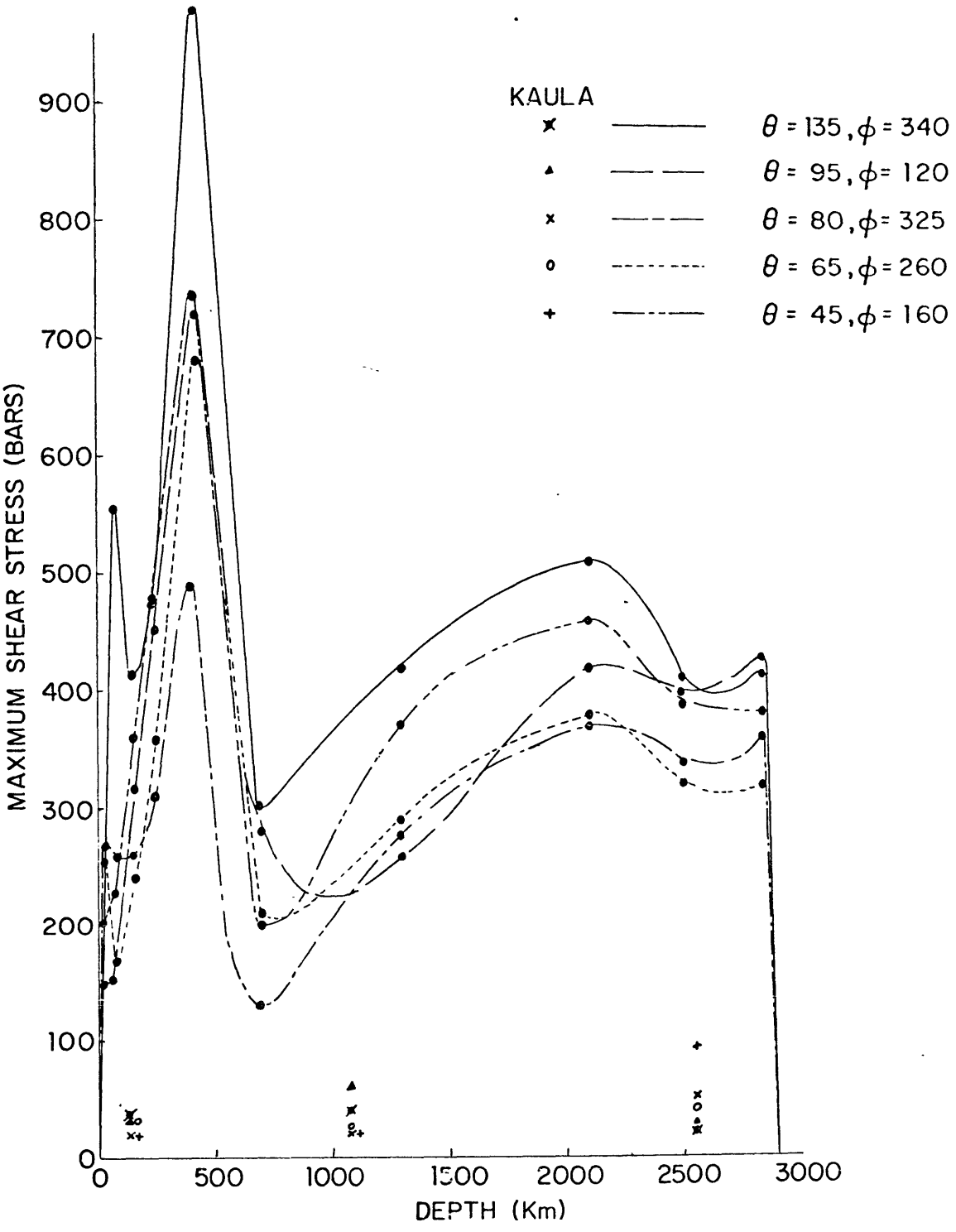
KAULA
θ = 135, ϕ = 340
θ = 95, ϕ = 120
θ = 80, ϕ = 325
θ = 65, ϕ = 260
θ = 45, ϕ = 160
MAXIMUM SHEAR STRESS (BARS)
DEPTH (Km)
0
100
200
300
400
500
600
700
800
900
0
500
1000
1500
2000
2500
3000

Fig. (3-24)

CHAPTER 4

Geophysical Interpretation of the Density Anomalies

In Chapter 3 we were concerned with the mathematical studies of the elastic deformation of an earth model subject to the surface and body loads. We solved a boundary value problem, through which the density perturbations in the mantle were determined. This chapter is devoted to the geophysical interpretation of these density anomalies. Before going into the interpretation let us emphasize, once more, that the solution of the problem is not unique. The density anomalies selected have relatively smooth radial variations and satisfy the boundary conditions imposed, while they produce a minimum total shear strain energy in the earth. Furthermore, these density anomalies yield the seismic travel time residuals and the gravitiational perturbations similar to those discussed in Chapter 2.

In this chapter we compare the computed density anomalies and the corresponding stress field in the earth with the lateral variations of the seismic structure of the mantle and tectonically active regions. We also discuss the anelastic behavior of the earth and determine the relaxation time of the stress field.

(4-1) - Lateral variations of seismic structure of the mantle

Lateral variations of the upper mantle velocities have been observed (Dorman, et al., 1960; Takeuchi, et al., 1962; and Toksöz,

et al., 1967), and it has been concluded that the oceanic and the continental upper mantle shear wave velocities differ by about 0.3 km./sec. Assuming that the variations of P and S wave velocities of the upper mantle are related by:

$$\delta V_p = [(2\sigma-2)/(2\sigma-1)]^{1/2} \cdot \delta V_s \qquad (4\text{-}1)$$

where σ is Poisson's ratio ($\sigma \sim .28$), the corresponding lateral variation of P wave velocity is found to be about 0.5 km./sec. On the other hand, Hayles and Doyle's (1967) empirical relationship for the upper mantle beneath the United States:

$$\delta V_p = 0.8\, \delta V_s \qquad (4\text{-}2)$$

yields a value of about 0.2 km./sec. Therefore, lateral variations of approximately 0.3 km./sec. seem to be plausible for P wave velocities in the upper mantle. Using Birch's (1964) equation, these variations correspond to density perbations of about 0.1 g/cc which agrees with the average density difference between the shield and the oceanic upper mantle obtained in our study.

Very little study has been devoted to lateral variations in the lower mantle. From his studies of the $\partial t/\partial \Delta$ curves of seismic arrivals at LASA, Montana, Fairborn (1968) deduced a value of about 0.1 km./sec. for the lateral variation of the P wave velocity at about

1900 km. depth. Assuming that this velocity variation is due to the density difference we determine the latter by Anderson's (1967) equation of state,

$$\rho = 0.048\, \bar{m}\, \phi^{0.323} \tag{4-3}$$

where

$$\phi = V_p^2 - \frac{4}{3} V_s^2 \tag{4-4}$$

and $\bar{m}$ is the mean atomic weight. Differentiating equation (4-3) with respect to V_p at constant radius yields

$$\left(\frac{\partial \rho}{\partial V_p}\right)_r = 0.0155\, \bar{m}\, \phi^{-0.677} \left(\frac{\partial \phi}{\partial V_p}\right)_r + 0.048\, \phi^{0.323} \left(\frac{\partial \bar{m}}{\partial V_p}\right)_r \tag{4-5}$$

setting $\sigma = .29$ (Birch, 1952), $V_p = 12.8$ km./sec., $V_s = 6.9$ km./sec. (Table 3-1), and $\bar{m} = 22$, equation (4-5) is then reduced to

$$\left(\frac{\partial \rho}{\partial V_p}\right)_r = 0.24 + 0.21 \times \left(\frac{\partial \bar{m}}{\partial V_p}\right)_r \tag{4-5a}$$

$\left(\partial \bar{m}/\partial V_p\right)_r$ equals zero if we assume no lateral variations of the chemical composition at 1900 km. depth. In that case

$$\Delta \rho = 0.24\, \Delta V_p \tag{4-5b}$$

which yields a lateral density variation of .024 g/cc at that depth. This density variation is larger than the maximum value of 0.01 g/cc, obtained in Chapter 3. Thus, both in the upper and the lower mantles the lateral density variations computed in this study are comperable with, or less than, those implied by the seismic observations.

(4-2) - Strenght of the Mantle

It is pertinent to question whether the real mantle can support the stress field obtained in Chapter 3. Very little is known about the creep strengths of materials at the high temperature and pressure conditions existing in the mantle. Therefore, we can only estimate them either by extrapolating laboratory data or from other geophysical measurements, such as the gravity anomalies or the stress drops through earthquakes.

A few laboratory data are available for igneous rocks (Lomnitz, 1956; Griggs and Handin, 1960). In any case the environmental conditions (confining pressure, temperature and strain rate) achieved in the laboratory experiments are not representative for the mantle. The confining pressures and temperatures employed in the laboratory studies are too low and the strain rates are too high in comparison with the conditions in the mantle (Heard, 1968). Nevertheless, from the extrapolation of the laboratory measurements,

a creep strength on the order of 100 bars has been postulated for the mantle materials (Orowan, 1960; and Robertson, 1964).

The gravity anomalies such as those associated with the Appalachian Mountains, Hawaii, and the Indonesian arc, indicate a value of about 100 bars for the strength of the mantle (Jeffreys, 1943; Birch, 1955, 1964). Moreover, to support the extra buldge of the equator a minimum strength of approximately 40 bars is required for the mantle materials (Jeffreys, 1964; and Caputo, 1965).

Additional information about the strength (most probably the yield strength) of the mantle can be deduced from the stress drops associated with earthquakes. For intermediate magnitude earthquakes, stress drops of about 100 to 1000 bars are estimated at focal depths between 10 to 700 km. (Aki, 1965; Berckhemer and Jacob, 1968).

In summary, the available data indicate a creep strength of about a hundred bars for the mantle materials, though their yield strengths may be as high as one thousand bars. The average value of maximum shear stresses resulted from our computed density anomalies, however, is about 400 bars (Figures 3-21 to 24). Therefore, we conclude that the real mantle can not support the density anomalies presented in Chapter 3 and the density anomalies will diminish in time unless they are supported by some dynamic processes.

(4-3) - Tectonically active regions

Although the radial variations of the maximum shear stresses obtained in Chapter 3 depend on the choice of the radial variations of the density anomalies, their lateral variations depend strongly on the input data (the lateral perturbations of geopotential, surface topography of the earth, density anomalies in the crust and the upper mantle deduced from seismic data). These input data are closely related to the real earth. Therefore, assuming that the earthquake foci are the regions where the existing shear stresses exceed the strength of the materials, it would be interesting to compare these regions with the maximum shear stresses obtained in Chapter 3.

Figure (4-1) shows the geographic location of the earthquakes with focal depths from 0 - 100 km. which occured from 1961 through 1967 (Barazangi and Dorman, 1968). Comparison of this figure with figure (3-21) indicates that the maxima of the shear stresses correlate with the earthquake epicenters in Central America, the west Pacific region, and the eastern part of India. These are the regions where our input data were reliable and relatively abundant. The correlation is very poor where no data were available and the spherical harmonic representations of the input data were unreliable. Such is the case for the western part of South America. The lack of correlation between the maxima of the shear-stress field and deep earthquake epicenters is most probably due to the

localization of the epicenters which cannot be resolved by the low degree spherical harmonics considered in the present study.

(4-4) - Relaxation Time of Stress Field

It has been pointed out previously in this chapter that the shear stresses associated with the density perturbations obtained in Chapter 3 are larger than the creep strength of the mantle. Thus, the density anomalies can either be created by some dynamic process such as convection (Runcorn, 1964) or be the residuals of large anomalies creater in the past that are presently decaying (Munk and MacDonald, 1960; and McConnel, 1968). With the available geophysical data it is difficult to study the time variations of the former cast. Considering the latter one, however, it is interesting to find out the relaxation time of the stress field associated with the density anomalies.

Relaxation times of surface loads with horizonal dimensions of about 2000 km. have been observed to be about 4000 years (Heiskanen and Vening Meinesz, 1958; and McConnel, 1965, 1968). For the surface loads specified by the second degree harmonics, such as the extra bulge of the equator, time constants varying between a thousand to about one hundred million years are proposed (Jeffreys and Crampin, 1960; Munk and MacDonald, 1960; Wang, 1966; and, McConnel, 1968).

For the perturbations specified by the spherical harmonics with, n - 1, . . . , 6, the relaxation time of a surface load does not differ

significantly from that of a body load. In comparison with the lateral dimensions of these harmonics, the mantle is like a shell whose responses for surface and body loads differ by less than a factor of 2. To demonstrate this behavior the radial displacements of the earth model adopted in Chapter 3 (Table 3-1) are determined for a mass anomaly distributed; a) on the earth's surface; and, b) from the surface to the core-mantle boundary, with constant radial dependence. The following table shows the ratio of these displacements at the earth's surface for different zonal harmonics

n	y_1 surf. / y_1 body
2	1.09
3	1.19
4	1.43
5	1.67
6	1.96

Assuming that the mantle of the earth model obeys the creep law of Jeffreys (1958) and following Jeffreys and Crampin (1960), the relaxation times of the stress fields produced in the earth by the surface loadings, are computed and listed in Table (4-1). It is evident from the table that Jeffreys' creep law yields longer relaxation times than the viscous models used in other studies. With the present knowledge about the earth's interior it is difficult to draw conclusions about the relaxation times of the stress field in the earth. But, it is most likely that the low viscosity upper mantle will play an important

role in the decay of the loads.

(4-5) - Comparison with Model 1 of Kaula (1963)

To compare our density model with Model 1 of Kaula (1963), the degree powers of Kaula's crustal density and the density of the surface layer presented in Chapter 2 are computed and listed in Table (4-2). It is evident from the table that the density anomalies of our surface layer are about twice as large as Kaula's crustal density variations. This table also includes the degree correlation coefficients that display a negative correlation for the second degree harmonic and positive ones for the higher harmonics. In the case of the mantle, Kaula has only listed the maximum values of the density perturbations which are about two orders of magnitude smaller than the ones listed in table (3-3). This difference is due to 1) the large upper mantle density anomalies deduced from P wave travel time residuals, and 2) the difference between his polynomial model and the layered model adopted in the present studies.

Because of the large density anomalies the corresponding deformations and stress fields obtained in Chapter 3 are, respectively, about twice and four times greater than Kaula's results.

(4-6) - Conclusion

The main interest in this thesis has been to determine the lateral variations of density in the mantle, which gives rise to a gravitational field similar to the one deduced from artificial satellite data and which also takes into account the lateral variations of crustal thickness and P wave travel time residuals. We have been concerned with broad features specified by spherical harmonics through the sixth degree. From these studies the following conclusions can be deduced:

1) There is no linear correlation between geopotential and surface topography or crustal thickness. Thus, the perturbations of geopotential are due to density anomalies existing deep in the mantle.

2) P wave travel time residuals exhibit good correlation with crustal thickness. The negative sign of their correlation coefficients imply that the thicker crust is associated with shorter travel time and vice versa. Bearing in mind that the continental crust is thicker and has lower seismic velocity than the oceanic one, this correlation indicates that the upper mantle seismic velocities under continents are higher than those under oceans.

3) The negative correlation between the P wave travel time residuals and the geopotential shows that a common source affects both phenomena.

4) Radial variations of the density models determined by minimizing only the shear-strain energy of the earth have oscillatory behaviors. These oscillations disappear when we minimize both the

shear-strain and the gravitational energy of the earth.

5) The selected density model is characterized by a decrease with depth. A maximum value of about 0.3 g/cc is found in the surface layer with 50 km. thickness. In the upper mantle density variations are about 0.1 g/cc and in the lower mantle about 0.04 g/cc. These density variations are within the values indicated by seismic staudies and also they are closer to the actual ones than those obtained by Kaula (1963).

6) The selected density anomalies produce maximum shear stresses of about 400 bars throughout the mantle which are larger than the creep strengths proposed for the mantle materials. Thus, the real earth, subject to these density variations, is in a creeping state and the corresponding stress field will decay in time with a relaxation time on the order of one million years.

At shallow depths (less than 100 km.) the maxima of the stress field fall, in general, at the epicenters of shallow earthquakes.

LIST OF TABLES FOR CHAPTER 4

Table (4-1)

Relaxation times of surface loads

n	τ (my)
2	24
3	60
4	120
5	220
6	360

Table (4-2)

Correlation of Kaula's (1963) crustal model with the density of the surface layer

n	Degree power $(g/cc)^2$		Correlation coefficient
	surface layer	Kaula's crust	
2	0.0040	0.0006	-.54
3	0.0053	0.0015	.94
4	0.0038	0.0013	.89

FIGURE CAPTIONS FOR CHAPTER 4

Figure

(4-1) Geographical locations of the epicenters of shallow earthquakes (0-100 km.) occurred from 1961 through 1967.

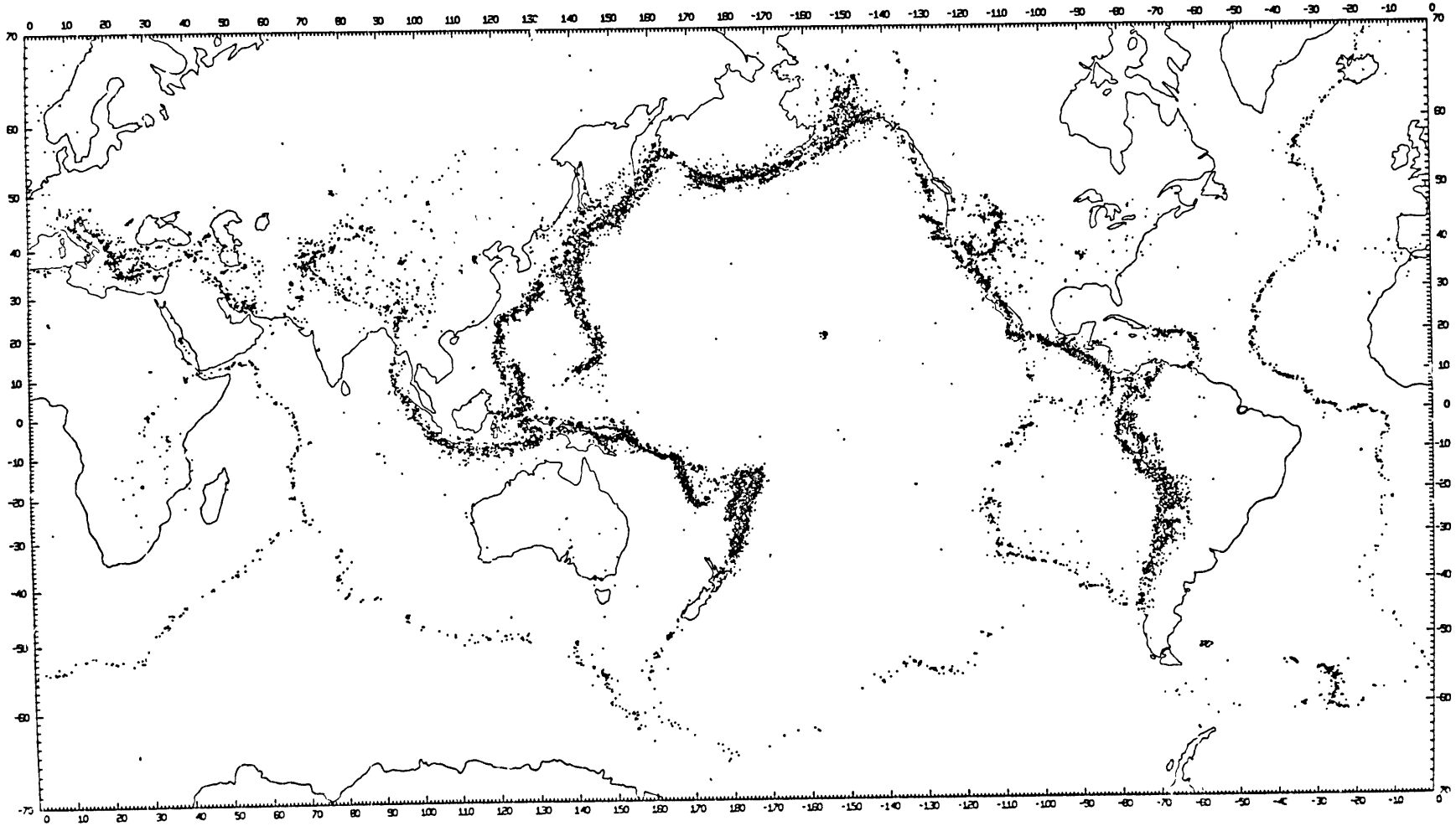

SEISMICITY OF THE EARTH, 1961-1967, ESSA, CGS EPICENTERS

Fig. (4-1)

CHAPTER 5

Suggestions for further studies

The density anomalies obtained through the treatments followed in the present studies suffer from two major areas: 1) the lack of sufficient available data, and 2) the unrealistic elastic model adopted for the mantle of the earth.

Having large amounts of crustal data, distributed all over the earth, will enable us to determine the density variations in the crust more accurately. The density anomalies in the upper mantle will be estimated more realistically from the large number of the observations on P and S wave travel time residuals by utilizing an adequate relationship between density and velocity which, in turn, will be obtained from the abundant laboratory measurements at high temperature and pressure conditions. The availability of large seismic arrays, such as LASA, at different parts of the earth will yield good information about the lateral variations in the properties of the lower mantle. This information together with the periods of the free oscillations of the earth can be used as an other independent constraint to be satisfied in computing the density anomalies in the mantle. To achieve this goal some intensive world wide studies are required which may take several decades.

To overcome the modeling errors it is necessary to adopt a thermo-visco-elastic mantle in our studies. A viscus mantle model has already been used to study post-glacial isostatic adjustments of small regions (McConnel, 1963; and, Crittenden, 1963). Most recently the deformation of a visco-elastic earth model subject to surface loading was also studied (Campbell, 1968). In the present chapter we formulate the equilibrium equations of a thermo-visco-elastic mantle model subject to surface as well as body loadings. The numerical computation of the boundary value problem analogous to the one treated in Chapter 3 is a suggestion for further studies.

(5-1)- Stress Analysis in a Thermo-Visco-Elastic Mantle

The fundamental equations for a thermo-visco-elastic mantle are the same as those for an elastic one except the stress-strain relationship (equation 3-5a) which should be modified in order to take into account the effects of temperature and viscosity.

Temperature variations in a medium causes a dilatational strain due to the thermal expansion of the medium and produces the following stress field (Sokolnikoff, 1956):

$$T_{ij} = -\alpha (3\lambda + 2\mu) \Theta \delta_{ij} \qquad (5\text{-}1)$$

Where Θ is the temperature and α is the volume thermal expansion coefficient.

The stress-strain relationship in a visco-elastic body can be expressed as (Lee, 1955, 1960):

$$P\, T_{ij} = Q\, e_{ij} \quad , \tag{5-2}$$

$$P'\, T_{ij} = Q'\, e_{ij} \tag{5-3}$$

where P, P', Q, and Q' are, in general, different polynomials of $\frac{\partial}{\partial t}$. That is,

$$(P, P', Q, Q') = \sum_i (p_i, p_i', q_i, q_i')\, \frac{\partial^i}{\partial t^i} \quad . \tag{5-4}$$

For the Maxwellian visco-elastic body (Bland, 1960)

$$\bar{t}_{ij} = \lambda \bar{e}_{kk}\, \delta_{ij} + 2\mu \bar{e}_{ij} + \eta \frac{\partial}{\partial t} \bar{e}_{ij} \quad . \tag{5-5}$$

Assuming that the visco-elastic properties of the mantle are approximately the same as a Maxwellian body, the stress-strain relationship of the mantle can be formulated by:

$$T_{ij} = \left[\lambda e_{kk} - p_o + u_r \frac{\partial}{\partial r} p_o - \alpha(3\lambda+2\mu)\Theta\right]\delta_{ij} + 2\left(\mu + \frac{\eta}{2}\cdot\frac{\partial}{\partial t}\right) e_{ij} \quad . \tag{5-6}$$

Replacing equation (3-5a) by equation (5-6) and following the same technique adopted in Chapter 3 yields the following differential equations.

$$\rho_o g_o \tilde{\Delta} + \rho_o \frac{\partial}{\partial r}\tilde{\psi} - \rho_o \frac{\partial}{\partial r}(g_o \tilde{u}_r) + \frac{\partial}{\partial r}\left[\lambda\tilde{\Delta} + (2\mu+\eta\gamma)\frac{\partial}{\partial r}\tilde{u}_r\right]$$
$$+ \frac{1}{r}\frac{\partial}{\partial\theta}\{(2\mu+\eta\gamma)\tilde{e}_{r\theta}\} + \frac{1}{r\sin\theta}\cdot\frac{\partial}{\partial\varphi}\{(2\mu+\eta\gamma)\tilde{e}_{r\varphi}\} - g_o\tilde{\delta\rho}$$
$$+ \frac{(2\mu+\eta\gamma)}{r}(2\tilde{e}_{rr} - \tilde{e}_{\theta\theta} - \tilde{e}_{\varphi\varphi} + \operatorname{cotan}\theta\,\tilde{e}_{r\theta}) - \frac{\partial}{\partial r}\{\alpha(3\lambda+2\mu)\tilde{\Theta}\} = 0 \qquad (5\text{-}7)$$

$$\frac{\rho_o}{r}\frac{\partial}{\partial\theta}\tilde{\psi} + \frac{\partial}{\partial r}\{(2\mu+\eta\gamma)\tilde{e}_{r\theta}\} + \frac{1}{r\sin\theta}\cdot\frac{\partial}{\partial\varphi}\{(2\mu+\eta\gamma)\tilde{e}_{\theta\varphi}\}$$
$$+ \frac{1}{r}\frac{\partial}{\partial\theta}\{\lambda\tilde{\Delta} - g_o\rho_o\tilde{u}_r + (2\mu+\eta\gamma)\tilde{e}_{\theta\theta}\} + \frac{(2\mu+\eta\gamma)}{r}\{3\tilde{e}_{r\theta} +$$
$$(\tilde{e}_{\theta\theta} - \tilde{e}_{\varphi\varphi})\operatorname{cotan}\theta\} - \frac{1}{r}\frac{\partial}{\partial\theta}\{\alpha(3\lambda+2\mu)\tilde{\Theta}\} = 0 \qquad (5\text{-}8)$$

$$\frac{\rho_o}{r\sin\theta}\cdot\frac{\partial}{\partial\varphi}\tilde{\psi} + \frac{\partial}{\partial r}\{(2\mu+\eta\gamma)\tilde{e}_{r\varphi}\} + \frac{1}{r}\cdot\frac{\partial}{\partial\theta}\{(2\mu+\eta\gamma)\tilde{e}_{\theta\varphi}\}$$
$$+ \frac{1}{r\sin\theta}\frac{\partial}{\partial\varphi}\{\lambda\tilde{\Delta} - g_o\rho_o\tilde{u}_r + (2\mu+\eta\gamma)\tilde{e}_{\varphi\varphi}\} + \frac{(2\mu+\eta\gamma)}{r}\{3\tilde{e}_{r\varphi} +$$
$$2e_{\theta\varphi}\operatorname{cotan}\theta\} - \frac{1}{r\sin\theta}\cdot\frac{\partial}{\partial\varphi}\{\alpha(3\lambda+2\mu)\tilde{\Theta}\} = 0 \qquad (5\text{-}9)$$

$$\nabla^2\tilde{\psi} - 4\pi G(\rho_o\tilde{\Delta} + \tilde{u}_r\frac{\partial}{\partial r}\rho_o - \tilde{\delta\rho}) = 0 \qquad (5\text{-}10)$$

Here $\tilde{\Delta}$ is the Laplace transformation of $\tilde{\Delta}$,

$$\tilde{\Delta} = \int_0^\infty \Delta\, e^{-\gamma t}\, dt \quad , \tag{5-11}$$

and so on. It is worthwhile to notice that equations (5-7 to 11) are analogous to those of the elastic case (equations 3-6 to 9) with the following differences:

1. The equations are expressed in terms of Laplace transformations of the variables.

2. The value $-\alpha(3\lambda+2\mu)\Theta$ contributes to the perturbations of the gravitational potential appearing in equations (5-8 to 10).

3. The rigidity μ is modified to $\mu + \frac{\eta\gamma}{2}$ in order to include the viscosity term.

4. A new parameter γ is added to the equations because of the Laplace transformations.

In the foregoing formulations it is assumed that ρ , λ , μ , α, and η are time independent and furthermore all the second order terms are negligible.

We will again consider a spheroidal motion:

$$\bar{U} = \sum_{nm} \left(U_{nm}(r) \;,\; V_{nm}(r) \frac{\partial}{\partial\theta} \;,\; \frac{V_{nm}(r)}{\sin\theta} \frac{\partial}{\partial\varphi} \right) S_{nm}(\theta,\varphi) \tag{5-12}$$

and, if we assume that,

$$[\lambda, \mu, \alpha, \eta, \Theta] = \sum_{nm} [\lambda_{nm}, \mu_{nm}, \alpha_{nm}, \eta_{nm}, \Theta_{nm}] S_{nm}(\theta, \varphi) \tag{5-13}$$

we will have terms like

$$A^{kl}_{nm} S_{nm}(\theta, \varphi) \cdot S_{kl}(\theta, \varphi)$$

appearing in the equations. Although we can, in general, express them in terms of single harmonics, $\sum_{ij} C_{ij} S_{ij}(\theta, \varphi)$ where C_{ij} is given by:

$$C_{ij} = \frac{\int_0^{\pi}\int_0^{2\pi} \sin\theta \, d\theta \, d\varphi \, A^{kl}_{nm} S_{nm}(\theta,\varphi) S_{kl}(\theta,\varphi) S_{ij}(\theta,\varphi)}{\int_0^{\pi}\int_0^{2\pi} \sin\theta \, d\theta \, d\varphi \, S^2_{ij}(\theta,\varphi)} \tag{5-14}$$

it is better to avoid complexity, in this state of the treatment, and assume that λ, μ, α, η, and Θ are laterally independent.

Now we define some dependent variables, analogous to what we did for the elastic case.

$$Y_1 = \tilde{U} \qquad Y_4 = (\mu + \frac{\eta\gamma}{2})(\frac{d}{dr}\tilde{V} - \frac{\tilde{V}}{r} + \frac{\tilde{U}}{r})$$

$$Y_2 = \lambda \tilde{X} + (2\mu + \eta\gamma)\frac{d}{dr}\tilde{U} \qquad Y_5 = \tilde{\psi} \tag{5-15}$$

$$Y_3 = \tilde{V} \qquad Y_6 = \frac{d}{d}\psi - 4\pi G \rho_o \tilde{U}$$

Following the procedure adopted in Chapter 3 equation (5-7 to 10) are reduced to the following simultaneous differential equations.

$$\frac{d}{dr}Y_1 = \frac{-2\lambda}{(\lambda+2\mu+\eta\gamma)r}Y_1 + \frac{1}{(\lambda+2\mu+\eta\gamma)}Y_2 + \frac{n(n+1)\lambda}{(\lambda+2\mu+\eta\gamma)r}Y_3 .$$

$$\frac{d}{dr}Y_2 = \left[-4g_0\rho_0 r + \frac{2(2\mu+\eta\gamma)(3\lambda+2\mu+\eta\gamma)}{\lambda+2\mu+\eta\gamma}\right]\frac{Y_1}{r^2} - \frac{2(2\mu+\eta\gamma)}{(\lambda+2\mu+\eta\gamma)r}Y_2 +$$
$$\left[n(n+1)g_0\rho_0 r - \frac{(2\mu+\eta\gamma)n(n+1)(3\lambda+2\mu+\eta\gamma)}{\lambda+2\mu+\eta\gamma}\right]\frac{Y_3}{r^2} + \frac{n(n+1)}{r}Y_4 - \rho_0 Y_5$$
$$+\Delta\rho g_0 - \frac{\partial}{\partial r}\left[\alpha(3\lambda+2\mu)\bar{\Theta}_1\right] .$$

$$\frac{d}{dr}Y_3 = -\frac{Y_1}{r} + \frac{Y_3}{r} + \frac{2Y_4}{2\mu+\eta\gamma} .$$

$$\frac{d}{dr}Y_4 = \left[g_0\rho_0 r - \frac{(2\mu+\eta\gamma)(3\lambda+2\mu+\eta\gamma)}{\lambda+2\mu+\eta\gamma}\right]\frac{Y_1}{r^2} - \frac{\lambda}{(\lambda+2\mu+\eta\gamma)r}Y_2$$
$$+\frac{(2\mu+\eta\gamma)}{(\lambda+2\mu+\eta\gamma)}\left[\lambda(2n^2+2n-1) + (2\mu+\eta\gamma)(n^2+n+1)\right]\frac{Y_3}{r^2}$$
$$-\frac{3Y_4}{r} - \rho_0\frac{Y_5}{r} - \frac{\partial}{\partial r}\left[\alpha(3\lambda+2\mu)\bar{\Theta}_1\right] .$$

$$\frac{d}{dr}Y_5 = 4\pi G\rho_0 Y_1 + Y_6 .$$

$$\frac{d}{dr}Y_6 = \frac{-4\pi G\rho_0 n(n+1)}{r}Y_3 + \frac{n(n+1)}{r^2}Y_5 - \frac{2}{r}Y_6 - 4\pi G\Delta\rho .$$

Boundary conditions of this problem are again analogous to the elastic case. Thus, in order to carry out numerical computations it is required to have the time variations of the boundary conditions at the earth's surface. The time dependence of surface topography

and crustal density may be estimated from the rate of continental drift. For geopotential, on the other hand, we need long time measurements which may take several decades. Therefore, the satisfactory numerical calculations require long time data collection. However, the thermo-elastic model does not need time varying boundary conditions. So, with the presently available data, this problem is solvable and will be considered in the near future.

APPENDIX I

Spherical Harmonic Analysis

In this appendix we describe the two different techniques used to analyze the observed geophysical data, $D(\theta, \varphi)$, in terms of the following spherical harmonics:

$$Z(\theta,\varphi) = \sum_{n=1}^{N} \sum_{m=0}^{n} \left\{ A_{nm} S^{e}_{nm}(\theta,\varphi) + B_{nm} S^{o}_{nm}(\theta,\varphi) \right\} \tag{I-1}$$

where

θ = co-latitude

φ = east longitude

S_{nm} = fully normalized spherical harmonic

e = even harmonics

o = odd harmonics

1) - Simple least-squares method

This method requires a minimum squared error, E^2;

$$\frac{\partial}{\partial A_{nm}} E^2 = \frac{\partial}{\partial B_{nm}} E^2 = 0 \tag{I-2}$$

where

$$E^2 = \sum_{i=1}^{q} \left\{ Z(\theta_i, \varphi_i) - D(\theta_i, \varphi_i) \right\} \sin\theta_i \cdot \tag{I-3}$$

Here q is the number of data points.

Combining equations (I-1 to 3) yields:

$$\bar{\bar{V}} \cdot \bar{X} = \bar{R} \tag{I-4}$$

$\bar{\bar{V}}$ is a symmetric matrix, any element of which is a 2x2 matrix:

$$V_{k\ell}^{nm} = \begin{bmatrix} \sum_{i=1}^{q} S_{nm}^{e}(\theta_i,\varphi_i)\, S_{k\ell}^{e}(\theta_i,\varphi_i) \sin\theta_i & \sum_{i=1}^{q} S_{nm}^{o}(\theta_i,\varphi_i) S_{k\ell}^{e}(\theta_i,\varphi_i) \sin\theta_i \\ \sum_{i=1}^{q} S_{nm}^{e}(\theta_i,\varphi_i)\, S_{k\ell}^{o}(\theta_i,\varphi_i) \sin\theta_i & \sum_{i=1}^{q} S_{nm}^{o}(\theta_i,\varphi_i) S_{k\ell}^{o}(\theta_i,\varphi_i) \sin\theta_i \end{bmatrix} \tag{I-5}$$

and $\bar{X}$ and $\bar{R}$ are two column vectors given by:

$$X^{nm} = \begin{bmatrix} A_{nm} \\ B_{nm} \end{bmatrix} \quad , \quad R_{k\ell} = \begin{bmatrix} \sum_{i=1}^{q} D(\theta_i,\varphi_i)\, S_{k\ell}^{e}(\theta_i,\varphi_i) \sin\theta_i \\ \sum_{i=1}^{q} D(\theta_i,\varphi_i)\, S_{k\ell}^{o}(\theta_i,\varphi_i) \sin\theta_i \end{bmatrix} . \tag{I-6}$$

If there were infinite numbers of evenly distributed data points we would use the orthogonality properties of the harmonics in order to solve equation (I-4) for $\bar{X}$. In practice, however, there are limited and unevenly scattered data. So we utilize Gauss-Jordan reduction technique to determine $\bar{X}$ (Hildebrand, 1961).

2) - Weighted least-squares method

In the case of very limited and unevenly scattered data points,

$\bar{\bar{V}}$ is an ill posed matrix and the coefficients obtained through the simple least-squares method are mutually dependent. To make $\bar{\bar{V}}$ to be well posed we find a weighting factor, w_i, for the i^{th} data point such that different spherical harmonics are orthogonal on the weighted points. That is:

$$\sum_{i=1}^{q} w_i S_{kl}(\theta_i, \varphi_i) \cdot S_{nm}(\theta_i, \varphi_i) = \delta_{kn} \cdot \delta_{lm} \cdot \delta_{eo} \sum_{i=1}^{q} \sin\theta_i \cdot S^2_{nm}(\theta_i, \varphi_i) \qquad \text{(I-7)}$$

where δ_{ij} is the Kronecker delta function. If the harmonics were orthogonal w_i would be equal to Sin θ_i. Therefore, w_i's are determined to be close to Sin θ_i by minimizing η^2, where η^2 is defined by:

$$\eta^2 = \sum_{i=1}^{q} \{ w_i - \sin\theta_i \}^2 \qquad \text{(I-8)}$$

In computation we first solve equations (I-7) and (I-8) for w_i. Rewriting these equations in a more compact form we obtain,

$$\bar{\bar{F}} \cdot \bar{w} = \bar{B} \qquad \text{(I-9)}$$

$$(\bar{w} - \bar{\xi})^T \cdot (\bar{w} - \bar{\xi}) = \text{Minimum} \qquad \text{(I-10)}$$

Where $\bar{\bar{F}}$ is a pxq matrix:

$$F^{nm}_{kl}(\theta_i, \varphi_i) = S_{nm}(\theta_i, \varphi_i) \cdot S_{kl}(\theta_i, \varphi_i) \qquad \text{(I-11)}$$

with

$$P = (N+1)(N+2)\{(N+1)(N+2)+1\}/2 \quad . \tag{I-12}$$

N is the highest degree of the harmonics considered. $\bar{W}$, $\bar{\xi}$, and $\bar{B}$ are column vectors with q, q, and p rows respecitvely:

$$\underset{i}{\xi} = \sin\theta_i \; , \quad B_{kl}^{nm} = \delta_{nk}\,\delta_{lm}\,\delta_{eo}\sum_{i=1}^{q} \sin\theta_i \, S_{nm}^{2}(\theta_i, \varphi_i) \tag{I-13}$$

and $(\bar{W}-\bar{\xi})^T$ is the transpose of $(\bar{W}-\bar{\xi})$.

Equations (I-9) and (I-10) are solved approximately by minimizing G_o which is defined by:

$$G_o = (\bar{\bar{F}}\cdot\bar{W}-\bar{B})^T\cdot(\bar{\bar{F}}\cdot\bar{W}-\bar{B}) + \varepsilon(\bar{W}-\bar{\xi})^T\cdot(\bar{W}-\bar{\xi}) \tag{I-14}$$

and the weighting factors are computed through:

$$\bar{W} = (\bar{\bar{F}}^T\cdot\bar{\bar{F}} + \varepsilon\bar{\bar{I}})^{-1}\cdot(\bar{\bar{F}}^T\cdot\bar{B} + \bar{\varepsilon}) \quad , \tag{I-15}$$

where $\bar{\bar{I}}$ is an identity matrix.

Having obtained the factors we then expand the data in terms of spherical harmonics, the coefficients of which are determined by the following weighted least-squares formula.

$$\sum_{i=1}^{q} \omega_i \left\{ Z(\theta_i, \varphi_i) - D(\theta_i, \varphi_i) \right\}^2 = \text{Minimum} \qquad \text{(I-16)}$$

The coefficients A and B are calculated by an equation similar to (I-4) where Sin θ_i is replaced by ω_i.

APPENDIX II

Correlation Coefficients and Regression Analysis

In Chapter 2 we correlated the spherical harmonic coefficients of geophysical data. Moreover, the raw data of crustal thickness was correlated with those of density of the surface layer. This appendix is devoted to the explanation of linear correlation coefficients between two continuous and two discrete data. In the latter case the constants of the regression line is also calculated.

Let $f(\theta,\varphi)$ and $f'(\theta,\varphi)$ be two continuous functions expressed in terms of the following spherical harmonics:

$$\begin{bmatrix} f(\theta,\varphi) \\ f'(\theta,\varphi) \end{bmatrix} = \sum_{n=1}^{N}\sum_{m=0}^{n} \left\{ \begin{bmatrix} A_{nm} \\ A'_{nm} \end{bmatrix} S^{e}_{nm}(\theta,\varphi) + \begin{bmatrix} B_{nm} \\ B'_{nm} \end{bmatrix} S^{e}_{nm}(\theta,\varphi) \right. \quad . \tag{II-1}$$

Their linear correlation coefficient is defined by:

$$r_{ff'} = \frac{\int_0^{2\pi}\int_0^{\pi} \sin\theta \, d\theta \, d\varphi \, f f'}{\left[\int_0^{2\pi}\int_0^{\pi} \sin\theta \, d\theta \, d\varphi \, f^2\right]^{1/2} \cdot \left[\int_0^{2\pi}\int_0^{\pi} \sin\theta \, d\theta \, d\varphi \, f'^2\right]^{1/2}} \quad . \tag{II-2}$$

Putting equation (II-1) into (II-2) and using the ortogonality properties of the harmonics we obtain:

$$r_{ff'} = \frac{\sum_{n=1}^{N}\sum_{m=0}^{n} \{ A_{nm} \cdot A'_{nm} + B_{nm} \cdot B'_{nm} \}}{\left[\sum_{n=1}^{N}\sum_{m=0}^{n} \{ A_{nm}^2 + B_{nm}^2 \}\right]^{1/2} \cdot \left[\sum_{n=1}^{N}\sum_{m=0}^{n} \{ A'^2_{nm} + B'^2_{nm} \}\right]^{1/2}} \tag{II-2a}$$

In the case of two sets of discrete data, X_i and Y_i, the linear correlation coefficient is defined by (Lee, 1956):

$$r_{xy} = \frac{\overline{(x-\bar{x})\cdot(y-\bar{y})}}{\sigma_x \cdot \sigma_y} \tag{II-3}$$

where $\bar{X}$ is the mean value of X and σ_x is the standard deviation of X. Equation (II-3) can be written in more explicit form as:

$$r_{xy} = \frac{q\sum_{i=1}^{q} x_i y_i - \left(\sum_{i=1}^{q} x_i\right)\left(\sum_{i=1}^{q} y_i\right)}{\left[q\sum_{i=1}^{q} x_i^2 - \left(\sum_{i=1}^{q} x_i\right)^2\right]^{1/2} \cdot \left[q\sum_{i=1}^{q} y_i^2 - \left(\sum_{i=1}^{q} y_i\right)^2\right]^{1/2}} \tag{II-3a}$$

The regression line fitted to this data is given by:

$$Y = aX + b \tag{II-4}$$

where

$$\begin{bmatrix} a \\ b \end{bmatrix} = \frac{1}{q\sum_{i=1}^{q} x_i^2 - \left(\sum_{i=1}^{q} x_i\right)^2} \cdot \begin{bmatrix} \sum_{i=1}^{q} i & -\sum_{i=1}^{q} x_i \\ -\sum_{i=1}^{q} x_i & \sum_{i=1}^{q} x_i^2 \end{bmatrix} \cdot \begin{bmatrix} \sum_{i=1}^{q} x_i y_i \\ \sum_{i=1}^{q} y_i \end{bmatrix} \tag{II-5}$$

APPENDIX III

Matricant Method

In Chapter 3 we adopted the matricant method in order to integrate the following set of simultaneous linear first order ordinary differential equations:

$$\frac{d}{dr}\bar{y} = \bar{\bar{A}} \cdot \bar{y} + \bar{S} \quad , \tag{III-1}$$

throughout the earth. In this appendix the properties of the matricant are briefly outlined and the solution of equation (III-1) is given in a compact form.

Let $Y(r_o)$ and $y(r)$ be the values of y at $r=r_o$ and $r=r$ respectively. Y (r) can be expressed in terms of $y(r_o)$, the matricant of the medium between r_o and r, $\bar{\bar{\Omega}}_{r_o}^{r}(\bar{\bar{A}})$, and the term due to the sources, S(r), located in this region in the following form (Gantmacher, 1960):

$$\bar{y}(r) = \bar{\bar{\Omega}}_{r_o}^{r}(\bar{\bar{A}}) \cdot \bar{y}(r_o) + \int_{\tau=r_o}^{r} \bar{\bar{\Omega}}_{\tau}^{r}(\bar{\bar{A}}) \cdot \bar{S}(\tau)\, d\tau \tag{III-2}$$

where the matricant is defined by:

$$\bar{\bar{\Omega}}_{r_o}^{r}(\bar{\bar{A}}) = \bar{\bar{I}} + \int_{r_o}^{r} \bar{\bar{A}}(\tau)\, d\tau + \int_{r_o}^{r} \bar{\bar{A}}(\tau_1)\, d\tau_1 \cdot \int_{r_o}^{\tau_1} \bar{\bar{A}}(\tau_2)\, d\tau_2 + \cdots \tag{III-3}$$

If the coefficient matrix $\bar{\bar{A}}$ is independent of r,

$$\bar{\bar{\Omega}}_{r_o}^{r}(\bar{\bar{A}}) = e^{(r-r_o)\bar{\bar{A}}} \quad . \tag{III-4}$$

Inside the earth $\bar{\bar{A}}$ and the source vector $\bar{S}$ are radially dependent. However, we divide each layer into sub-layers thin enough that inside each sub-layer $\bar{\bar{A}}$ and $\bar{S}$ can be regarded as constants. We then use equation (III-4) to express the matricant of that sub-layer. The size of the sub-layer is determined by the following procedure. First, the matricant of the total layer is calculated and then the layer is divided into two equally thick layers and the matricant of the total layer is again calculated through the matricant of each sub-layer and the following property of the matricant:

$$\bar{\bar{\Omega}}_{r_o}^{r}(\bar{\bar{A}}) = \bar{\bar{\Omega}}_{r_1}^{r}(\bar{\bar{A}}) \cdot \bar{\bar{\Omega}}_{r_o}^{r_1}(\bar{\bar{A}}) \quad . \tag{III-5}$$

The two results should be close to each other within a given tolerance. Otherwise we continue to divide the layer into many sub-layers, until the closeness of the matricants are justified.

We also assume that $\bar{S}$ is located at the center of each sub-layer. That is:

$$\bar{S}_j = \bar{s}_j \cdot \delta\left(r - \frac{r_j + r_{j-1}}{2}\right) \tag{III-6}$$

where δ is the Kroniker delta function and

$$\bar{S}_j = \int_{r_{j-1}}^{r_j} \bar{S}_j(\tau)\, d\tau \quad . \tag{III-7}$$

Using equations (III-5 and 6), equation (III-2) is reduced to:

$$\bar{y}(r_i) = \left[\prod_{j=1}^{i} \bar{\bar{\Omega}}_{r_{j-1}}^{r_j}(\bar{\bar{A}}_j) \right] \cdot \bar{y}(r_0) + \sum_{j=1}^{i} \bar{\bar{\Omega}}_{r_j}^{r_i}(\bar{\bar{A}}_{j+1}) \cdot \bar{\bar{\Omega}}_{r_{j-1}}^{r_j}\left(\frac{\bar{\bar{A}}_j}{2}\right) \cdot \bar{S}_j \quad . \tag{III-8}$$

In our case the source term is a product of a scalor, d (density perturbation), and a vector, element of which depend only on the properties of the medium so that:

$$\bar{S}_j = d_j \bar{D}_j \quad . \tag{III-9}$$

Putting equation (III-9) into (III-8) yields:

$$\bar{y}(r_i) = \left[\prod_{j=1}^{i} \Omega_{r_{j-1}}^{r_j}(\bar{\bar{A}}_j) \right] \cdot \bar{y}(r_0) + \sum_{j=1}^{i} d_j \bar{M}_j \tag{III-10}$$

where

$$\bar{M}_j = \bar{\bar{\Omega}}_{r_j}^{r_i}(\bar{\bar{A}}_{j+1}) \cdot \bar{\bar{\Omega}}_{r_{j-1}}^{r_j}\left(\frac{\bar{\bar{A}}_j}{2}\right) \cdot \bar{D}_j \quad . \tag{III-11}$$

It is worthwhile to notice that the coefficients of $Y(r_0)$ and d_j depend only on the properties of the medium (in our case the unperturbed earth model.

A Remark on the Determination of $e^{\bar{\bar{P}}}$

If $\bar{\bar{P}}$ has a large number of rows or its elements have large magnitudes, a great number of terms should be included in the power series expansion in order to obtain a good approximation. The following procedure is used to avoid this difficulty.

Let us write

$$e^{\bar{\bar{P}}} = \left[e^{\bar{\bar{P}}/2^n} \right]^{2^n} \tag{III-12}$$

and expand inside the parenthesis in power series,

$$e^{\bar{\bar{P}}} = \left[\bar{\bar{I}} + \frac{\bar{\bar{P}}}{2^n} + \frac{1}{2} \left(\frac{\bar{\bar{P}}}{2^n}\right) \cdot \left(\frac{\bar{\bar{P}}}{2^n}\right) + \cdots + \frac{1}{(m-1)!} \left(\frac{\bar{\bar{P}}}{2^n}\right)^{m-1} + \bar{\bar{\epsilon}} \right]^{2^n} \tag{III-13}$$

where $\bar{\bar{\epsilon}}$ is the truncation error:

$$\bar{\bar{\epsilon}} \leq \frac{(K\rho)^m}{m!} \cdot e^{K\rho} \cdot [\bar{\bar{I}}] \quad . \tag{III-14}$$

Here K is the number of rows (or column) of $\bar{\bar{P}}$ and ρ is the elements of $\bar{\bar{P}}$ with greatest absolute value (Frazer, et al., 1965). There are two parameters in equation (III-14), n and m, which should be chosen such that the ratio

$$\left(2^n \left(\bar{\bar{B}}\right)^{2^n - 1} \cdot \bar{\bar{\epsilon}} \right) / \left(\bar{\bar{B}}\right)^{2^n} \tag{III-15}$$

falls within a given error, η . That is:

$$\left[2^n \left(\bar{\bar{B}} \right)^{2^{n-1}} \cdot \bar{\bar{\epsilon}} \right] \leqslant \eta \left(\bar{\bar{B}} \right)^{2^n} . \tag{III-16}$$

or

$$\bar{\bar{\epsilon}} < \frac{\eta \bar{\bar{B}}}{2^n} \tag{III-16a}$$

where

$$\bar{\bar{B}} = \bar{\bar{I}} + \frac{\bar{\bar{P}}}{2^n} + \cdots + \frac{1}{(m-1)!} \left(\frac{\bar{\bar{P}}}{2^n} \right)^{m-1} . \tag{III-17}$$

Putting equation (III-16) into (III-14) yields:

$$\frac{(K\varphi)^m}{m!} e^{K\varphi} \cdot [\bar{\bar{1}}] \leqslant \frac{\eta}{2^n} \bar{\bar{B}} \tag{III-18}$$

The minimum amount of calculation, at least in our case, is when φ is between .2 and .5. Thus, we determined n in order to make φ to be within this limit and then determined m from equation (III-18). Once we find $\bar{\bar{B}}$ it needs only n multiplications to recover $e^{\bar{\bar{P}}}$.

REFERENCES FOR TABLE (2-1)

1. Adams, R. D., Thickness of the earth's crust beneath the Pacific-Antarctic Ridge, New Zeal. J. Geol. Geophys., 7, 529, 1964.

2. Aki, K., Crustal structure in Japan from the phase velocity of Rayleigh waves, Part 1, Bull. Earthquake Res. Inst., 39, 255, 1961.

3. Andrew, A. P., V. V. Brodovoy, V. E. Goldsmidt, U. E. Koozmin, M. D. Morozov, and R. A. Aydlin, Crustal structure in Kazakhstan and method of its study, Akad. Nauk Kazakhskoi SSR, IZV. Ser. Geo., 4, 3, 1964.

4. Antoine, J. and J. Ewing, Seismic refraction measurements on the margins of the Gulf of Mexico, J. Geop. Res., 68, 1975, 1963.

5. Barrett, D. L., M. Berry, J. E. Blanchard, M. J. Keen, and R. E. McAlester, Seismic studies on the eastern seaboard of Canada: The Atlantic Coast of Nova Scotia, Canad. J. Earth Scien., 1, 10, 1964.

6. Bath, M. and E. Tryggvason, Deep seismic reflection experiments at Kiruna, Geofisica Pure et Applicata, 51, 79, 1962.

7. Belaussov, V. G., B. S. Volvovski, I. S. Volvovski, and V. A. Rayaboi, Experimental investigation of the recording of deep reflected waves, Acad. Sci. U.S.S.R. Bull. Geofiz. Ser., 7, 662, 1962.

8. Bentley, C. R., and J. L. Worzel, Geophysical Investigations in the emerged and submerged Atlantic coastal plain part X: Continental slope and continental rise south of the Grand Banks, Bull. Geol. Soc. Am., 67, 1, 1956.

9. Berckhemer, H., Rayleigh wave dispersion and crustal structure in the east Atlantic ocean basin, Bull. Seis. Soc. Am., 46, 83, 1956.

10. Berg, J. W., L. Trembly, D. A. Emilia, J. R. Hutt, J. M. King, L. T. Long, W. R. McKnight, S. K. Sarmah, R. Souders, J. V. Thiruvathukal, and D. A. Vossler, Crustal refraction profile, Oregon coast range, Bull. Seis. Soc. Am., 56, 1357, 1966.

11. Blanchard, J. E., A. M. Dainty, G. N. Ewing, C. E. Keen, M. J. Keen, G. S. Moore, and C. F. Tsong, Seismic Studies on the eastern seaboard of Canada, Maritime Sed., 1, 2, 23, 1965.

12. Bott, M. H. P., The deep structure of the northern Irish Sea - A problem of crustal dynamics, Submarine Geol. Geoph., 179, 1965.

13. Bullin, N. K., Earth's crust in central Turkman in Sermyy Zavod region, Akad. Nauk S. S. S. R., IZV, Geofiz. Ser., 9, 1389, 1964.

14. Bynce, E. T., and D. A. Fahlquist, Geophysical investigation of the Puerto Rico trench and outer ridge, J. Geophy. Res., 67, 3955, 1962.

15. Collette, B. J. and R. A. Lagaay, Depth to the Mohorovicic discontinuity under the north sea basin, Nature, 205, 688, 1965.

16. Cram, I. H., Jr., A crustal structure refraction survey in south Texas, Geophysics, 26, 560, 1961.

17. Eaton, J. P., Crustal structure from San Francisco, California, to Eureka, Nevada, from seismic refraction measurements, J. Geoph. Res., 68, 5789, 1963.

18. Evison, F. F., C. E. Ingham, R. H. Orr, and J. H. LeFort, Thickness of the earth's crust in Antarctic and surrounding oceans, Geophy. J., 3, 289, 1960.

19. Ewing, J. I., J. Antoine and M. Ewing, Geophysical measurements in the western Caribbean Sea and in the Gulf of Mexico, J. Geophys. Res., 65, 4087, 1960.

20. Ewing, M., J. I. Ewing and W. J. Luduring, Seismic-refraction measurements in the Atlantic Ocean basins, in the Mediterranean Sea, on the Mid-Atlantic ridge and in the Norwegian Sea, Bull. Geol. Soc. Am., 74, 275, 1963.

21. Ewing, J., and M. Ewing, Geophysical Investigations in the submerged Argentine costal plain, Bull. Geol. Soc. Am., 70, 291, 1959.

22. Ewing, M., G. H. Sutton and C. R. Officer, Jr., Seismic refraction measurements in the Atlantic ocean, part VI, typical deep stations North American basin, Bull. Seis. Soc. Am., 44, 21, 1954.

23. Fahlquist D. A., Seismic refraction measurements in the Western Mediterranean Sea, Ph. D. thesis, Mass. Inst. of Technology, Cambridge, Mass., 1963.

24. Finetti, J., S. Bellemo and G. DeVisintini, Preliminary investigation on the earth's crust in the South Adriatic Sea. Boll. Geofisica Teor., ed. Appl., 8, 21, 1966.

25. Fisher, R. L. and R. W. Raitt, Topography and structure of the Peru-Chile trench, Deep-Sea Res., 9, 423, 1962.

26. Francis, T. J. G., D. Davies and M. N. Hill, Crustal Structure between Kenya and the Seychelles, Roy. Soc. London, Phil. Tran., 259, 240, 1966.

27. Francis, T. J. G. and R. W. Raitt, Seismic refraction measurements in the Southern Indian ocean, J. Geophys. Res., 72, 3015, 1967.

28. Fuchs, K., S. T. Muller, E. Peterschmitt, J. P. Rothe, A. Stein and K. Strobach, Krustenstruktur der Westalpen Nach Refraktionsseismischen Mussugen, Gerlands Beitrage Zur Geoph., 72, 149, 1963.

29. Furumoto, A. S., N. J. Thompson and G. P. Woolard, The structure of Koolau Volcanic from seismic refraction studies, Pacific Sci., 19, 306, 1965

30. Gabriel, V. C. and J. T. Kuo, Heigh Rayleigh wave phase velocity for the New Delhi, India--Lahore, Pakistan profile, Bull. Seis. Soc. Am., 56, 1137, 1966.

31. The German Research Group for Explosion Seismology, Crustal structure in Western Germany, Zeit. Geophys., 30, 209, 1964.

32. Gilbert, D. and M. N. Toksöz, Crustal structure in east Antarctic from surface wave dispersion, Geophy. J., 10, 127, 1965.

33. Gupta, H. K. and H. Narain, Crustal structure in Himalayan and Tibet plateau region from surface wave dispersion, Bull. Seis. Soc. Am., 57, 235, 1967.

34. Hall, D. H. and W. C. Brislan, Crustal structure from converted head waves in Central Western Manitoba, Geophysics, 30, 1053, 1965.

35. Healy, J. H., Crustal structure along the coast of California from seismic refraction measurements, J. Geoph. Res., 68, 5777, 1963.

36. Hersey, J. B., E. T. Bunce, R. F. Wyrick, and F. T. Dietz, Geophysical investigation of the continental margin between Cape Henry, Virginia and Jacksonville, Florida, Bull. Geol. Soc. Am., 70, 437, 1959.

37. Houtz, R.E. and J.I. Ewing, Detailed sedimentary velocities from seismic refraction profiles in the western North Atlantic, J. Geoph. Res., 68, 5233, 1963.

38. Jackson, W.H. and L.C. Pakiser, Seismic study of crustal structure in the southeastern Rocky Mountains, U.S.G.S. Prof. papers, 525, D.P.D. 85, 1965.

39. Johnson, L.R., Crustal structure between Lake Mead, Nevada and Mono Lake, California, J. Geophys. Res., 70, 2863, 1965.

40. Kanasewich, E.R. and G.L. Cumming, Near-Vertical-Incidence seismic reflection from Conrad discontinuity, J. Geophys. Res., 70, 3441, 1965.

41. Karasnopevtseva, G.V., K. Voprosoo o gloobinnom stroenee zemnoy kore zakavkazya, Sovt. Geol., 2, 159, 1966.

42. Katz, S. and M. Ewing, Seismic refraction measurements in the Atlantic Ocean, Part VII: Atlantic Ocean basin, west of Bermuda, Bull. Geol. Soc. Am., 67, 475, 1956.

43. Khalevin, N.E., V.S. Drooghenin, V.M. Rebalka, A.A. Nezolenova, and L.N. Chodankova, On the results of deep seismic sounding of the earth's crust in Central Ural, Akad. Nauk SSSR, IZV. Fizika Zemli, 4, 36, 1966.

44. Knopoff, L., S. Mueller and W. L. Pilant, Structure of the crust and upper mantle in the Alps from the phase velocity of Rayleigh waves, Bull. Seis. Soc. Am., 56, 1009, 1966.

45. Kosminskaya, I.P., G.G. Mikhota and Y.V. Tulina, Stoeneye Aemnoy kor v pamiro-Alayeskoy zone po dannim gloobinnogo seismicheskogo zondirovania, Akad. Nauk SSSR IZV. Ser. Geofiz., 1162, 1958.

46. Kiplov, S.V., V.S. Surkov and A.R. Meeshenkina, Stroeneye zemnoy kor V Uoghnoy chasti zapadno-seberskoy nizmennosti, Akad. Nauk SSSR Sibirskoy ot deleney, Geol Geofiz, 1, 62, 1965.

47. Lee, W.H.K. and P.T. Taylor, Global analysis of seismic refraction measurements, Geophy. J., 11, 389, 1966.

48. Lepichon, X., R.E. Houtz, C.L. Drake and J.E. Nate, Crustal structure of the mid-ocean ridges, 1: seismic refraction measurements, J. Geoph. Res., 70, 319, 1965.

49. Liebscher, H. J. Deutugsuersuche für die struktur de Tieferen Erdruste nach reflexionsseismischen und granimetrischen messugen im deutschen Alpennorland, Zeit, Geophy., 30, 51, 1964.

50. Matuzawa, T., T. Matumoto and S. Asano, On the crustal structure derived from observations of the second Hokoda Explosion, Bull. Earthquake Res. Inst. Tokyo Univ., 37, 509, 1959.

51. Mikumo, T., M. Otsuka, T. Utsu, T. Terashima and A. Okada, Crustal structure in Central Japan as derived from the Miboro Explosion - seismic observations, part 2: On the crustal structure, Bull. Earthquake Res. Inst. Tokyo Univ., 39, 327, 1961.

52. Murauchi, S., N. Den, S. Asano, H. Hotta, J. Chujo, T. Asanama, K. Ichikawa and I. Noguchi, A seismic refraction exploration of Kuman Nada (Kumano Sea), Japan, Japan Acad. Proc., 40, 111, 1964.

53. Naprochnov, Yu. P., A. F. Neprochnova, S. M. Zverev, V. I. Mironova, R. A. Bokun and A. V. Chekunov, Fresh information on the crustal structure of the Black Sea trough south of the Crimea, Doklady Akad. Nauk, SSSR, 156, 51, 1964.

54. Officer, C. B., J. I. Ewing, J. F. Hennion, D. G. Harkrider and D. E. Miller, Geophysical investigations in the eastern Caribbean: summary of 1955-1956 cruises, Physics and chemistry of the earth, 3, Pergamon Press, New York, 1959.

55. Officer, C. B., M. Ewing and P. C. Wuenschel, Seismic refraction measurements in the Atlantic Ocean; Bermuda, Bermuda rise, and Nares Basin, Bull. Geol. Soc. Am., 63, 777, 1952.

56. Payo, G., Crustal structure of the Mediterranean Sea by surface waves, Part I: Group velocity, Bull. Seis. Soc. Am., 57, 151, 1967.

57. Pomerantseva, E. V., Results of studying the crystalline layer of crust in Russian platform regions, Prikladnaya Geofizica, 11, 1961.

58. Press, F., M. Ewing and J. Oliver, Crustal structure and surface wave dispersion in Africa, Bull. Seis. Soc. Am., 46, 97, 1956.

59. Raitt, R. W., Seismic refraction studies of the Pacific Ocean basin, part I: Crustal thickness of the central equatorial Pacific, Bull. Geol. Soc. Am., 67, 1623, 1956.

60. Reich, H., O. Foerstsch and G.A. Schulze, Results of seismic observations in Germany on the Heligsland explosion of April 18, 1947, J. Geoph. Res., 56, 147, 1951.

61. Rezanov, I.A., O geologicheskoy interpretachiy profilya gloobinogo seismicheskogo zondirovania Magadam-Kolima, Akad. Nauk SSSR, IZV, ser. Geofiz., 7, 865, 1962.

62. Richards, T.C. and D.J. Walker, Measurement of the thickness of the crust in the Albertan plains of Western Canada, Geophysics, 24, 262, 1959.

63. Roller, J.C., Crustal structure in the eastern Colorado plateaus province from seismic refraction measurements, Bull. Seis. Soc. Am., 55, 107, 1965.

64. Roller, J.C., and J.H. Healy, Seismic-Refraction measurements of crustal structure between Santa Monica Bay and Lake Mead, J. Geoph. Res., 68, 5837, 1963.

65. Sander, G.W. and A. Overton, Deep seismic refraction investigations in the Canadian Arctic Archipelago, Geophysics, 30, 87, 1965.

66. Savarenskii, E.F. and B.N. Shechkov, On the determination of variation of crustal thickness from group velocity of seismic waves, Akad Nauk SSSR, IZV, Phys. of the solid earth, 751, 1965.

67. Shekov, B.N., Dispersion of seismic surface waves and structure of the crust, Akad. Nauk SSSR, IZV, Ser. Geofiz., 3, 313, 1964.

68. Shore, G.G., Jr., Crustal structure of the Hawaiian Ridge near Gardner Pinnacles, Bull. Seis. Soc. Am., 50, 563, 1960.

69. Shore, G.G., Jr., Seismic refraction studies of the coast of Alaska, Bull. Seis. Soc. Am., 52, 37, 1962.

70. Shore, G.G., Jr., Structure of the Bering Sea and the Aleutian Ridge, Marine Geol., 1, 213, 1964.

71. Shore, G.G., Jr., and R.L. Fisher, Middle Atlantic Trench: Seismic-Refraction studies, Bull. Geol. Soc. Am., 72, 721, 1961.

72. Shore, G.G., Jr., and D.D. Pollard, Mohole site selection studies North of Maui, J. Geophys. Res., 69, 1627, 1964.

73. Smith, J. T., J. S. Stainhart and L. T. Aldrich, Lake Superior crustal structure, J. Geophys. Res., 71, 1141, 1966.

74. Sollogoob, V. B., H. E. Povlenkova, A. V. Chekoonov and L. A. Kheeleenskiy, Gloobinoy stroeneye zemnoy kori v dom meridionalnogo peresecheniya chernoe more - Voponeghskii massiv, Akad. Nauk Ukrayenskii SSR Prob. fiziki zemli, 15, 46, 1966.

75. Stuart, D. J., J. C. Roller, W. H. Jackson and G. B. Mangan, Seismic propagation paths, regional travel times, and crustal structure in the western United States, Geophysics, 29, 178, 1964.

76. Thompson, A. A., and F. F. Evison, Thickness of the crust in New Zealand, J. Geol. Geoph., 5, 1962.

77. Thompson, G. A., and M. Talwani, Crustal structure from Pacific basin to central Nevada, J. Geophys. Res., 69, 4813, 1964.

78. Usami, T., T. Mikumo, E. Shima, I. Tamaki, S. Asano, T. Asada, and T. Matuzawa, Crustal structure in Northern Kwanto district by explosion-seismic observations, part II, Models of Crustal structure, Bull. Earthquake Res. Inst., Tokyo Univ., 36, 349, 1958.

79. Veytsman, P. S., Features of the deep structure of the Kurile-Kamchatka Zone, Acad. Nauk, SSSR. IZV. Fiziki Zemli, 9, 13, 1965.

80. Volvovski, B. S., E. S. Volvovski and V. Z. Reyaboy, Nekotopiy danni o seismicheskekh volna, sootvetstvooyoosheekh podkorovomoo sloyo, Prikhladnay a Geofizica, 31, 3, 1961.

81. White, W. R. H. and J. C. Savage, A seismic refraction and gravity study of the earth's crust in British Columbia, Bull. Seis. Soc. Am., 55, 463, 1965.

82. Willden, R., Seismic refraction measurements of crustal structure between American Falls Reservoir, Idaho, and Flaming Gorge Reservoir, Utah, USGS. prof. papers, 525, C. P. C. 44, 1965.

GENERAL REFERENCES

Aki, K., Generation and propagation of G waves from the Niigata earthquake of June 16, 1964, part 2: Estimation of earthquake moment, released energy, and stress-strain drop, Bull. Earthquake Res. Inst., 44, 73-88, 1966.

Alterman, Z., H. Jarosh, and C.L. Pekeris, Oscillations of the earth, Proc. Roy. Soc., Ser. A, 252, 80-95, 1959.

Alterman, Z., H. Jarosh and C.L. Pekeris, Propagation of Rayleigh waves in the earth, Geophys. J. R. Astr. Soc., 4, 219-241, 1961.

Anderson, D.L., A seismic equation of state, Geophys. J. Roy. Astr. Soc., 13, 9-30, 1967.

Arkani-Hamed, J. and M.N. Toksöz, Analysis and correlation of geophysical data, Suppl. al Nuovo Cimento, 6, 1968, in press.

Arley, N., and K.R. Buch, Introduction to the Theory of Probability and Statistics, John Wiley & Sons, New York, 196-198, 1950.

Barazangi, M. and J. Dorman, World seismicity maps compiled from ESSA, Coast and Geodetic Survey, epicenter data, 1961-1967, presented at the meeting of the Eastern Section, Seis. Soc. Am., 1968.

Berckhemer, H. and K.H. Jacob, Investigation of the dynamic process in earthquake foci by analyzing the pulse shape of body waves, Berichte des Institutes für Meteorologic und Geophysik der Universität Frankfurt/Main, 13, 1968.

Birch, F., Elasticity and constitution of the earth's interior, J. Geophys. Res., 57, 227-286, 1952.

Birch, F., Physics of the Crust, Geol. Soc. Am., special paper, 62, 101-108, 1955.

Birch, F., The velocity of compressional waves in rocks to 10 kilobars, Part 2, J. Geophys. Res., 66, 2199-2224, 1961.

Birch, F., Megageolacial consideration in rock mechanics, in State of Stress in the Earth's Crust, ed. W.R. Judd, 55-80, 1964.

Birch, F., Density and compostion of mantle and core, J. Geophys. Res., 69, 4377-4388, 1964.

Bland, D.R., The Theory of Linerar Visco-elasticity, Intr. Ser. Monog. Pure and Appl. Math, 10, 1960.

Burridge, R. and L. Knopoff, The effect of initial stress or residual stress on elastic energy correlations, Bull. Seismo. Soc. Am., 56, 421-424, 1966.

Campbell, D.L., Deformation of a loaded visco-elastic planet, Trans. Am. Geophys. Union, 49, 752-753, 1968.

Caputo, M., The minimum strength of the earth, J. Geophys. Res., 70, 955-963, 1965.

Carder, D.S., D.W. Gordon and J.N. Jordan, Analysis of surface-foci travel times, Bull. Seism. Soc. Am., 56, 815-840, 1966.

Chinnery, M.A. and M.N. Toksöz, P-wave velocities in the mantle below 700 km., Bull. Seism. Soc. Am., 57, 199-226, 1967.

Cleary, J.R. and A.L. Hales, An analysis of the travel times of P-waves to North American stations, in the distance range of 32° to 100°, Bull. Seism. Soc. Am., 56, 467-490, 1966.

Crittenden, M.D., Effective viscosity of the earth derived from isostatic loading of Pleistocene Lake Bonneville, J. Geophys. Res., 68, 5517-5530, 1963.

Dorman, J., M. Ewing, and J. Oliver, Study of shear-velocity distribution in the upper mantle by mantle Ralyeigh waves, Bull. Seismo. Soc. Am., 50, 87-115, 1960.

Doyle, H.A. and A.L. Hales, An analysis of the travel times of S waves to North American stations in the distance range of 28° to 82°, Bull. Seism. Soc. Am., 57, 761-772, 1967.

Fairborn, J.W., Mantle P and S wave velocity distributions from dt/d measurements, Ph.D. Thesis, Mass. Inst. of Tech. 1968.

Frazer, R.A., W.J. Duncan and A.R. Collar, Elementary Matrices, Cambridge University Press, 42-42, 1960

Gantmacher, F.R., The theory of matrices, Vol. II, Chelsea Pub. Co., 1960.

Gaposchkin, E.M., A dynamic solution for the tesseral harmonics of the geopotential and station coordinates using Baker-Nunn data, Space Res., VII, 2, North Holland Pub., 685-693, 1967.

Giuer, W.H., Determination of the non-zonal harmonics of the geopotential from satellite doppler data, Nature, 200, 124-125, 1963.

Giuer, W.H. and R.R. Newton, The earth's gravity field as deduced from the doppler tracking of five satellites, J. Geophys. Res., 70, 4613-4626, 1965.

Griggs, D.T., and J. Handin, Editors, Rock Deformation, Geol. Soc. Am. Mem., 79, 347-364, 1960.

Hales, A.L., and H.A. Doyle, P and S travel time anomalies and their interpretation, Geophys. J. Roy. Astr. Soc., 13, 403-415, 1967.

Heard, H.C., Experimental deformation of rocks and the problem of extrapolation to nature, Rock Mechanics Seminar, 2, 439-507, 1968.

Heiskanen, W.A. and F.A. Vening Meinesz, The Earth and its Gravity Field, McGraw-Hill Book Co., Inc., 368-369, 1958.

Herrin, E., and J. Taggart, personnal communication, 1966.

Herrin, E., and J. Taggart, Regional variations in P travel times, Bull. Seism. Soc. Am., 58, 1325-1337, 1968.

Hildebrand, F.B., Methods of Applied Mathematics, Prentice-Hall, Inc., 1-4, 1961.

Hoskins, L.M., The strain of a gravitating, compressible elastic sphere, Am. Math. Soc. Trans. 11, 203-248, 1910.

Hoskins, L.M., The strain of a gravitating sphere of variable density and elasticity, Am. Math. Soc. Trans., 21, 1-43, 1920.

Izack, I. M., Tesseral harmonics of the geopotential and corrections to station coordinates, J. Geophys. Res., 69, 2621-2630, 1964.

Jeffreys, H., The determination of the earth's gravitational field, Roy. Soc. Mon. Not., 5, 1-22, 1941.

Jeffreys, H., The stress differences in the earth's shell, Roy. Astr. Soc. Month. Not. Geophys. Suppl., 5, 71-88, 1943.

Jeffreys, H., Rock Creep, tidal friction and the moons ellipticity, Month. Not., 118, 14-17, 1958.

Jeffreys, H., The Earth, 4th Ed., Cambridge Univ. Press, 195-210, 1959.

Jeffreys, H., On the hydrostatic theory of the figure of the earth, Geophys. J. Roy. Astr. Soc., 8, 196-202, 1964.

Jeffreys, H., and S. Crampin, Rock creep, a correction, Month. Not. Roy. Astr. Soc., 121, 571-577, 1960.

Kaula, W.M., Elastic models of the mantle corresponding to variations in the external gravity field, J. Geophys. Res., 68, 4967-4978, 1963.

Kaula, W.M., Determination of earth's gravitational field, Rev. of Geophys., 1, 507-551, 1963.

Kaula, W.M., Tesseral harmonics of the earth's gravitational field from Camera tracking of staellites, J. Geophys. Res., 71, 4377-4388, 1966.

Kaula, W.M., Geophysical implications of satellite determinations of the earth's gravitational field, Space Sci. Rev., 7, 769-794, 1967.

Kellogg, O.D., Foundations of Potential Theory, Dover Pub., Inc., 79-81, 1953.

Kovach, R.L. and D.L. Anderson, Study of the energy of the free oscillations of the earth, J. Geophys. Res., 72, 2155-2168, 1967.

Lee, E.H., Stress analysis in visco-elastic bodies, Quart. Appl. Math., 13, 183-190, 1955.

Lee, E.H., Visco-elastic stress analysis, Structural Mechanics, Pergamon Press, 456-482, 1960

Lee, Y.W., Statistical Theory of Communication, John Wiley & Sons, Inc., 220, 1960.

Lee, W.H.K. and W.M. Kaula, A spherical harmonic analysis of the earth's topography, J. Geophys. Res., 72, 753, 758, 1967.

Lee, W.H.K. and P.T. Taylor, Global analysis of seismic refraction measurements, Geophys. J. Roy. Astr. Soc., 11, 389-413, 1966.

Lomnitz, C., Creep measurements in igneous rocks, J. Geol., 64, 473-479, 1956.

Longman, I.M., A green's fraction for determining the deformation of the earth under surface mass loads, Part 1; Theory, J. Geophys. Res., 67, 845-850, 1962.

Longman, I.M., A green's function for determining the deformation of the earth under surface mass loads, part 2: computations and numerical results, J. Geophys. Res., 68, 485-496, 1963.

Love, A.E.H., Some problems of geodynamics, Dover Pub. Inc., 28-31, 1967.

McConnel, R.K., Jr., Isostatic adjustment in the layered earth, J. Geophys. Res., 70, 5171-5187, 1965.

Munk, W.H., and G.J.F. MacDonald, Continentality and the gravitational field of the earth, J. Geophys. Res., 65, 2169-2172, 1960.

Orowan, E., Mechanism of seismic faulting, Rock Defromation, Geol. Soc. Am. Mem., 79, 323-345, 1960.

Pekeris, C.L., and H. Jarosh, The free oscillations of the earth, in Contribution in Geophysics, Pergamon Press, 1, 177, London, 171-192, 1958.

Press, F., Earth models obtained by Monte Carlo inversion, J. Geophys. Res., 73, 5223-5233, 1968.

Rayleigh, O.M., On the dilalational stability of the earth, Proc. Roy. Soc., Ser. A., 77, 486-499, 1906.

Robertson, E.C., Visco-elasticity of rocks, State of Stress in the Earth's Crust, Ed. W.R. Judd, 181-233, 1964.

Runcorn, S.K., Satellite gravity measurements and a laminar viscous flow model of the earth's mantle, J. Geophys. Res., 69, 4389-4894, 1964.

Slicter, L.B., and M. Caputo, Deformation of an earth model by surface pressures, J. Geophys. Res., 65, 4151-4156, 1960.

Sokolnikoff, I.S., Mathematical theory of elasticity, McGraw-Hill Book Co., Inc., 1956.

Spencer Jones, Dimensions and Rotation, in The Earth as a Planet, Sol. Sys., Vol. II, 1-41, 1954.

Takeuchi, H., M. Saito and N. Kobayashi, Statical deformation and free oscillation of a model earth, J. Geophys. Res., 67, 1141-1154, 1962.

Takeuchi, H., M. Saito and N. Kobayashi, Study of shear velocity distribution in the upper mantle by mantle Rayleigh and Love waves, J. Geophys. Res., 67, 2831-2839, 1962.

Toksöz, M. N. and J. Arkani-Hamed, Seismic delay times: correlation with other data, Science, 158, 783-785, 1967.

Toksöz, M. N. M. A. Chinnery and D. L. Anderson, Inhomogeneities in the earth's mantle, Geophys. J. Roy. Astr. Soc., 13, 31-59, 1967.

Vening Meinesz, F. A., Thermal convection in the earth's mantle, Continental drift, Inter. Geophys. Ser., 3, 145-176, 1962.

Wang, C., Some geophysical implications from gravity and heat flow data, J. Geophys. Res., 70, 5629-5634, 1965.

Wange, C. Y., Earth's zonal deformations, J. Geophys. Res., 71, 1713-1720, 1966.

Woolard, G. P., Crustal structure from gravity and seismic measurements, J. Geophys. Res., 64, 1521-1544, 1959.